UNIVERSITY OF CALIFORNIA SAN DIEGO

Metabolic and physiological functions of sphingolipid biosynthetic flux in cardiovascular disease

A Dissertation submitted in partial satisfaction of the requirements
for the degree Doctor of Philosophy

in

Bioengineering

by

Jivani Manovathy Gengatharan

Committee in charge:

Professor Christian M. Metallo, Chair
Professor Pedro Cabrales, Co-Chair
Professor Adam Engler
Professor Philip Gordts
Professor Nathan Lewis

2023

The Dissertation of Jivani Manovathy Gengatharan is approved, and it is acceptable in quality and form for publication on microfilm and electronically.

University of California San Diego

2023

DEDICATION

To my parents Gengatharan Retnasingam and Ratnavathany Gengatharan for their continuous encouragement, love, and support.

TABLE OF CONTENTS

LIST OF FIGURES

LIST OF TABLES

ACKNOWLEDGEMENTS

There are several people I have to thank for their encouragement and support during the course of my graduate research. I am most grateful to my advisor, Dr. Christian Metallo, for his guidance and support through graduate school and for fostering an environment to grow and develop as a scientist. I want to thank current and former members of the Metallo lab for their valuable scientific discussions and the wonderful memories we've shared: Martina Wallace, Courtney Green, Thekla Cordes, Mehmet Badur, Le You, Avi Kumar, Thangaselvam Muthusamy, Esther Lim, Michal Handzlik, Noah Meurs, Justin Hover, Anna Trimble, Grace McGregor, Ramya Kuna, Sanika Khare, Karl Wessendorf-Rodriguez, Becky Chinn, Mo Ruchhoeft, Elena Diaz, Shrikaar Kambhampati, Emeline Joulia, Aurélie Laguerre, Sam Kerk, Emily Fennell, Addii Estrada-Cardenas, Patrick Tseng, Ethan Ashley, and finally, Zoya Chih. I have learned so much from each and every lab member and I appreciate the supportive atmosphere our lab has maintained over my graduate school journey to make each day in lab enjoyable. I also would like to express my gratitude to my collaborator and Committee member Dr. Philip Gordts for his guidance in learning new techniques to broaden the scope of my research and to his lab members Patrick Secrest, Joanna Coker, and Chelsea Painter for insightful scientific discussions and training to guide experiments and analysis. I would also like to thank my other Committee members, Dr. Pedro Cabrales, Dr. Adam Engler, and Dr. Nathan Lewis for their advice and support through my graduate career.

I want to thank my friends in San Diego and elsewhere for always being there for me, providing endless fun and laughter outside of work, and being my cheerleaders. I would also like to thank my constant source of joy Vaibhav Menon for his unwavering support and encouragement over the last several years. Finally, I would like to thank my parents Genga

Retnasingam and Vathany Gengatharan for their unconditional love and countless sacrifices throughout my life that have led me to where I am. Your support means the world to me.

Chapter 1 is an introduction to the literature and methods related to my dissertation. This chapter includes an overview of aberrant lipid metabolism in atherosclerotic cardiovascular disease, sphingolipid metabolism, mass spectrometry measurements, and stable isotope tracing techniques.

Chapter 2 has been submitted for publication and under review. Jivani M. Gengatharan is the primary author of this manuscript. Michal K. Handzlik, Zoya Y. Chih, Maureen L. Ruchhoeft, Patrick Secrest, Ethan L. Ashley, Courtney R. Green, Martina Wallace, and Philip L.S.M. Gordts are co-authors of the paper. Christian M. Metallo is the corresponding author of this manuscript.

Chapter 3 has been submitted in the same publication as Chapter 2 and is under review. Jivani M. Gengatharan is the primary author of this manuscript. Michal K. Handzlik, Zoya Y. Chih, Maureen L. Ruchhoeft, Patrick Secrest, Ethan L. Ashley, Courtney R. Green, Martina Wallace, and Philip L.S.M. Gordts are co-authors of the paper. Christian M. Metallo is the corresponding author of this manuscript.

Chapter 4 is the concluding chapter of this dissertation. This chapter compiles critical findings from each chapter and identifies avenues for future research.

VITA

2018 Bachelor of Science in Bioengineering, University of California San Diego

2023 Doctor of Philosophy in Bioengineering, University of California San Diego

PUBLICATIONS

Handzlik MK, **Gengatharan JM**, Frizzi KE, McGregor GH, Martino C, Rahman G, Gonzalez A, Moreno AM, Green CR, Guernsey LS, Lin T, Tseng P, Ideguchi Y, Fallon RJ, Chaix A, Panda S, Mali P, Wallace M, Knight R, Gantner ML, Calcutt NA, Metallo CM. Insulin-regulated serine and lipid metabolism drive peripheral neuropathy. *Nature*. (2023)

Cordes T, Kuna RS, McGregor GH, Khare SV, **Gengatharan J**, Muthusamy T, Metallo CM. 1-Deoxysphingolipid synthesis compromises anchorage-independent growth and plasma membrane endocytosis in cancer cells. *J Lipid Res*. (2022)

Martino C, Zaramela LS, Gao B, Embree M, Tarasova J, Parker SJ, Wang Y, Chu H, Chen P, Lee KC, Galzerani DD, **Gengatharan JM**, Lekbua A, Neal M, Knight R, Tsukamoto H, Metallo CM, Schnabl B, Zengler K. Acetate reprograms gut microbiota during alcohol consumption. *Nat Commun*. (2022)

Lim EW, Handzlik MK, Trefts E, **Gengatharan JM**, Pondevida CM, Shaw RJ, Metallo CM. Progressive alterations in amino acid and lipid metabolism correlate with peripheral neuropathy in *Polg*^{D257A} mice. *Sci Adv*. (2021)

Sawh MC, Wallace M, Shapiro E, Goyal NP, Newton KP, Yu EL, Bross C, Durelle J, Knott C, Gangoiti JA, Barshop BA, **Gengatharan JM**, Meurs N, Schlein A, Middleton MS, Sirlin CB, Metallo CM, Schwimmer JB. Dairy Fat Intake, Plasma Pentadecanoic Acid, and Plasma Iso-heptadecanoic Acid Are Inversely Associated With Liver Fat in Children. *J Pediatr Gastroenterol Nutr*. (2021)

Lee YM, Mu A, Wallace M, **Gengatharan JM**, Furst AJ, Bode L, Metallo CM, Ayres JS. Microbiota control of maternal behavior regulates early postnatal growth of offspring. *Sci Adv*. (2021).

Jung SM, Hung CM, Hildebrand SR, Sanchez-Gurmaches J, Martinez-Pastor B, **Gengatharan JM**, Wallace M, Mukhopadhyay D, Caleiman CM, Luciano AK, Hsiao WY, Tang Y, Li H, Daniels DL, Mostoslavsky R, Metallo CM, Guertin DA. Non-canonical mTORC2 Signaling Regulates Brown Adipocyte Lipid Catabolism through SIRT6-FOXO1. *Mol Cell* (2019).

Muthusamy T, Cordes T*, Handzlik MK*, You L*, Lim EW, **Gengatharan J**, Pinto AFM, Badur MG, Kolar MJ, Wallace M, Saghatelian A, Metallo CM. Serine deprivation drives 1-deoxysphingolipid synthesis to restrict tumor growth. *Nature* (2020).

Fernandez S, Viola JM, Torres A, Wallace M, Trefely S, Zhao S, Affronti HC, **Gengatharan JM**, Guertin DA, Snder NW, Metallo CM, Wellen KE. Adipocyte ACLY Facilitates Dietary Carbohydrate Handling to Maintain Metabolic Homeostasis in Females. *Cell Rep* (2019).

Wallace M, Green CR, Roberts LS, Lee YM, McCarville JL, Sanchez-Gurmaches J, Meurs N, **Gengatharan JM**, Hover JD, Phillips SA, Ciaraldi TP. Enzyme promiscuity drives branched-chain fatty acid synthesis in adipose tissues. *Nat Chem Biol* (2018).

ABSTRACT OF THE DISSERTATION

Metabolic and physiological functions of sphingolipid biosynthetic flux in cardiovascular disease

by

Jivani Manovathy Gengatharan

Doctor of Philosophy in Bioengineering

University of California San Diego, 2023

Professor Christian M. Metallo, Chair
Professor Pedro Cabrales, Co-Chair

Lipid metabolism plays a role in the pathogenesis of atherosclerotic cardiovascular disease (ASCVD) through aberrant lipid biosynthesis and trafficking via lipoproteins. The dysregulation of these pathways occurs across various tissues and understanding tissue-specific lipid biosynthetic flux can unravel the metabolic contribution to physiological responses.

Furthermore, understanding how these fluxes are regulated at the genetic level may uncover new mechanisms to be exploited as clinical targets. Sphingolipids constitute a pool of bioactive lipids that are critical in maintaining cell function and lipid homeostasis. Owing to their abundance in circulation and enrichment in lipoproteins, sphingolipids have been emerging as biomarkers of several diseases including ASCVD.

In this dissertation, we study the intersection of sphingolipid metabolism and dietary fat in the progression of ASCVD and other co-morbidities of metabolic syndrome. First, we applied mass spectrometry to quantify the metabolic flux of cis (CFAs) and trans monounsaturated fatty acids (TFAs) into sphingolipids by the initial, rate-limiting enzyme serine palmitoyltransferase (SPT). We identified novel sphingolipids synthesized from TFAs that exhibit high affinity for the sphingolipid pathway through their preferential incorporation into the long-chain base of sphingolipids and secretion from hepatocarcinoma cells.

Next, we designed custom high-fat diets (HFDs) with identical macronutrient composition enriched in either CFAs or TFAs to characterize the role of sphingolipid metabolism in the progression of hepatic steatosis and atherosclerosis induced by dietary fat. Administration of a HFD enriched in TFAs to low-density lipoprotein receptor deficient (*Ldlr-/-*) mice accelerated liver steatosis, hepatic very-low-density lipoprotein (VLDL) secretion, and atherogenesis compared to a HFD enriched in CFAs. Mechanistically, we demonstrate that *in vivo* SPT inhibition mitigated these phenomena while significantly diminishing atherogenic VLDL consisting of TFA-derived polyunsaturated sphingolipids. SPT inhibition additionally remodeled the lipidome by shifting hepatic fatty acids towards phospholipids, indicating that diverting fatty acids away from SPT and downstream sphingolipids may be beneficial on these HFDs.

Collectively, we elucidate a novel mechanism in which SPT flux synergizes with hepatic lipoprotein secretion to deliver atherogenic sphingolipids into circulation. Thus, we uncovered a critical metabolic link between sphingolipids and lipoprotein metabolism that can be therapeutically targeted in ASCVD in response to specific dietary fats.

Chapter 1 Elucidating the role of sphingolipid metabolism in atherosclerotic cardiovascular disease using mass spectrometry

1.1 Introduction

Metabolism is a set of chemical reactions that convert nutrients to energy to maintain cellular processes, synthesize macromolecules, and eliminate waste. Since this complex network of metabolic pathways is critical for maintaining homeostasis, perturbations to pathway flux can result in disease states. Within this large network, the subsection of lipid metabolism is essential for membrane formation, signaling, and energy storage and its disruption in various tissues has been implicated in several diseases.

The subject of this dissertation is the contribution of sphingolipid metabolism to ASCVD induced by dietary fat. My studies focus on promiscuity of the rate-limiting enzyme of sphingolipid biosynthesis, serine palmitoyltransferase (SPT), leading to aberrant fatty acid incorporation and its influence on the atherogenicity of dietary trans fat. Specifically, we have used stable isotope tracing via mass spectrometry and dietary interventions to quantitatively highlight altered sphingolipid biosynthetic flux as a critical node in the pathogenesis of liver steatosis and atherosclerosis induced by trans fat intake.

1.2 Dietary fat influences progression of atherosclerotic cardiovascular disease

Cardiovascular disease (CVD) is the leading cause of death globally, accounting for approximately 18 million deaths each year. Several factors contribute to cardiovascular disease including atherosclerosis, high blood cholesterol, hypertension, obesity, diabetes, smoking, physical inactivity, and genetic risk factors. Dietary fat intake has long been proposed to

influence lipid and lipoprotein metabolism and initiate the progression of CVD and other associated co-morbidities. Specifically saturated fat intake is known to raise low-density lipoprotein cholesterol (LDL-C) [1], a key marker of cardiovascular risk due to its tendency to aggregate in atherosclerotic lesions. While the total fat intake of the Western diet is similar to that of the Mediterranean diet, the difference in fat composition to include more monounsaturated fatty acids (MUFAs) and reduce saturated fatty acids (SFAs) in the Mediterranean diet is sufficient to reduce cardiovascular risk[2].

Atherosclerosis is initiated by endothelial dysfunction allowing retention and oxidation of atherogenic LDL or other lipoproteins in the intima. Endothelial cells are then activated to promote the adhesion of monocytes and leukocytes and facilitate the infiltration of smooth muscle cells into the intima. Monocytes then differentiate into macrophages and transform into foam cells as they take up oxidized LDL and lipids via scavenger receptors. Subsequent release of cytokines from foam cells enables the further development of atherosclerosis.

While clinical studies have measured effects on dietary fats on cardiovascular risk factors such as lipid and lipoprotein profiles, mechanistic studies have been more thoroughly explored in animal models. The most common models are mice with a deficiency in apolipoprotein E (Apoe)[3] or the low-density-lipoprotein receptor (Ldlr) [4], which both develop hypercholesterolemia. Mutations in these genes in humans are also associated with various types of hypercholesterolemia or hyperlipidemia with increased ASCVD risk. Mice carry the majority of their cholesterol in high-density lipoprotein (HDL) and do not typically develop atherosclerosis. Humans contrastingly carry the majority of their cholesterol in LDL, which enables the development of atherosclerosis. Therefore, developing non-HDL-derived hypercholesterolemia, similar to humans, is required to induce atherosclerosis. ApoE is a ligand

on chylomicrons, very low-density lipoproteins, and their remnants required for their uptake by hepatic LDL receptor and LDL receptor-related protein. Therefore, *Apoe-/-* mice exhibit accumulation of atherogenic lipoproteins in circulation and advanced atherosclerotic lesions even on a chow diet as early as 8 weeks[5]. LDLR is a membrane receptor required to endocytose circulating LDL. *Ldlr-/-* mice exhibit reduced clearance of LDL, thereby emulating a similar lipoprotein profile to humans. This atherogenic lipoprotein profile with elevated LDL-C can drive atherosclerosis in the presence of dietary cholesterol [6] or at least a high fat diet [7]. Therefore, both murine models of atherosclerosis have been utilized to study the influence of dietary fat on the progression of atherosclerosis.

1.3 Sphingolipids are a diverse class of bioactive lipids

Sphingolipids are bioactive lipids that play critical roles in maintaining cellular and physiological homeostasis. Within the cell, they are essential structural components of the plasma membrane in lipid rafts with cholesterol [8]–[13] and mediate several signaling cascades in processes such as cell death [14], [15], differentiation [16], and proliferation [17]. The synthesis of sphingolipids is initiated in the endoplasmic reticulum (ER) by the rate-limiting enzyme serine palmitoyltransferase (SPT), which canonically condenses the amino acid serine and the 16 carbon palmitoyl-CoA to synthesize sphinganine d18:0 (**Figure 1.1**). This long-chain base (LCB) SA d18:0 can be N-acylated by one of six ceramide synthases (CerS) responsible for adding fatty acids of specific chain lengths to form dihydroceramides (DHCer d18:0/N-acyl). The final step of *de novo* sphingolipid synthesis is mediated by delta 4-desaturase (DEGS) to add a double bond to form ceramides (Cer d18:1/N-acyl) (**Figure 1.1**). This central hub of ceramides is transported to the Golgi and can then be further modified with sugar groups to form hexosyl-

ceramides, lactosyl-ceramides, and complex glycosphingolipids (**Figure 1.1**). Ceramides can also be modified with a phosphocholine head group via sphingomyelin synthases (SMS1/2) to synthesize sphingomyelin (SM), the most abundant sphingolipid in the body (**Figure 1.1**). Sphingomyelin synthase pairs the synthesis of sphingomyelin with the conversion of phosphatidylcholine (PC) to diacylglycerol (DAG) by transferring the phosphocholine head group to ceramides to form SM. Ceramide can also be directly phosphorylated to form ceramide-1-phosphate via ceramide kinase (CERK).

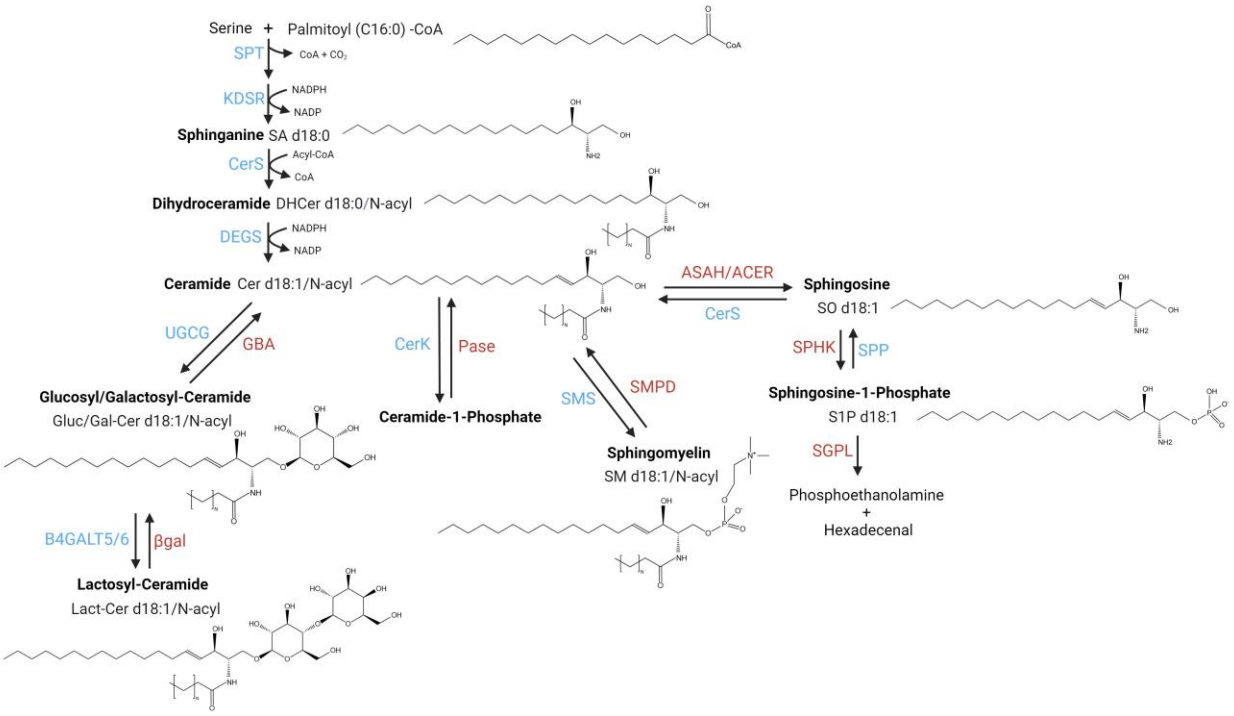

Figure 1.1 Sphingolipid biosynthetic pathway.

SPT: serine palmitoyltransferase; KDSR: 3-dihydrosphingosine reductase; CerS: ceramide synthase; UGCG: UDP-glucose ceramide glucosyltransferase; B4GALT5/6: beta-4,5/4,6-galactosyltransferase; βgal: beta-galactosidase; GBA: glucocerebrosidase; CerK: ceramide kinase; Pase: phosphatase; SMS: sphingomyelin synthase; SMPD: sphingomyelinase; ASAH/ACER: acid ceramidase; SPHK: sphingosine kinase; SPP: sphingosine-1-phosphate phosphatase; SGPL: sphingosine-1-phosphate lyase.

Sphingolipids can be degraded beginning with the conversion of complex sphingolipids back into ceramides. This process is catalyzed by acid, neutral, or alkaline ceramidases and can occur in several cellular compartments including the plasma membrane, ER, Golgi, or lysosome (**Figure 1.1**). Ceramides are then broken into their LCB backbone sphingosine (SO d18:1) and further phosphorylated by sphingosine kinase (SPHK1/2) (**Figure 1.1**). The phosphorylated product sphingosine-1-phosphate (S1P) is degraded by the enzyme S1P lyase (SGPL1) to release hexadecenal and phosphoethanolamine. The free LCB SO d18:1 can be re-acylated by Cers to fuel sphingolipid recycling (**Figure 1.1**). Defects in the sphingolipid degradation pathway will result in aberrant increase in sphingolipid intermediates that can give rise to lysosomal storage disorders[18]. S1P is a critical signaling molecule that plays a role in various diseases and processes including cancer[19]–[21], inflammation[22]–[24], atherosclerosis[25]–[27], angiogenesis[28]–[30], and cell growth[31], [32].

Sphingolipid biosynthesis is tightly regulated by the feedback inhibition of ORMDL proteins. The ORMDL family consists of ORMDL1, ORMDL2, and ORMDL3. These regulators normally inhibit SPT in the presence of excess ceramides. However, free cholesterol induces autophagy of ORMDL and thereby increases SPT flux[33]. ORMDL3 has been linked to childhood asthma[34], ulcerative colitis[35], type I diabetes[36], and Crohn's disease[37]. Dysregulation of sphingolipid biosynthesis is implicated in several diseases[38]–[40]. Increased SPT flux can lead to toxic accumulation of pathway intermediates, which may have effects on membrane fluidity, ER stress, and other cell functions.

1.4 Sphingolipids contribute to pathogenesis of atherosclerotic cardiovascular disease

Several studies over the years have characterized the role of sphingolipids in the progression of atherosclerotic cardiovascular disease. Analysis of human aortas from autopsies 60 years ago

revealed the presence of sphingomyelin in atherosclerotic lesions that, like cholesterol, increase with severity and account for up to 60-70% intimal phospholipids [41]. These sphingolipids can be derived from local endothelial cells or from deposition of lipoproteins enriched in sphingolipids. Specifically, LDL and VLDL, both of which contribute to atherosclerotic plaque formation, contain more sphingolipids than HDL[42]. Early studies discovered further processing of LDL sphingolipids by local sphingomyelinases increase the endothelial ceramide content, which induces lipoprotein aggregation and subendothelial retention mediating the initial stages of atherosclerosis[43], [44]. Ceramide content in LDL localized to atherosclerotic lesions was 10-50 fold higher compared with ceramide levels in circulating plasma LDL [43], thereby highlighting further enrichment within lesions beyond initial deposition of circulating lipoproteins.

Studies focused on the role of particular nodes of sphingolipid metabolism in pathogenesis of atherosclerosis have used either the *Apoe-/-* or *Ldlr-/-* mouse models. Acid sphingomyelinase deficiency on either the *Apoe-/-* or *Ldlr-/-* background both reduced aortic root lesions[45]. Deficiency of either sphingomyelin synthase (Sgms1/2) on *Apoe-/-* or *Ldlr-/-* background was also sufficient to reduce lesions in the aortic arch and root[46]. The sphingolipid degradation product S1P can be either pro- and anti-inflammatory depending on its localization and receptor cascade [47] and its role in atherogenesis has been studied. However, mixed results were achieved via genetic manipulations. S1PR3 deficiency on an *Apoe-/-* background had no effect on lesion size while increasing smooth muscle cell content of lesions and decreasing macrophage/monocyte recruitment. In contrast, S1PR2 deficiency on an *Apoe-/-* background reducing atherosclerotic lesion area while reducing circulating inflammatory cytokines [48]. This discrepancy is also reflected with S1P mimetic and S1PR agonist FTY-720 (fingolimod), in

which it reduced atherosclerotic lesion formation in *Ldlr-/-* mice on a high cholesterol (1.25%) diet [49], but had no effect with moderate levels of dietary cholesterol (0.25%) in *Ldlr-/-* mice [50]. Inhibition of *de novo* sphingolipid synthesis has also been explored to reduce atherosclerotic lesions. Dietary incorporation or intraperitoneal administration of the SPT inhibitor myriocin reduced atherosclerotic lesion areas in *Apoe-/-* mice fed chow long-term or atherogenic western diets containing cholesterol [51]–[53].

Numerous clinical studies have revealed strong correlations between sphingolipids and ASCVD prognosis. Sphingomyelin was the first sphingolipid identified as elevated in coronary artery disease (CAD) patients compared to healthy controls[54]. Further clinical studies revealed sphingomyelin was associated with myocardial infarction but not in patients with stable angina [55]. S1P typically localizes to HDL; however, non-HDL-S1P increased with severity of CAD symptoms and degree of stenosis in patients [27], [56]. Following this strong association of sphingolipids and ASCVD, the Mayo Clinic (USA) has established a clinical test to measure plasma ceramides in patients due to their strong ability to predict cardiovascular risk[57].

1.5 Stable isotope tracing via mass spectrometry can reveal changes in metabolism

Mass spectrometry is a robust analytic technique to identify and quantify several compounds in a given sample through their mass-to-charge ratio (m/z). Mass spectrometers are commonly coupled to gas or liquid chromatography (GC, LC) to additionally distinguish and identify compounds via their retention time. The mass spectrum at a given time consisting of a unique fragmentation pattern enables the identification of distinct compounds. Advancements in mass spectrometry have fueled the field of metabolomics and lipidomics to take advantage of

various chromatography tools and powerful mass spectrometers including high resolution to broaden the number and range of metabolites that can be measured in a single sample.

Metabolites such as fatty acids, amino acids, and cholesterol are identified commonly via GC-MS with one round of fragmentation. However, more complex lipids such as sphingolipids, triglycerides, and phospholipids require more advanced mass spectrometry, typically using two rounds of fragmentation via LC-MS/MS to further identify distinct components of these complex lipids. Multiple reaction monitoring (MRM) is a common quantitative method using the transition of the precursor and product ion via MS/MS to identify and quantify sphingolipids and other complex lipids. This is especially critical in sphingolipid quantitation as isobaric species such as Cer d18:1/22:0 and Cer d16:1/24:0 co-elute via LC and MRMs specific to the LCB enable accurate identification. For example, while both ceramides will have a precursor ion of m/z 622.6, the product ion is m/z 264.2 for Cer d18:1/22:0 and m/z 236.2 for Cer d16:1/24:0. This distinction in product ion will allow specific quantitation of each of the two species as well as numerous other isobaric metabolites. Using standardized MRMs for sphingolipids[58], we have expanded our assay to include MRMs for atypical sphingolipids.

While metabolite abundances can provide insight on major changes contributing to phenotypes, these stationary measurements do not comprehensively capture metabolism. Stable isotope tracing enables the quantitation of metabolic flux to capture synthesis of metabolic intermediates beyond their abundances. Changes in abundances may not reflect changes in biosynthetic flux as rate of synthesis can be altered while pools are maintained. Stable isotope tracers can be administered in cell culture medium *in vitro* or through drinking water, infusion, oral gavage, or intraperitoneal injection *in vivo*. Metabolic flux can be quantified by measuring the mass isotopologue distribution (MID) of a given metabolite. This distribution presents the

isotope labeling pattern as fractions. For example, when mice are provided the deuterated water (D_2O) as a stable isotope tracer via drinking water and *de novo* lipogenesis is measured, the presence of a M+1, M+2, M+3, or more isotopic enrichment on palmitate is noted in the MID representing incorporation of deuterium into palmitate. This labeling pattern can be corrected for natural isotope abundance and modeled to quantify the rate of synthesis of palmitate or other metabolites.

Calculating metabolic flux of complex lipids requires other techniques given the incorporation of various fatty acids. Using MRMs via LC-MS/MS, the incorporation of fatty acids into complex lipids and their biosynthetic flux can be measured. For example, cells treated with the tracer palmitate (C16:0)-d4, which replaced 4 hydrogens atoms for deuterium atoms, can be scanned for +4 mass shifts in the MRMs of complex lipids via LC-MS/MS to determine their incorporation of the tracer. If palmitate-d4 were only incorporated into the LCB of Cer d18:1/22:0 to produce Cer d18:1-d4/22:0, then the MRM would include a precursor ion of m/z 626.6 and product ion of m/z 268.2, both of masses 4 Daltons greater than the MRM for Cer d18:1/22:0. If palmitate-d4 were only incorporated into the N-acyl of Cer d18:1/22:0 in its elongated form to produce Cer d18:1/22:0-d4, then the MRM would include the same precursor ion of m/z 626.6 but a product ion of m/z 264.2 due to maintaining an unlabeled d18:1 LCB. Therefore, MRMs can be precisely crafted to uncover the specific incorporation of stable isotope fatty acid tracers into sphingolipids and other complex lipids via LC-MS/MS.

1.6 Acknowledgments

Chapter 1 is an introductory chapter to this dissertation. Jivani M. Gengatharan is the primary author. Christian M. Metallo is the corresponding author.

Chapter 2 Unraveling the selective flux of CFAs versus TFAs through sphingolipid metabolism

2.1 Abstract

Lipid metabolism is essential for membrane formation, signaling, and energy storage and its disruption in various tissues has been implicated in the progression of several diseases. Industrially-produced trans unsaturated fatty acids (TFAs) are associated with atherosclerotic cardiovascular disease (ASCVD) in humans due to elevated total cholestererol, increased LDL-C, and decreased HDL-C. Sphingolipids are diverse class of bioactive lipids due to substrate promiscuity of the rate-limiting enzyme of sphingolipid biosynthesis, serine palmitoyltransferase (SPT). Through liquid chromatography-mass spectrometry, we identified novel sphingolipids preferentially incorporating the TFA elaidate into the long-chain base (LCB) of sphingolipids in contrast to CFA isomer oleate *in vitro*. CFAs are instead predominantly incorporated into phospholipids or the N-acyl chain of sphingolipids. This high affinity of TFAs to sphingolipid biosynthesis is reflected in increased sphingomyelin extracellular flux from Huh7 hepatocarcinoma cells, predominantly polyunsaturated sphingomyelin derived from TFAs as determined via stable isotope tracing. These findings suggest SPT selectivity for atypical TFAs may play a role in modulating flux through sphingolipid biosynthesis and lipid remodeling, which in turn may contribute to the progression of atherosclerosis induced by trans fat intake.

2.2 Introduction

Sphingolipids are a class of bioactive lipids comprised of a long-chain base (LCB) backbone that can be modified with an acyl chain or various head groups to construct more complex species. They are essential structural components of the plasma membrane in lipid rafts[8]–[11]

and ceramide-rich domains[12], [13] and are key molecules in signal transduction pathways mediating apoptosis[14], [15], proliferation[17], differentiation[16], and other processes[59].

The initial rate-limiting enzyme of sphingolipid biosynthesis, serine palmitoyltransferase (SPT), canonically condenses the amino acid serine and palmitoyl-CoA to synthesize the long-chain base (LCB) of sphingolipids. SPT is known to be promiscuous for the amino acid substrate as it can use alanine or glycine as the amino acid substrate instead of its canonical substrate serine. Specifically, promiscuity with the amino acid substrate is linked to disease states as alanine incorporation forms the non-canonical products deoxysphingolipids[60], which are implicated in implicated in hereditary sensory and autonomic neuropathy type 1 (HSAN 1)[61], [62], diabetes mellitus[63], cancer[64], [65], and macular telangiectasia type 2[66]. Although SPT's canonical acyl-CoA substrate is palmitoyl-CoA, it can also use various acyl-CoAs from 10-26 carbons to make a diverse set of LCBs[67], [68]. The SPT enzyme complex comprises two primary subunits and several accessory proteins that influence substrate choice and enzyme activity[69]–[73]. *SPTLC1* encodes an obligate component of the enzyme with either *SPTLC2* or *SPTLC3* required for catalytic activity. While *SPTLC1* and *SPTLC2* are ubiquitously expressed, *SPTLC3* is more selectively expressed across tissues including placenta, skin, some glands, kidney, and liver [68], [74], [75]. *SPTLC3* variants have been associated with elevated LDL-C[76], myocardial infarction[77], and dyslipidemia[78]. Additionally, SPTLC3 has been shown to enhance LCB diversity by facilitating incorporation of short-chain acyl-CoAs[70] and the monomethyl branched-chain fatty acid (mmBCFA) anteiso-C17:0[73]. While saturated acyl-CoAs are commonly used by SPT, unsaturated acyl-CoAs have been shown to differentially modulate SPT activity[67]. However, the mechanism of utilization of unsaturated acyl-CoAs by SPT has not been thoroughly explored.

Several types of unsaturated fatty acids are found in the body with varying degrees of desaturation and can be synthesized *de novo* or derived from the diet. Unsaturated fatty acids are proposed to be beneficial as they do not induce the same toxicity as saturated fatty acids including endoplasmic reticulum (ER) stress[79] and a reduction in membrane fluidity[80]. Monounsaturated fatty acids (MUFAs) such as oleic acid C18:1 (9Z) have been promoted as part of the healthy Mediterranean diet for their ability to reduce atherogenic low density lipoprotein-cholesterol (LDL-C) and other risk factors for metabolic syndrome and atherosclerotic cardiovascular disease (ASCVD) [81], [82]. MUFAs such as oleic acid can be derived from the diet in fat sources such as olive oil, avocado, nuts, and canola oil. Additionally, they can be synthesized via *de novo* lipogenesis followed by desaturases such as stearoyl-coA desaturase (SCD1). These desaturases provide an additional mechanism to reduce saturated fat toxicity by diverting saturated fatty acids towards unsaturated fatty acids [83]. Natural unsaturated fatty acids derived from diet or synthesized *de novo* contain one or more cis double bond, leading to a kinked structure that affords more fluidity in membranes [80] .

In recent decades, trans unsaturated fatty acids (TFAs) have been incorporated into the food supply through partial hydrogenation of vegetable oils to enhance flavor and improve shelf life. TFAs contain one or more double bond in the trans configuration, leading to a straight-chain structure similar to saturated fatty acids unlike the kinked structure of cis unsaturated fatty acids (CFAs). Typically, the most abundant TFA in these processed fat sources is elaidic acid C18:1 (9E), the isomer of oleic acid C18:1 (9Z). Several clinical studies over the years revealed TFAs induce an unfavorable blood lipid profile including increased total cholesterol and LDL-C as well as decreased high-density lipoprotein-cholesterol (HDL-C)[84].

Given SPT's preference for saturated acyl-CoA substrates, we hypothesized that trans unsaturated acyl-CoAs could be incorporated into the LCB of sphingolipids through SPT promiscuity and this atypical incorporation could contribute to the toxicity and atherogenicity of trans fats. We combined stable isotope tracing and mass spectrometry to reveal insights into trans fat-induced sphingolipid biosynthetic flux.

2.3 Results

TFAs are preferentially metabolized by SPT over CFAs

The SPT complex catalyzes synthesis of LCBs and many studies [70], [73] have highlighted its promiscuity with respect to amino acid and acyl-CoA substrate usage **(Figure 2.1A)**. Consistent with these findings, Huh7 hepatocarcinoma cells treated with diverse saturated fatty acid species bound to albumin for 48 hours contained LCBs for each of the fatty acids tested including the canonical substrate C16:0 palmitate, C18:0 stearate, odd-chain fatty acid C17:0, and monomethyl branched chain fatty acids (mmBCFAs) iso-C16:0, anteiso-C17:0, or iso-C17:0 **(Figure 2.1B)**. While saturated acyl-CoAs have been primarily explored as alternate substrates for SPT, monounsaturated fatty acids (MUFAs) are highly abundant in the diet and tissues, and microsomal enzyme activity assays have previously indicated that both cis-C18:1(9Z) oleate and trans-C18:1(9E) elaidate are metabolized by SPT to LCBs [67]. To examine the extent of MUFA incorporation into LCBs and beyond, we cultured Huh7 cells with 100 μM of fatty acid bound to albumin for 48 hours and measured SPT activity through quantification of hydrolyzed sphingolipids to detect chromatographically-resolved, isobaric LCBs derived from oleate or elaidate **(Figures 2.1C-D)**. Elaidate was incorporated into its respective sphinganine d20:1 (SA d20:1) and sphingosine d20:2 (SO d20:2) LCBs at levels 8-fold and 15-fold more than oleate, respectively **(Figure 2.1E)**. In contrast to oleate-derived LCBs, the elaidate-derived LCB SA

d20:1(E) was produced at similar levels to other non-canonical LCBs, including those generated in cells treated with odd- and branched-chain fatty acids **(Figure S1.1A)**. To examine the fates of oleate and elaidate through the lipidome more directly, we treated Huh7 cells with the ^{2}H-labeled tracers oleate-d9 and elaidate-d17 and used multiple-reaction monitoring (MRM) to quantify SA d20:1 and SO d20:2 with mass shifts of 9 or 17, respectively **(Table S3.1)**. Elaidate-d17 was incorporated into its respective SA LCB 5-fold and SO LCB 13-fold more than oleate-d9 **(Figure 2.1F)**. When Huh7 cells were treated with an equimolar mix of both tracers in direct competition for SPT, we observed elaidate-d17 incorporation to be 17-fold higher for SA and 60-fold higher for SO as compared to oleate-d9 **(Figure S1.1B)**.

Figure 2.1 TFAs are preferentially metabolized by SPT over CFAs.

(**A**) Schematic depicting promiscuity of the initial rate-limiting enzyme of sphingolipid biosynthesis SPT in both amino acid and acyl-CoA substrates. Created with Biorender.com. (**B**) Hydrolyzed LCBs synthesized from supplemented fatty acid treatments in Huh7 cells (n=3 per group). (**C**) Hypothesized LCBs from oleate or elaidate incorporation by SPT. Oleate or elaidate would first form a SA 20:1 (9Z) or SA d20:1 (9E) LCB, respectively, after SPT and KDSR reactions and these LCBs would be maintained through CerS. They would next form a SO d20:2 (4E,11Z) or SO d20:2 (4E,11E) LCB, respectively, after CerS and DEGS reactions. The LCBs derived from oleate or elaidate will be noted by their unique double bond configuration as SA d20:1(Z) and SO d20:2(Z) from oleate and SA d20:1(E) and SO d20:2(E) from elaidate. Created with Biorender.com. (**D**) After hydrolyzing sphingolipids from either oleate or elaidate treatment to their LCBs, unique peaks were identified via LC-MS in only cells treated with elaidate, corresponding to both the expected SA d20:1 (E) and SO d20:2 (E) LCBs. Another peak with the same MRM eluting prior to this novel peak was present at low levels in vehicle-treated cells and was increased upon oleate treatment. Through peak area increases corresponding to treatments of the different fatty acids, the first peak was identified as derived from oleate while the second peak was identified as derived from elaidate. (**E**) Hydrolyzed SA and SO LCBs synthesized from 100 μM oleate or 100 μM elaidate, respectively, in Huh7 cells (n=3 per group). (**F**) Hydrolyzed SA and SO LCBs synthesized from oleate-d9 or elaidate-d17, respectively, in Huh7 cells (n=3 per group). Data are mean ± standard error of mean (SEM) and were analyzed using an independent t-test (E-F). *$p < 0.05$, **$p < 0.01$, or *** $p< 0.001$ unless otherwise noted.

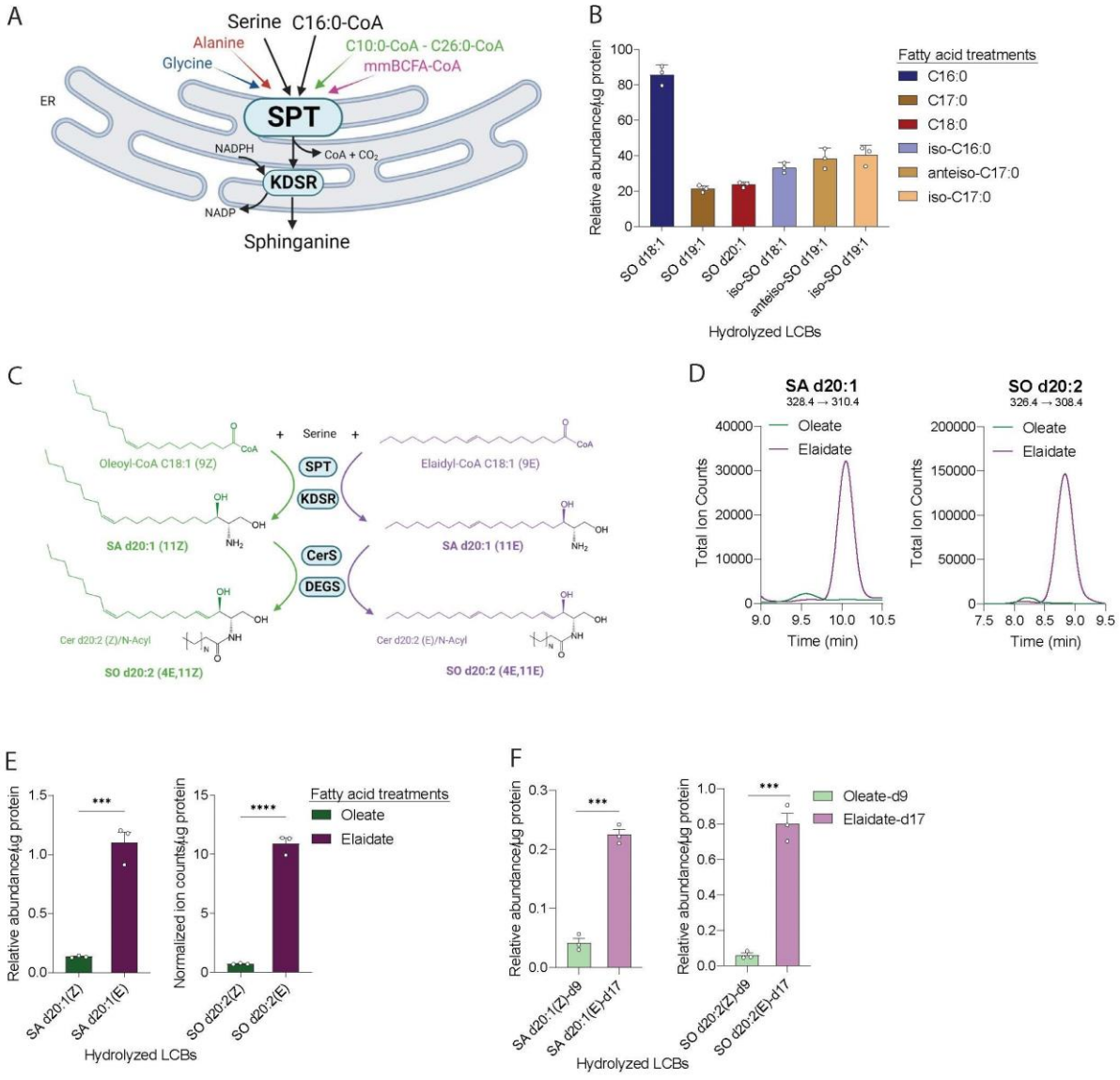
A
Serine
C16:0-CoA
Alanine
Glycine
C10:0-CoA - C26:0-CoA
mmBCFA-CoA
ER
SPT
NADPH
CoA + CO2
KDSR
NADP
Sphinganine
B
Relative abundance/µg protein
Fatty acid treatments
C16:0
C17:0
C18:0
iso-C16:0
anteiso-C17:0
iso-C17:0
SO d18:1
SO d19:1
SO d20:1
iso-SO d18:1
anteiso-SO d19:1
iso-SO d19:1
Hydrolyzed LCBs
C
Serine
Oleoyl-CoA C18:1 (9Z)
Elaidyl-CoA C18:1 (9E)
SPT
KDSR
SA d20:1 (11Z)
SA d20:1 (11E)
CerS
DEGS
Cer d20:2 (Z)/N-Acyl
Cer d20:2 (E)/N-Acyl
SO d20:2 (4E,11Z)
SO d20:2 (4E,11E)
D
SA d20:1
328.4 → 310.4
SO d20:2
326.4 → 308.4
Oleate
Elaidate
Total Ion Counts
Time (min)
E
Relative abundance/µg protein
Normalized ion counts/µg protein
Fatty acid treatments
Oleate
Elaidate
SA d20:1(Z)
SA d20:1(E)
SO d20:2(Z)
SO d20:2(E)
Hydrolyzed LCBs
F
Relative abundance/µg protein
Oleate-d9
Elaidate-d17
SA d20:1(Z)-d9
SA d20:1(E)-d17
SO d20:2(Z)-d9
SO d20:2(E)-d17
Hydrolyzed LCBs

Molecular partitioning of CFAs and TFAs through sphingolipid metabolism

Next, we assessed MUFA incorporation into intact, cellular sphingolipids using specific MRMs **(Table S3.1)**. Consistent with its high abundance in obesogenic lard diets, oleate-d9 was highly incorporated into the N-acyl chain of canonical ceramides only after elongation to C24:1-d9 or further, not as its original form C18:1-d9 **(Figure 2.2A)**. On the other hand, elaidate was incorporated in a more versatile manner reminiscent of saturated acyl-CoAs **(Figure 2.2A)**. We additionally used specific MRMs to quantify incorporation into the LCB of ceramides and glycosphingolipids (GSLs) **(Figure 2.2B)**. While ceramides with an oleate-d9-derived LCB were below the detection limit, we found distinct ceramide (Cer), glucosyl/galactosyl-ceramide (Gluc/Gal-Cer), and lactosyl-ceramide (Lact-Cer) species with elaidate-d17 incorporated into the LCB, suggesting that TFA-containing sphingolipids are processed throughout the pathway **(Figure 2.2C)**. This ceramide N-acyl profile was similar to that obtained with palmitate or stearate treatments, indicating that ceramide synthases metabolize TFA-derived LCBs similarly to canonical LCBs **(Figures S1.2A-B)**. Only total incorporation of tracers into sphingomyelin (SM) pools is observable with available MRMs **(Table S3.1)**. Here, oleate-d9 was incorporated predominantly into SM 42:2-d9, presumably via the abundant, canonical Cer d18:1/24:1-d9. We detected no SM peaks with a mass shift of 18, indicating oleate-d9 is not incorporated into both the LCB and N-acyl at detectable levels **(Figure 2.2D)**. In contrast, elaidate-d17 was incorporated into more diverse SM species, including several species with a mass shift of 34 suggestive of elaidate incorporation into both the LCB and N-acyl. Overall, CFAs and TFAs appear to be molecularly partitioned in the sphingolipid biosynthetic pathway, as TFAs are structurally similar to canonical, saturated, SPT substrates and therefore preferentially incorporated in the LCB, while

CFAs feed the ceramide pool through N-acylation **(Figure 2.2E)**. Therefore, double bond configuration can affect flux through sphingolipid biosynthesis at different stages.

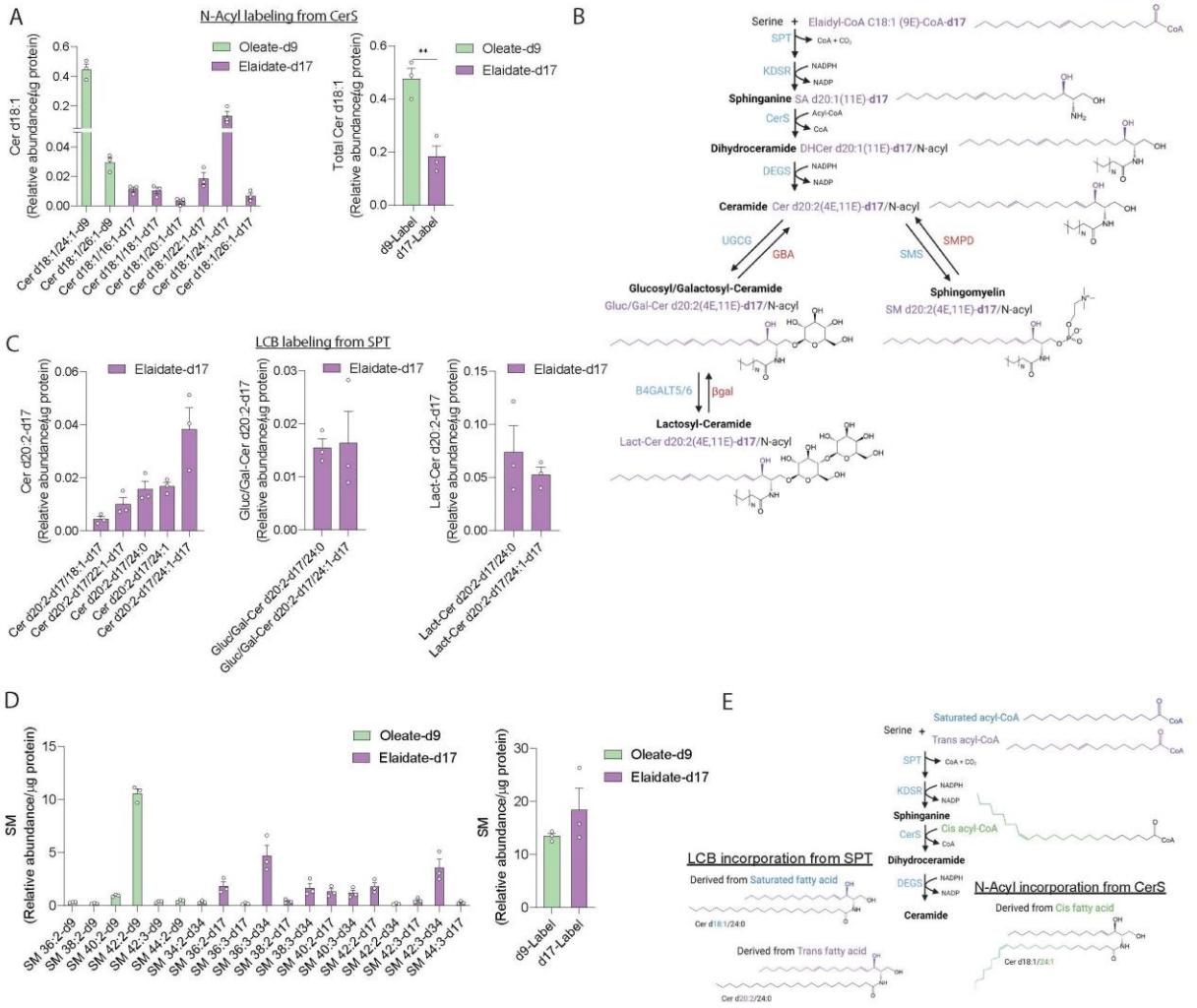

Figure 2.2 Molecular partitioning of CFAs and TFAs through sphingolipid metabolism.

(**A**) N-Acyl 2H labeling on canonical ceramides d18:1 from oleate-d9 or elaidate-d17 in Huh7 cells (n=3 per group). (**B**) Schematic of elaidate-d17 incorporation into the LCB of sphingolipids. (**C**) LCB 2H labeling from elaidate-d17 producing a d20:2-d17 LCB in ceramides, glucosyl/galactosyl-ceramides, and lactosyl-ceramides in Huh7 cells (n=3 per group). (**D**) 2H labeling on sphingomyelin from oleate-d9 or elaidate-d17 in Huh7 cells (n=3 per group). (**E**) Schematic of molecular partitioning of cis and trans fatty acids in the sphingolipid biosynthetic pathway. Created with Biorender.com. Data are mean ± standard error of mean (SEM) were analyzed using an independent t-test (A, D).*p < 0.05, **p < 0.01, or *** p< 0.001 unless otherwise noted.

TFAs drive aberrant sphingomyelin secretion

We next assessed how these CFA and TFA treatments influence the broader lipidome, quantifying the flux of oleate-d9 and elaidate-d17 into phospholipids and neutral lipids in Huh7 cells. Oleate was preferentially utilized in phospholipids phosphatidylcholine (PC) and phosphatidylethanolamine (PE) while elaidate was preferentially found in lysophospholipids **(Figures 2.3A, S1.3A-F)**. This preferential utilization of oleate for phospholipids suggests that the kinked structure provided by the cis double bond may be crucial for membrane fluidity and that alterations in double bond configuration could lead to different downstream fates of lipid flux, consistent with previous findings highlighting differential lipidomic profiles and incorporation of CFAs and TFAs [85], [86].

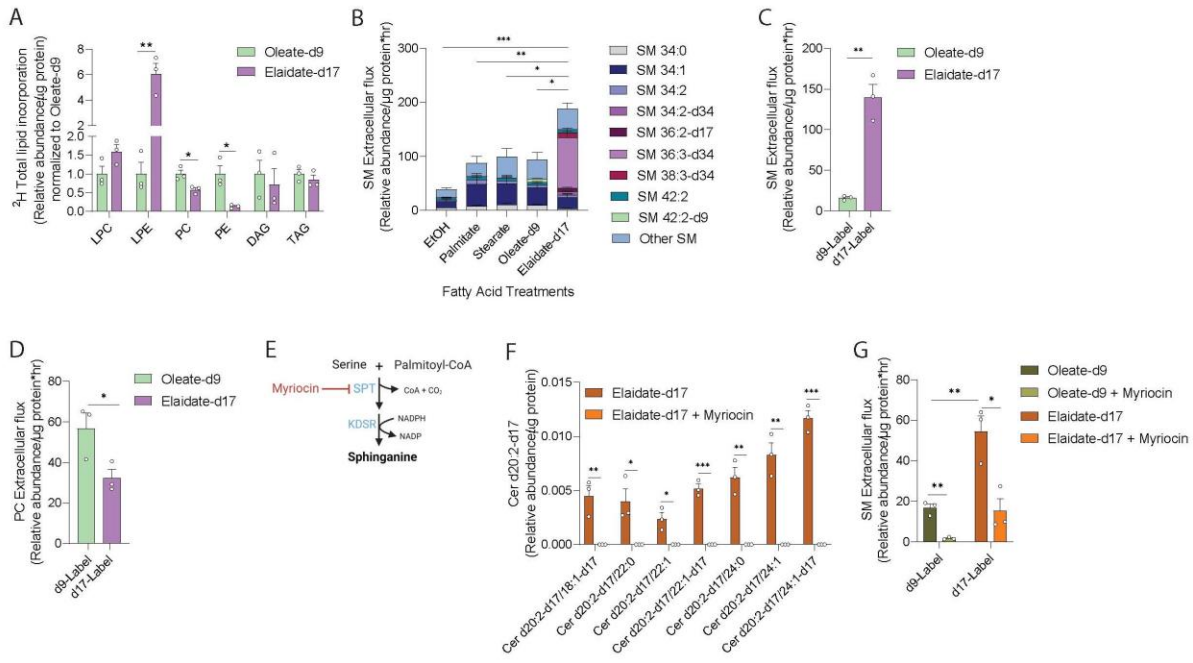

Figure 2.3 TFAs drive aberrant sphingomyelin secretion.

(**A**) Total abundances of lipids with 2H labeling from oleate-d9 or elaidate-d17 normalized to abundances following oleate-d9 supplementation in Huh7 cells (n=3 per group). (**B**) Stacked plot of sphingomyelin (SM) extracellular flux from Huh7 cells following fatty acid supplementation including oleate-d9 or elaidate-d17 (n=3 per group). (**C**) Total sphingomyelin (SM) extracellular flux from Huh7 cells with 2H labeling from oleate-d9 or elaidate-d17 (n=3 per group). (**D**) Total phosphatidylcholine (PC) extracellular flux from Huh7 cells with 2H labeling from oleate-d9 or elaidate-d17 (n=3 per group). (**E**) Schematic depicting mechanism of action of SPT inhibitor Myriocin. (**F**) LCB 2H labeling from elaidate-d17 producing a d20:2-d17 LCB in ceramides (Cer) in Huh7 cells treated with elaidate-d17 or elaidate-d17 and Myriocin (n=3 per group). (**G**) Total sphingomyelin (SM) extracellular flux from Huh7 cells with 2H labeling from oleate-d9 or elaidate-d17 in the presence or absence of myriocin (n=3 per group). Data are mean ± standard error of mean (SEM) were analyzed using an independent t-test (A, C-D, F), one-way ANOVA (B), or two-way ANOVA with Fisher's LSD post hoc test (G). Statistical analysis in (B) was performed using total abundance.*$p < 0.05$, **$p < 0.01$, or *** $p< 0.001$ unless otherwise noted.

SM is the most abundant sphingolipid present in blood predominantly in lipoproteins, and its presence in plasma correlates positively with ASCVD [87]. Therefore, we quantified secretion of SM from Huh7 cells into culture media under various fatty acid treatments, including oleate-d9 and elaidate-d17. Elaidate induced the highest total SM efflux from Huh7 cells compared to its cis isomer oleate or saturated palmitate and stearate **(Figure 2.3B)**. This increase in SM efflux was

significantly driven by SM with double incorporation of elaidate (36:3-d34) **(Figure 2.3B)**, such that nearly 10-fold more elaidate-incorporated SM was secreted compared to oleate-incorporated SM **(Figure 2.3C)**. This trend was specific to sphingolipids, as oleate-incorporated PCs were secreted more than elaidate-incorporated PCs **(Figure 2.3D)**, presumably due to the higher abundance of intracellular, oleate-derived PCs **(Figure S1.3C)**. This preferential secretion of elaidate-derived SM further highlights the distinct metabolism of TFAs in the sphingolipid biosynthetic pathway.

To determine if synthesis of these elaidate-derived sphingolipids can be modulated, we treated cells with myriocin, a pharmacological inhibitor of SPT **(Figure 2.3E)**. Myriocin reduced production of the LCBs SA d20:1 (Z)-d9 and SO d20:2 (Z)-d9 from oleate-d9 and SA d20:1 (E)-d17 and SO d20:2 (E)-d17 from elaidate-d17 following hydrolysis of sphingolipids **(Figure S1.3G)**. In cells treated with elaidate-d17, myriocin also reduced the intracellular abundance of several Cer d20:2-d17, Gluc/Gal-Cer d20:2-d17, Lact-Cer d20:2-d17, SM-d17, and SM-d34 species under elaidate-d17 treatment **(Figures 2.3F, S1.3H-J)**. Additionally, myriocin suppressed the efflux of TFA-derived SM-d17 and SM-d34 species, suggesting that SPT activity and fatty acid structure directly impact lipid secretion **(Figure 2.3G)**.

2.4 Discussion

In this study, we have applied stable isotope tracing and mass spectrometry *in vitro* to identify novel TFA-derived LCBs of sphingolipids. These TFA-derived LCBs are preferentially synthesized compared to CFA-derived LCBs, presumably due to structural similarity of a trans acyl-CoA to the canonical saturated palmitoyl-CoA substrate. The increased affinity of TFAs to SPT is supported by previous findings measuring SPT activity with a variety of acyl-CoA

substrates in rat brain microsomes[67]. These TFA-derived sphingomyelin are additionally secreted from Huh7 cells, thereby driving increased total sphingomyelin efflux. While there were was a trending increase in intracellular TFA-derived sphingomyelin compared to CFA-derived sphingomyelin, the critical distinction in their incorporation was reflected in the media, further highlighting the importance of considering sphingolipid secretion as part of sphingolipid biosynthetic flux, especially from hepatocytes as they are major contributors to circulating sphingolipids.

We additionally measured differential incorporation of elaidate and oleate into the broader lipidome, with oleate being preferentially utilized as an acyl chain for phospholipids PC and PE. Oleate is known to induce more fluidity in cell membranes compared to elaidate [88], which corresponds to our results demonstrating increased flux of oleate into phospholipids. This reduced ability for elaidate to be incorporated into phospholipids *in vitro* could influence the shift of TFAs towards sphingolipids and the preferential secretion of TFA-derived sphingolipids. Instead of altering membrane fluidity through phospholipid incorporation, the cell may prefer to direct TFAs towards sphingolipid metabolism for its degradation potential and secretion via very-low-density lipoproteins (VLDL) from hepatocytes.

Identifying novel substrates for SPT has been an ongoing area of research. While promiscuity with the amino acid substrate to synthesize 1-deoxysphingolipids has been implicated in HSAN1[61], [62], diabetes mellitus[40], and macular telangiectasia type 2[66], the consequence of SPT promiscuity with the acyl-CoA substrate is not clear. SPTLC3 facilitates the incorporation of a diverse set of acyl-CoAs[70], [73], [89]. SPTLC3 incorporates the mmBCFA anteiso-C17:0[73], which is derived from branched chain amino acids known to be elevated in type 2 diabetes[90]. Therefore, the presence of mmBCFAs-derived LCBs driven by increased

BCAA catabolism may be a biomarker in type 2 diabetes, though this has not been demonstrated. The largest diversity of LCBs with chain length C16-C26 was found in the skin [89], which also contains high expression of *SPTLC3*[73], [91]. This diversity may be required in a specialized tissue such as skin, which uses ceramides to maintain barrier function. Consistently, SPTLC3 expression is increased during differentiation of keratinocytes[89]. Therefore, determining the functional role of these TFA-derived LCBs in sphingolipids and the purpose of SPT promiscuity to incorporate these atypical fatty acids will be critical in understanding why SPT has evolved to incorporate a diverse set of acyl-CoAs.

2.5 Material and methods

Cell culture experiments

Huh7 cells were cultured in Dulbecco's modified Eagle's medium (DMEM) with 10% fetal bovine serum (FBS) and 1% penicillin/streptomycin (P/S). Media was supplemented with 100 μM fatty acid treatments conjugated with bovine serum albumin (BSA) for 48 hours. For ^{2}H flux measurements of intact sphingolipids and broader lipidome, cells were treated with elaidic acid-d17 (Cayman Chemical, 27715) or oleic acid-d9 (Avanti Polar Lipids, 861809) in DMEM supplemented with 10% delipidated FBS and 1% P/S. To test direct competition of both fatty acids, Huh7 cells were treated with an equimolar mix of elaidic acid-d17 and oleic acid-d9 at concentrations of 50 μM each. For hydrolysis assays measuring the LCB derived from oleic acid-d9 and elaidic acid-d17, standard FBS was utilized. To inhibit SPT flux in specific experiments, myriocin was used at a concentration of 100 nM in DMSO. To calculate extracellular flux, 1.5 mL of fresh or spent media was evaporated under vacuum at 4°C and resuspended into 0.1 mL of H_2O.

Concentrated media was extracted as described below. All cells were maintained at 37°C and 5% CO_2 and periodically tested for mycoplasma.

Long-chain base hydrolysis

Cells were spiked with internal standards sphinganine-d7 (Avanti Polar Lipids, Cat# 860658) and sphingosine-d7 (Avanti Polar Lipids, Cat# 860657) and tissues were homogenized or cells were scraped with 0.5 mL methanol. Homogenate aliquot of 50 µL was taken to determine protein content using the BCA protein assay (Thermo Scientific). Samples were placed on a mixer for 1 hr at 37°C and centrifuged at 2800g. Supernatant was transferred to a new Eppendorf tube and hydrolyzed for 16 hr at 65°C. 100 µL 10M KOH, 625 µL chloroform, 100 µL 2N NH_4OH, and 500 µL alkaline water were added to samples followed by vortexing for 5 min and centrifugation for 5 min at 16,000g. The lower organic phase was washed 3 times with alkaline water and dried under air. Quantification of hydrolyzed long chain bases was performed on an Agilent 6460 QQQ LC-MS/MS. Metabolite separation was achieved with a C18 column (Hypersil GOLD aQ C18 100 x 2.1 mm, 1.9 µm particle size, Thermo Scientific). Mobile phase A was composed of a 60:40 ratio of methanol:water containing 0.1% formic acid and 5 mM ammonium formate. Mobile phase B consisted of 100% methanol containing 0.1% formic acid and 5 mM ammonium formate. The gradient elution program consisted of holding at 40% B for 0.5 min, linearly increasing to 100% B over 15 min, and maintaining it for 9 min, followed by re-equilibration to the initial condition for 10 min. The capillary voltage was set to 3.5 kV, the drying gas temperature was 350 °C, the drying gas flow rate was 10 L/min, and the nebulizer pressure was 60 psi. Long chain bases were analyzed by multiple reaction monitoring (MRM) of the transition from precursor to product ions at associated optimized collision energies and fragmentor

voltages (Table S3.1). Long chain bases were then quantified from spiked internal standards corresponding to respective long chain base class.

Targeted sphingolipid quantification

Cells or media were spiked with internal standards sphinganine-d7 (Avanti Polar Lipids, Cat# 860658), deoxysphinganine-d3 (Avanti Polar Lipids, Cat# 860474), d18:0-d7/13:0 dihydroceramide (Avanti Polar Lipids, Cat# 330726), d18:1-d7/15:0 ceramide (Avanti Polar Lipids, Cat# 860681), d18:1-d7/15:0 glucosylceramide (Avanti Polar Lipids, Cat# 330729), d18:1-d7/15:0 lactosylceramide (Avanti Polar Lipids, Cat# 330727), sphingosine-d7 (Avanti Polar Lipids, Cat# 860657), and d18:1/18:1-d9 sphingomyelin (Avanti Polar Lipids, Cat# 791649) or 18:1 sphingomyelin (d18:1/18:1)-d9 (Avanti Polar Lipids, Cat#860740). Tissue was homogenized and cells were scraped with 0.5 mL methanol and 0.5 mL H_2O. Homogenate aliquot of 100 µL was taken to determine protein content using the BCA protein assay (Thermo Scientific). The remaining homogenate was transferred to a new Eppendorf tube and 1 mL chloroform was added. For media, 0.5 mL methanol, 0.5 mL H_2O, and 1 mL chloroform were added directly. Samples were vortexed for 5 min and centrifuged for 5 min at 4 ˚C at 15,000*g*. The organic phase was collected and 2 µL of formic acid was added to the remaining polar phase which was re-extracted with 1 mL of chloroform. Combined organic phases were dried under nitrogen.

Quantification of sphingolipids was performed on an Agilent 6460 QQQ LC-MS/MS. Sphingolipid species were separated on a C8 column (Spectra 3 µm C8SR 150 × 3 mm inner diameter, Peeke Scientific). 5 µL of sample was injected. Mobile phase A was composed of 100% HPLC-grade water containing 2 mM ammonium formate and 0.2% formic acid, and mobile phase B consisted of 100% methanol containing 0.2% formic acid and 1 mM ammonium formate. The

gradient elution program consisted of the following profile: 0 min, 82% B; 3 min, 82% B; 4 min, 90% B, 18 min, 99% B; 25 min, 99% B; 27 min; 82% B; 30 min, 82% B. Column re-equilibration followed each sample and lasted 10 min. The capillary voltage was set to 3.5 kV, the drying gas temperature was 350 °C, the drying gas flow rate was 10 L/min, and the nebulizer pressure was 60 psi. Sphingolipid species were analyzed by multiple reaction monitoring (MRM) of the transition from precursor to product ions at associated optimized collision energies and fragmentor voltages (Table S3.1). Sphingolipids were then quantified from spiked internal standards corresponding to respective sphingolipid class.

Targeted lipid quantification

Cells or media were spiked with internal standards 15:0-18:1(d7) phosphatidylcholine (Avanti Polar Lipids, Cat #791637), 15:0-18:1(d7) phosphatidylethanolamine (Avanti Polar Lipids, Cat #791638), 18:1(d7) lysophosphatidylcholine (Avanti Polar Lipids, Cat#791643), 18:1(d7) lysophosphatidylethanolamine (Avanti Polar Lipids, Cat #791644), 15:0-18:1(d7) diacylglycerol (Avanti Polar Lipids, Cat #791647), 15:0-18:1(d7)-15:0 triacylglycerol (Avanti Polar Lipids, Cat #791648). Cells were scraped with 0.5 mL methanol and 0.5 mL H_2O. Homogenate aliquot of 100 µL was taken to determine protein content using the BCA protein assay (Thermo Scientific). The remaining homogenate was transferred to a new Eppendorf tube and 1 mL chloroform was added. For media, 0.5 mL methanol, 0.5 mL H_2O, and 1 mL chloroform were added directly. Samples were vortexed for 5 min and centrifuged for 5 min at 4 ˚C at 15,000*g*. The organic phase was collected and 2 µL of formic acid was added to the remaining polar phase which was re-extracted with 1 mL of chloroform. Combined organic phases were dried under nitrogen.

Targeted lipids were quantified on an Agilent 6460 QQQ LC-MS/MS equipped with an Accucore C30, 150 × 2.1 mm, 2.6 µm particle (Thermo) column at 40°C. 5 µL of sample was injected. Mobile phase A was composed of a 60:40 ratio of acetonitrile:water containing 10 mM ammonium formate and 0.1% formic acid and mobile phase B consisted of a 90:10 ratio of isopropanol:acetonitrile with 10 mM ammonium formate and 0.1% formic acid. Both mobile phases utilized a flow rate of 0.2 mL/min. The liquid chromatography gradient ran from 30%- 43% B from 3-8 min, 43%-50% B from 8-9 min, 50-90% B from 9-18 min, 90-99% B from 18-26 min, then held at 99% B from 26-30 min before returning to 30% B in 6 min and held for a further 4 min. Column re-equilibration followed each sample and lasted 10 min. The capillary voltage was set to 3.5 kV, the drying gas temperature was 350 °C, the drying gas flow rate was 10 L/min, and the nebulizer pressure was 60 psi. Lipids were analyzed by multiple reaction monitoring (MRM) of the transition from precursor to product ions at associated optimized collision energies and fragmentor voltages (Table S3.1). Lipids were then quantified from spiked internal standards corresponding to respective lipid class.

Stastical analysis

Data are presented as mean ± standard error of mean (SEM) of at least three biological replicates as indicated in figure legends. Statistical analysis was performed with GraphPad Prism 9.3.1 using two-tailed independent *t*-test to compare two groups, one-way ANOVA with Fisher's least significant difference (LSD) post hoc test to compare more than two groups, and two-way ANOVA with Fisher's LSD post hoc test to compare two-factor study designs. For all tests, $p<0.05$ was considered significant with *$p < 0.05$, **$p < 0.01$, or *** $p< 0.001$ unless otherwise noted.

2.6 Acknowledgements

We thank all members of the Metallo Lab for helpful discussions. Chapter 2 has been submitted for publication and is under review. Jivani M. Gengatharan is the primary author of this manuscript. Michal K. Handzlik, Zoya Y. Chih, Maureen L. Ruchhoeft, Patrick Secrest, Ethan L. Ashley, Courtney R. Green, Martina Wallace, and Philip L.S.M. Gordts are co-authors of the paper. Christian M. Metallo is the corresponding author of this manuscript.

Chapter 3 Altered sphingolipid biosynthetic flux and lipoprotein trafficking contribute to trans fat-induced atherosclerosis

3.1 Abstract

Dietary fat drives the pathogenesis of atherosclerotic cardiovascular disease (ASCVD), in particular circulating cholesterol and triglyceride-rich lipoprotein remnants. Industrially produced trans-unsaturated fatty acids (TFAs) incorporated into food supplies significantly promoted ASCVD. However, the molecular trafficking of TFAs responsible for this association is not well understood. Here, we comprehensively trace how cis-monounsaturated fatty acids (CFAs) and TFAs are metabolized across the lipidome in cultured cells and low-density lipoprotein receptor (LDLr) knockout mice, a murine model of atherosclerosis. We previously demonstrated that TFAs are preferentially incorporated into sphingolipids by serine palmitoyltransferase (SPT) and secreted from cells *in vitro*. Administering high-fat diets (HFD) enriched in TFAs to *Ldlr-/-* mice accelerated liver steatosis, hepatic very-low-density lipoprotein (VLDL) secretion, and atherogenesis compared to a CFA-enriched HFD. SPT inhibition mitigated these phenotypes and reduced circulating atherogenic VLDL enriched in TFA-derived polyunsaturated sphingomyelin. Transcriptional analysis of the liver revealed distinct regulation of *SPTLC2* versus *SPTLC3* subunit expression consistent with human genetic correlations in ASCVD, further establishing sphingolipid metabolism as a critical node mediating the progression of ASCVD in response to specific dietary fats.

3.2 Introduction

Sphingolipids are a diverse class of bioactive lipids that consist of a long-chain base (LCB) with further modifications that can include an acyl chain or various head groups to construct more complex species. They play diverse roles in membrane biology [8]–[13]and signaling [14]–[17], [59] and are implicated in numerous diseases including ASCVD [41], [92], non-alcoholic fatty liver disease[93], [94], obesity and associated insulin resistance disorders [95]–[97], diabetes [98]–[101], peripheral neuropathy[102], [103] , and neurodegeneration [104]. Owing to their abundance and contribution to the blood lipid profile as components of VLDL, low-density lipoproteins (LDL), and high-density lipoproteins (HDL) [42], ceramides and other sphingolipid species are emerging as biomarkers for various diseases including ASCVD. Consequently, the Mayo Clinic (USA) has implemented a clinical test to measure plasma ceramides as a gauge of cardiovascular risk [57].

Dietary fat is absorbed and distributed throughout the body by the intestine and liver via chylomicrons and very-low-density lipoproteins (VLDL), respectively. In many cases, fatty acids are distinctly metabolized by cellular enzymes to influence their fate. Therefore, deciphering the molecular mechanisms of fatty acid trafficking through the lipidome and lipoproteins will improve our understanding of various diseases, including ASCVD where atherogenic lipoproteins are retained in the endothelium and initiate atherosclerosis. Trans fatty acids (TFAs) are unsaturated fatty acids with at least one double bond in the trans conformation, which leads to a straight-chain structure similar to saturated fatty acids (SFAs) unlike the kinked structure of cis unsaturated fatty acids (CFAs). A large percentage of TFAs are industrially produced through partial hydrogenation of vegetable oils, of which the most abundant TFA is elaidate C18:1 (9E), the isomer of oleate C18:1 (9Z). Trans fats were once widespread in the food supply and drove a marked increase in ASCVD in the population, supported by large clinical studies that linked TFAs to increased

cardiovascular risk and an unfavorable plasma lipid profile including increased total cholesterol and LDL-cholesterol (LDL-C) as well as decreased HDL-cholesterol (HDL-C) [84]. While dietary fatty acid composition influences the progression of various diseases, the contribution of fatty acid flux through downstream lipid pathways to their pathogenesis warrants further investigation.

Here, we comprehensively tracked the fate and diversity of fatty acids through the sphingolipid biosynthesis pathway to highlight how TFA incorporation by SPT promotes lipoprotein secretion and ASCVD. We designed HFDs with identical macronutrient compositions differing distinctly in their mono-unsaturated fatty acid species and used *Ldlr-/-* mice [4] to assess their impact on ASCVD and associated pathologies. We found CFA diets induced poor glucose handling and greater adiposity, while diets including TFAs exacerbated hepatic steatosis and drove atherosclerotic plaque formation. Inhibiting SPT activity via dietary administration of myriocin, a SPT inhibitor, profoundly reduced TFA-induced atherosclerosis while revealing specific regulation of *SPTLC2* and *SPTLC3* subunit expression. Collectively, these findings highlight the distinct trafficking of fatty acids through the lipidome and further establish sphingolipid biosynthesis as a target for ASCVD.

3.3 Results

Inhibition of sphingolipid biosynthesis mitigates trans fat-induced hepatic steatosis

Given the strong correlations of circulating ceramides, SM, and cholesterol with ASCVD[87], we hypothesized that inhibition of sphingolipid biosynthesis could modulate lipoprotein metabolism and reduce aortic plaque deposition induced by TFAs [105], [7], [106]. To test this *in vivo*, we utilized LDL receptor-deficient (*Ldlr-/-*) mice[4] to model the impact on hyperlipidemia and atherosclerosis. *Ldlr-/-* mice develop accelerated atherosclerosis due to

reduced clearance of circulating atherogenic LDL-C[4]. We designed custom, high-fat diets (HFDs) with identical macronutrient composition (60% kcal fat) enriched in either 62% cis monounsaturated C18:1 fatty acids (Cis HFD) or a mixture of 28% trans monounsaturated C18:1 fatty acids and 34% cis monounsaturated C18:1 fatty acids (Trans HFD) **(Figure 3.1A, Table S3.2)**. Each diet was also supplemented with Myriocin, and we administered all four diets to *Ldlr-/-* mice for 16 weeks to examine metabolic and physiological changes associated with hyperlipidemia, liver steatosis, and atherosclerosis. Cholesterol supplementation was not included in the diets to interrogate the dichotomy of CFA versus TFA ingestion without confounding dietary cholesterol intake[107]. Mice fed Cis HFD gained the most weight, followed by mice fed Trans HFD, while myriocin attenuated body weight gain under both dietary fat compositions **(Figure 3.1B)**. Food intake was reduced by 12% under Trans HFD + Myriocin but was not significantly different between the other diets **(Figure S2.1A)**. Body weight differences largely reflected changes in adiposity **(Figures 3.1C, S2.1B)**.

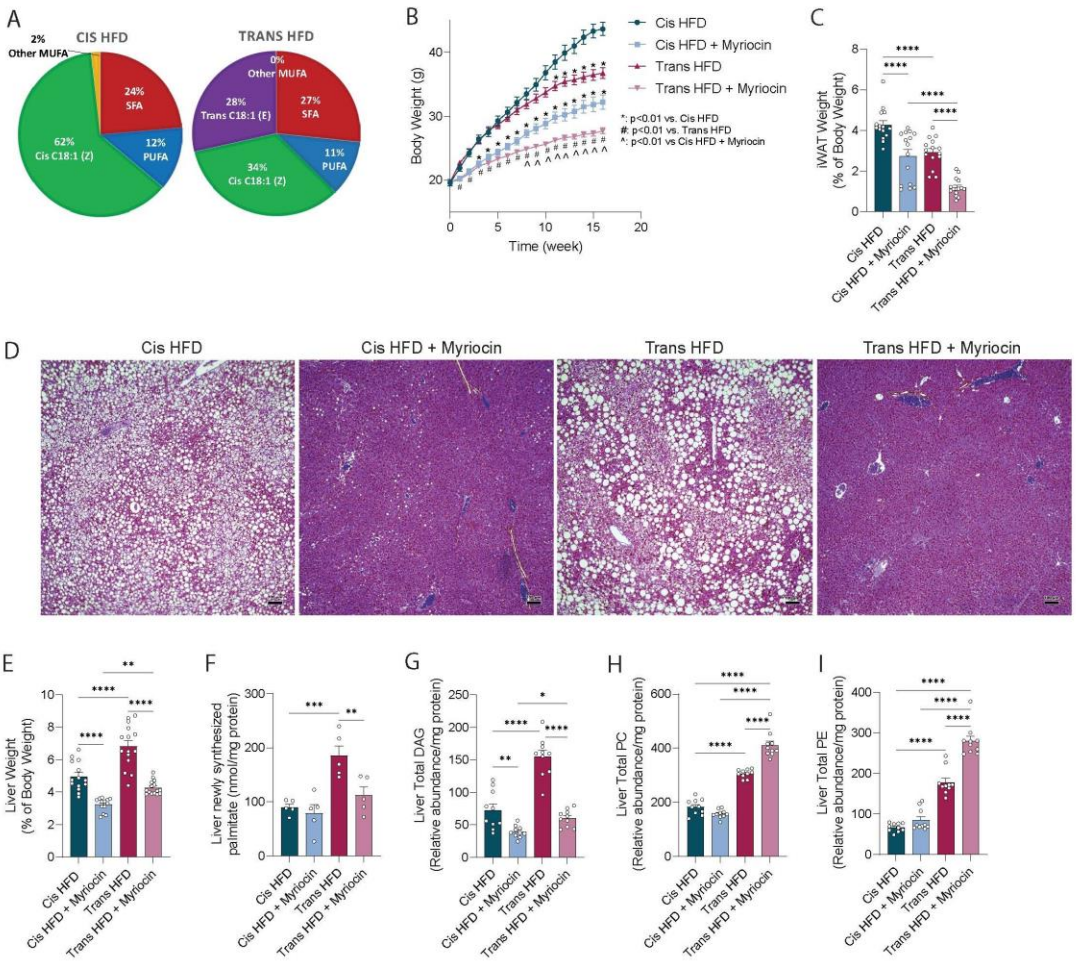

Figure 3.1 Inhibition of sphingolipid biosynthesis mitigates trans fat-induced liver steatosis.

(**A**) Fatty acid composition of Cis Unsaturated HFD derived from a combination of 34% lard and 66% olive oil and Trans Unsaturated HFD derived from 100% Primex. (**B**) Body weight over course of 16 weeks in mice fed Cis HFD, Cis HFD + Myriocin, Trans HFD, or Trans HFD + Myriocin (n=17 per group). (**C**) Inguinal adipose tissue (iWAT) weight in mice fed Cis HFD, Cis HFD + Myriocin, Trans HFD, or Trans HFD + Myriocin (n=15 per group). (**D**) Representative images of hematoxylin and eosin (H&E) staining of the liver at 10x magnification highlighting hepatic steatosis in mice fed Cis HFD, Cis HFD + Myriocin, Trans HFD, Trans HFD + Myriocin (n=10 per group). (**E**) Liver weight in mice fed Cis HFD, Cis HFD + Myriocin, Trans HFD, or Trans HFD + Myriocin (n=15 per group). (**F**) Hepatic *de novo* lipogenesis of palmitate in mice fed Cis HFD, Cis HFD + Myriocin, Trans HFD, or Trans HFD + Myriocin (n=5 per group). (**G**) Hepatic diacylglycerol (DAG) abundance in mice fed Cis HFD, Cis HFD + Myriocin, Trans HFD, or Trans HFD + Myriocin (n=10 per group). (**H**) Hepatic phosphatidylcholine (PC) abundance in mice fed Cis HFD, Cis HFD + Myriocin, Trans HFD, or Trans HFD + Myriocin (n=10 per group). (**I**) Hepatic phosphatidylethanolamine (PE) abundance in mice fed Cis HFD, Cis HFD + Myriocin, Trans HFD, or Trans HFD + Myriocin (n=10 per group). Data are mean ± standard error of mean (SEM) were analyzed using a two-way ANOVA with Fisher's LSD post hoc test (B-C,E-I). *p < 0.05, **p < 0.01, or *** p< 0.001 unless otherwise noted.

Cis HFD-fed mice exhibited elevated fasting blood glucose at 16 weeks **(Figure S2.1C)** and glucose tolerance was correspondingly compromised under the Cis HFD compared to all other diets **(Figure S2.1D)**. However, Trans HFD-fed mice exhibited more advanced liver steatosis than Cis HFD-fed mice **(Figure 3.1D)**, consistent with prior comparisons of TFAs, SFAs, and CFAs[108]–[110]. Liver weight was elevated on the Trans HFD compared to the Cis HFD, while myriocin reduced liver weight and steatosis in both diets **(Figure 3.1E)**. Expression of *Col1a1*, a marker of fibrosis, was increased on the Trans HFD and reduced by myriocin, indicating a mitigation of preliminary fibrosis **(Figure S2.1E)**. Stable isotope tracing via $^{2}H_2O$ to evaluate *de novo* lipogenesis (DNL) revealed elevated palmitate synthesis on the Trans HFD compared to the Cis HFD, which was attenuated by myriocin, consistent with previous observations of myriocin influencing SREBP1 mRNA and protein[111] **(Figure 3.1F)**.

To understand how these diets influenced molecular abundances across the lipidome, we quantified tissue lipids using high-resolution mass spectrometry. Within the liver, diacylglycerol (DAG) and total fatty acids were elevated under the Trans HFD compared to the Cis HFD, while these species along with neutral lipids triacylglycerol (TAG) and cholesteryl ester (ChE) were reduced by myriocin **(Figures 3.1G, S2.1F-H)**. In contrast, hepatic PC and PE, as well as lysophosphatidylcholine (LPC) and lysophosphatidylethanolamine (LPE) were all elevated on the Trans HFD versus Cis HFD but further increased by myriocin **(Figure 3.1H-I, Figure S3.1I-J)**. These results suggest myriocin reshapes lipid metabolism by diverting fatty acids away from sphingolipid pools and towards phospholipids rather than reducing lipid uptake overall.

Despite these changes in phospholipids and neutral lipids, hepatic sphingolipid content was not significantly altered between Cis and Trans HFD apart from deoxydihydroceramides (doxDHCer) **(Figure S2.1K)**. Since 1-deoxysphingolipids cannot be phosphorylated and further

degraded[112], this finding suggests that hepatic sphingolipid biosynthetic flux is increased under the Trans HFD. Myriocin effectively reduced total hepatic dihydroceramide (DHCer), ceramide (Cer), deoxysphinganine (doxSA), and doxDHCer while having no significant impact on more complex sphingolipids, suggesting that salvage pathways can compensate to maintain sphingolipid pools **(Figure S2.1K)**. Therefore, rather than accumulate in the liver, we hypothesized these complex sphingolipids are secreted in lipoproteins at higher rates in Trans HFD- versus Cis HFD-fed mice.

Trans fat-induced hepatic sphingolipid drive VLDL secretion and atherosclerosis

Dietary TFAs accelerate atherosclerosis compared to SFA, CFA or polyunsaturated fatty acid (PUFA)-enriched diets in *Ldlr-/-* mice[105], [106], [7] and in the human population[84]. The primary lipids in human atherosclerotic lesions are cholesterol, glycerophospholipids, and sphingolipids, with SM accounting for approximately 60-70% of intimal phospholipids in advanced human lesions[41], [113]. ApoB lipoproteins such as VLDL and LDL, which contain more sphingolipids than HDL[38], accumulate in atherosclerotic lesions and pose an ASCVD risk[114], [115]. Consistent with our hypothesis, the plasma lipoprotein profile was altered in Trans HFD-fed mice, with increased VLDL-cholesterol (VLDL-C) and VLDL-triacylglycerol (VLDL-TAG) compared to mice fed a Cis HFD, and myriocin attenuated the Trans HFD-induced response **(Figures 3.2A, S2.2A)**. We next measured hepatic VLDL secretion under these dietary treatments as we hypothesized SPT activity supports the synthesis, packaging, and secretion of VLDLs by the liver into blood **(Figure 3.2B)**. Trans HFD accelerated hepatic VLDL secretion compared to the Cis HFD, which was significantly mitigated by myriocin **(Figures 3.2C, S2.2B)**.

Figure 3.2 Trans fat-induced hepatic sphingolipids drive VLDL secretion and atherosclerosis.

(**A**) Lipoprotein analysis of plasma cholesterol from mice fed Cis HFD, Cis HFD + Myriocin, Trans HFD, Trans HFD + Myriocin (3 pooled plasma per group from n=3 each). CR: chylomicron remnant, VLDL: very-low-density lipoprotein, IDL: intermediate-density lipoprotein, LDL: low-density lipoprotein, HDL: high-density lipoprotein. (**B**) Schematic depicting mechanism of action of Tyloxapol, a lipoprotein lipase inhibitor, used to measure hepatic very-low-density lipoprotein (VLDL) secretion. Created with Biorender.com. (**C**) Hepatic VLDL secretion after injection of Tyloxapol relative to t=0 in mice fed Cis HFD, Cis HFD + Myriocin, Trans HFD, Trans HFD + Myriocin (n=4-5 per group). (**D**) Representative images of modified Van Gieson staining of the aortic root highlighting atherosclerotic lesions in mice fed Cis HFD, Cis HFD + Myriocin, Trans HFD, Trans HFD + Myriocin (n=10 per group). (**E**) Atherosclerotic lesion quantitation in the aortic root including area under curve (AUC) of mice fed Cis HFD, Cis HFD + Myriocin, Trans HFD, Trans HFD + Myriocin (n=9-10 per group). (**F**) Newly synthesized cholesterol in plasma of mice fed Cis HFD, Cis HFD + Myriocin, Trans HFD, Trans HFD + Myriocin (n=5 per group). (**G**) Abundance of plasma polyunsaturated sphingomyelin (SM) containing >3 double bonds in mice fed Cis HFD, Cis HFD + Myriocin, Trans HFD, Trans HFD + Myriocin (n=10 per group). (**H**) Lipoprotein analysis of plasma polyunsaturated sphingomyelin containing >3 double bonds from mice fed Cis HFD, Cis HFD + Myriocin, Trans HFD, Trans HFD + Myriocin (3 pooled plasma per group from n=3 each). CR: chylomicron remnant, VLDL: very-low-density lipoprotein, IDL: intermediate-density lipoprotein, LDL: low-density lipoprotein, HDL: high-density lipoprotein. (**I**) Hepatic mRNA expression of genes involved in sphingolipid metabolism in mice fed Cis HFD, Cis HFD + Myriocin, Trans HFD, Trans HFD + Myriocin (n=7-10 per group). (**J**) *SPTLC2* versus *SPTLC3* correlation to genes involved in hepatic VLDL secretion, including MTTP and APOB in human liver. Data are mean ± standard error of mean (SEM) were analyzed using a two-way ANOVA with Fisher's LSD post hoc test (C, E-G, I). *$p < 0.05$, **$p < 0.01$, or *** $p< 0.001$ unless otherwise noted.

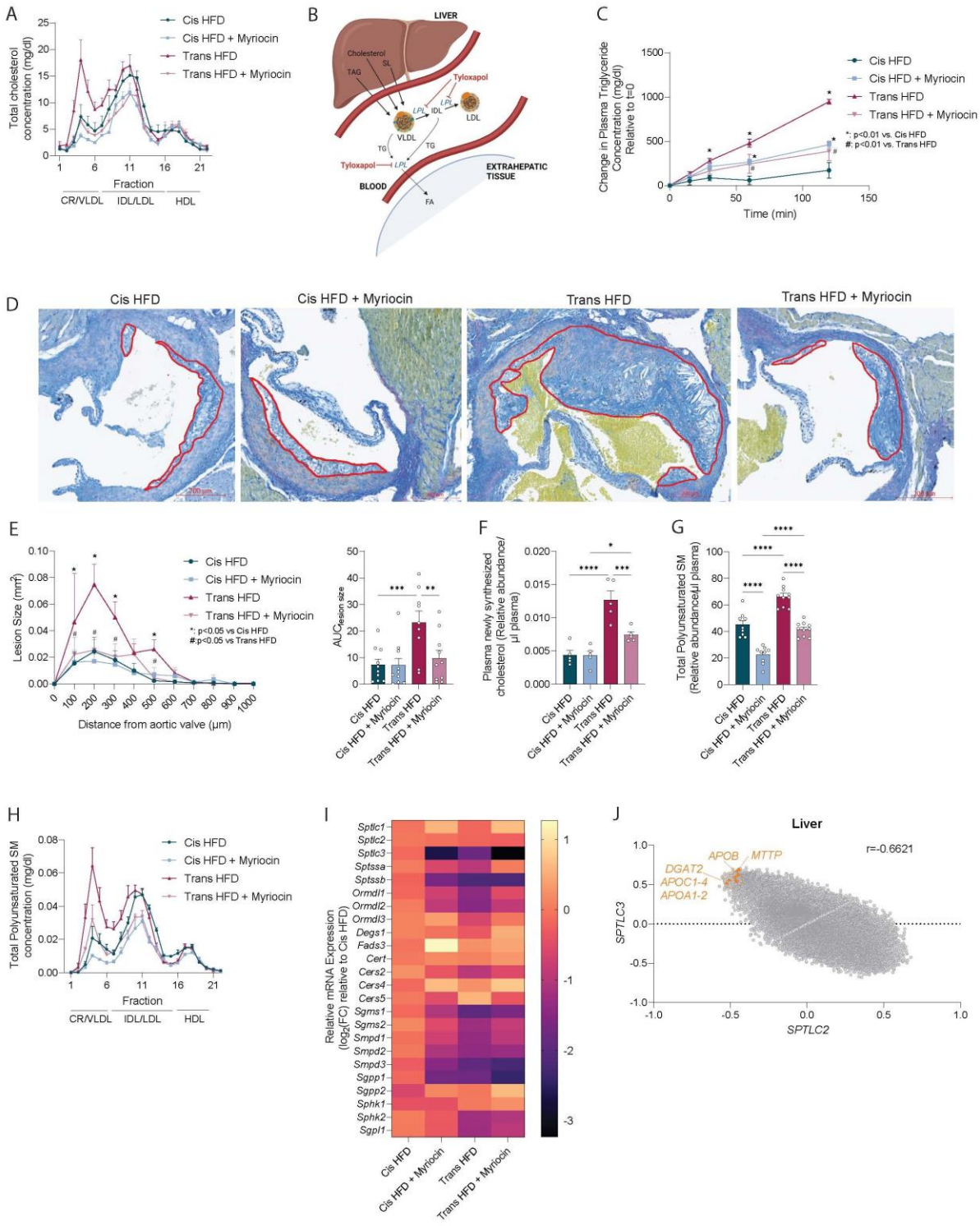
A
Total cholesterol concentration (mg/dl)
Fraction
CR/VLDL
IDL/LDL
HDL
Cis HFD
Cis HFD + Myriocin
Trans HFD
Trans HFD + Myriocin
B
LIVER
Cholesterol
SL
TAG
Tyloxapol
LPL
IDL
LDL
VLDL
TG
EXTRAHEPATIC TISSUE
BLOOD
FA
C
Change in Plasma Triglyceride Concentration (mg/dl) Relative to t=0
Time (min)
*: p<0.01 vs. Cis HFD
#: p<0.01 vs. Trans HFD
D
Cis HFD
Cis HFD + Myriocin
Trans HFD
Trans HFD + Myriocin
E
Lesion Size (mm²)
Distance from aortic valve (µm)
*: p<0.05 vs Cis HFD
#:p<0.05 vs Trans HFD
AUC lesion size
F
Plasma newly synthesized cholesterol (Relative abundance/ µl plasma)
G
Total Polyunsaturated SM (Relative abundance/µl plasma)
H
Total Polyunsaturated SM concentration (mg/dl)
I
Relative mRNA Expression (log2(FC) relative to Cis HFD)
Sptlc1
Sptlc2
Sptlc3
Sptssa
Sptssb
Ormdl1
Ormdl2
Ormdl3
Degs1
Fads3
Cert
Cers2
Cers4
Cers5
Sgms1
Sgms2
Smpd1
Smpd2
Smpd3
Sgpp1
Sgpp2
Sphk1
Sphk2
Sgpl1
J
Liver
r=-0.6621
APOB
MTTP
DGAT2
APOC1-4
APOA1-2
SPTLC3
SPTLC2

We next aimed to understand how SPT activity and TFAs influence the progression of ASCVD by measuring atherosclerotic lesions in the valves of the aortic root. The Trans HFD significantly increased atherosclerotic lesion area within the aortic root, characterized by intima thickening and cholesterol crystals compared to the fatty streaks found with the Cis HFD. Myriocin attenuated atherosclerotic lesion area under the Trans HFD **(Figures 3.2D-E)**, consistent with previous findings in *Apoe-/-* mice fed long-term chow or a Western diet[51]–[53]. $^{2}H_2O$ tracing revealed increased newly synthesized cholesterol and palmitate in plasma from mice fed a Trans HFD, indicating the increased lipid biosynthetic flux entering the pool of circulating lipids **(Figures 3.2F, S2.2C)**. Myriocin attenuated this elevation in newly synthesized plasma cholesterol and palmitate **(Figures 3.2F, S2.2C)**. Targeted plasma lipidomics additionally highlighted that myriocin effectively reduced several lipid classes elevated on the Trans HFD, most notably the sphingolipids DHCer, doxDHCer, SM, and phospholipids PC and PE **(Figure S2.2D)**. The Trans HFD also increased plasma levels of polyunsaturated SM species with 3 or more double bonds that presumably include both cis- sphingadienes derived from FADS3[116], [117] and TFA-containing LCBs as observed with stable isotope tracing *in vitro*, while myriocin reduced these species **(Figures 3.2G, S2.2E, 2.3B)**. Plasma dihydrosphingomyelin (DHSM) and monounsaturated SM were unchanged between the Cis and Trans HFD **(Figures S2.2F-G)**. Diunsaturated SM, which can include a variety of canonical LCB and N-acyl combinations in addition to TFA-derived LCBs, were slightly, but significantly, increased under the Trans HFD and attenuated by Myriocin **(Figures S2.2H)**. However, total VLDL-SM was elevated under the Trans HFD including enrichment in polyunsaturated SM that was suppressed by myriocin **(Figures 3.2H, S2.2I)**. Collectively, these results suggest that TFA-driven SPT flux drives hepatic lipoprotein secretion and atherosclerosis in *Ldlr-/-* mice.

Finally, to gain insights into the molecular regulation of sphingolipid homeostasis, we quantified the expression of various sphingolipid pathway enzymes in the livers of mice fed each diet. While several biosynthetic and catabolic enzymes were downregulated under the Trans HFD compared to Cis HFD, the most dramatic change we observed across all diets was downregulation of the *Sptlc3* expression upon long term dietary myriocin treatment **(Figure 3.2I)**. In contrast, prolonged reduction of SPT activity by dietary myriocin slightly increased *Sptlc1* expression and had no effect on *Sptlc2* expression, suggesting distinct regulation and function of these subunits **(Figure 3.2I)**.

SPTLC3 variants are associated with elevated LDL-C[76], myocardial infarction[77], and dyslipidemia[78]. Furthermore, this subunit is primarily expressed in cells that mediate lipid processing and/or serve as epithelial barriers including liver, intestine, and skin[43]. Given the above regulation by myriocin **(Figure 3.2I)**, we hypothesized that SPTLC3 has specialized function and regulation associated with vesicular processing of lipids, which is critical for lipoprotein secretion. To this end, we used Correlation AnalyzeR[118] to identify genes co-regulated with *SPTLC3* and *SPTLC2* in publicly available human transcriptional datasets. We identified that *SPTLC3* has a strong positive correlation with numerous VLDL secretion genes, including *MTTP* and *APOB* as well as other *APO* genes in human liver. In contrast, *SPTLC2* has a strong negative correlation with *MTTP*, *APOB*, and other APO genes, establishing these genes among the top differentially correlated genes between *SPTLC2* and *SPTLC3* **(Figure 3.2J, Table S3.5)**. These differential correlations indicate opposing functions of SPTLC2 and SPTLC3 in regulating hepatic lipid secretion that correspond to the demonstrated promiscuity of SPTLC3[70], [73]. Consistent with human disease correlations, SPTLC3 acts to bridge hepatic sphingolipid biosynthetic flux to lipid secretion via lipoproteins, which ultimately leads to atherosclerosis.

3.4 Discussion

Here, using a combination of *in vitro* metabolic tracing, dietary manipulations, pharmacological interventions, and physiological analyses, we have highlighted a functional role for SPT in hepatic steatosis, lipoprotein metabolism, and ASCVD progression. We specifically characterized distinct TFA-derived sphingolipids that are selectively secreted from cells, promote VLDL secretion from liver, and accelerate deposition of atherosclerotic plaques in *Ldlr-/-* mice. By quantifying how these species are trafficked through the lipidome in cells and animals, we have elucidated key molecular mechanisms through which SPT activity contributes to the progression of ASCVD.

While cholesterol metabolism has been identified as a major driver of trans fat-induced ASCVD, there are many underlying mechanisms controlling the early pathogenesis that have not been thoroughly explored. Ceramides in circulation are similarly linked to ASCVD pathogenesis[119], and our results highlight specific benefits in reducing their production and dissemination as sphingomyelin in lipoproteins. Arterial wall SMase is thought to hydrolyze sphingomyelin to ceramides, and this increase in ceramides stimulates lipoprotein aggregation and subendothelial retention in artery walls[43], [45], thereby mediating the initial stages of atherosclerosis. We demonstrate that pharmacological inhibition of sphingolipid biosynthesis *in vivo* reduces *de novo* lipogenesis to diminish TFA-induced liver steatosis and VLDL secretion, which delivers sphingolipids, cholesterol, and triglycerides to blood. This reduction in circulating atherogenic lipids including sphingomyelin on VLDL and subsequent transfer to LDL is sufficient to restrict the progression of atherosclerosis induced by dietary TFAs. While these studies focused on hepatic sphingolipid metabolism, SPT activity in enterocytes may also contribute to circulating

atherogenic sphingolipids as dietary fatty acids are initially packaged and trafficked in chylomicrons.

Although myriocin has previously been shown to mitigate progression of atherosclerosis, most of these studies included cholesterol in the diet[51], [53], which is known to advance atherosclerosis. Additionally, the majority of studies were performed in *Apoe-/-* mice[51]–[53], which develop accelerated atherosclerosis on atherogenic diets and carry the majority of cholesterol via VLDL unlike LDL in humans[120]. Here, we directly interrogated the role of different MUFAs in atherosclerosis progression with specifically customized diets varying in CFA versus TFA content without the influence of dietary cholesterol, using *Ldlr-/-* mice that have a similar lipoprotein profile to humans. Myriocin can induce gastrointestinal dysfunction[121] and limit intestinal cholesterol absorption[122]. A minor reduction in food intake was noted only in mice fed Trans HFD + Myriocin in certain weeks. We also observed increased hepatic phospholipid abundances under the Trans HFD + Myriocin diet, demonstrating that dietary lipids are effectively absorbed and processed into complex lipids within tissues. This remodeling indicates that shifting fatty acids away from SPT and downstream sphingolipids is beneficial on these HFDs. Therefore, the absence of dietary cholesterol, increased abundance of hepatic phospholipids, and potent reduction of circulating lipoproteins suggest that a reduction of hepatic SPT activity can mitigate liver steatosis and atherosclerosis.

Our studies also highlight key differences in the fate of TFAs from CFAs, predominantly oleate, which are readily incorporated into phospholipids and sphingolipids by ceramide synthases, promote more adiposity, yet induce far less VLDL secretion and atherosclerotic plaque formation compared to TFAs. We hypothesize that TFAs are more atherogenic due to their structural mimicry of SFAs and reduced ability to be desaturated. Unlike SFAs that have mechanisms such as stearoyl-

CoA desaturase (SCD1) and fatty acid desaturase (FADS3) to be converted to CFAs or sphingadienes[116], [117], respectively, to reduce saturated toxicity, TFAs may be ineffective substrates for these desaturases, leading to greater accumulation and toxicity in ASCVD compared to SFAs as has been reported[84]. The FADS3 gene has similarly been implicated in ASCVD through human genetics[77], and SCD1 mediates saturated fat-induced inflammation and associated atherosclerosis[83]. This dichotomy between CFAs and TFAs provides molecular evidence for the benefit of Mediterranean diets enriched in CFAs compared to high SFA diets.

Characterization of SPT subunit expression in response to myriocin also suggested distinct regulatory functions. We identified a strong positive correlation between *SPTLC3* and hepatic VLDL secretion genes in publicly available human liver transcriptional datasets. These findings suggest distinct functions associated with lipid secretion encoded by *SPTLC3*, a gene that is strongly linked to ASCVD by variants in human populations demonstrated in genome-wide association studies (GWAS)[76]–[78]. Therefore, SPTLC3 may prove to be a more direct target for reducing hepatic VLDL secretion and circulating atherogenic lipoproteins that typically carry sphingolipids with a propensity to aggregate and initiate atherosclerosis.

Collectively, we highlight how SFAs, the canonical substrate for SPT, and similarly structured TFAs heavily influence sphingolipid metabolism to promote ASCVD. CFAs are differentially metabolized by enzymes in this pathway and drive divergent phenotypes including glucose intolerance and obesity. While TFAs are largely banned worldwide, they are acceptable at levels below 0.5 g per serving and naturally present in dairy and meat products. We have described a biochemical pathway where TFAs and SPT flux synergize with hepatic lipoprotein secretion to deliver atherogenic sphingolipids and cholesterol into circulation. Thus, SPT may serve as a potential therapeutic target for mitigating TFA- and SFA-induced ASCVD.

3.5 Materials and methods

Animal experiments

Experimental protocols were approved and performed according to the Institutional Animal Care and Use Committee (IACUC) of the Salk Institute for Biological Studies. Four-five-week-old *Ldlr-/-* C57BL/6J male and female mice (JAX# 002207) were fed with irradiated 60% high fat diets (HFD) prepared by Dyets for 16 weeks. These diets include Cis Unsaturated HFD (105063GI), Cis Unsaturated HFD with 2.2 mg/kg Myriocin Added (105064GI), Trans Unsaturated HFD (105061GI), and Trans Unsaturated HFD with 2.2 mg/kg Myriocin Added (105061GI). The Trans Unsaturated HFD was designed with 100% Primex, a partially hydrogenated vegetable oil, and the Cis Unsaturated HFD was designed with 34% lard and 66% olive oil. Dietary fatty acid composition is detailed in Table S3.2. Tissues were collected after mice were fasted for 6 hours. Mice were anesthetized with isoflurane and tissues were freeze-clamped immediately using Wollenberger clamps pre-cooled to the temperature of liquid nitrogen and stored at -80°C until analysis. Liver, epididymal white adipose tissue (eWAT), and inguinal white adipose tissue (iWAT) were weighed prior to being frozen. Blood was collected in EDTA-coated tubes (Sarstedt Inc.) and centrifuged at 2000g for 5 min. The supernatant was transferred to a new Eppendorf tube and stored at -80°C until analysis.

Glucose tolerance test

Ldlr-/- C57BL/6J male mice (n=10) fed the diets for 15 weeks were fasted overnight with water provided ad libitum. Mice were weighed the following morning and baseline fasting blood glucose was measured via tail bleed with a Contour Next glucometer (Bayer). Mice received an

intraperitoneal bolus injection of 2 g glucose/kg body weight. Blood glucose was measured via tail bleed at 15, 30, 60, 120, and 180 min post-injection.

Hepatic VLDL-TG secretion

Ldlr-/- C57BL/6J mice (n=5: 3 female, 2 male) fed the diets for 16 weeks were fasted for 5 hours with water provided ad libitum. Mice were weighed and baseline fasting blood was collected via tail bleed. Tyloxapol (10% w/v in H_2O) at a dose of 0.5 g/kg body weight was injected via tail vein after mice were anesthetized. Plasma was collected via tail vein at 15 min, 30 min, 60 min, and 120 min post-injection. Triglyceride and cholesterol levels were quantified via enzymatic kits (234-60, 236-60, SE-035, Sekisui).

Fast protein liquid chromatography

Plasma from *Ldlr-/-* C57BL/6J male mice (n=9) per diet were combined into 3 pooled plasma samples and separated via gel-filtration fast-protein liquid chromatography (FPLC). Samples were loaded on a GE Superose 6 10/30 GL column in 0.15 M sodium chloride containing 1 mM ethylenediaminetetraacetic acid and 0.02% sodium azide with pH 7.4. Fractions of 0.5 mL were collected at a flow rate of 0.5 mL/min. Triglyceride and cholesterol levels were quantified via enzymatic kits (Sekisui, 234-60, 236-60, SE-035). Sphingomyelin was measured as described below with the UltimateSPLASH One Mix (Avanti Polar Lipids, Cat #330820) used as internal standards for quantification.

Histology

Liver sections and the top half of the heart were fixed overnight in 10% neutral buffered formalin. Fixed liver was washed with PBS and stored in 70% ethanol until sectioning. Fixed heart for aortic root analysis was washed with PBS and stored in PBS with 30% sucrose and 0.01% sodium azide until sectioning. Liver sections were stained with H&E (hematoxylin & eosin) to visualize hepatic steatosis. Aortic root sections were stained with modified Van Gieson to visualize atherosclerotic lesions.

Atherosclerotic plaque quantitation

Serial 5 µm sections of the aortic root from *Ldlr-/-* C57BL/6J male mice (n=9-10) were stained with modified Van Gieson to measure atherosclerotic lesion sizes sequentially from the beginning of the aortic valves and area under the curve. Aortic root cross-sectional atherosclerotic lesion size was quantified via QuPath.

^2H_2O De novo lipogenesis measurements

Ldlr-/- C57BL/6J male mice (n=5) fed the diets for 16 weeks were administered ^2H_2O in 0.9% NaCl at a dose of 0.027 mL/g body weight via intraperitoneal injection. Drinking water was replaced with 8% ^2H_2O drinking water for 30 hours. 24 hours post-injection, mice were fasted for 6 hours with 8% ^2H_2O drinking water provided ad libitum. Tissues and blood were collected as described above.

^2H_2O enrichment in plasma from samples or standards was measured via deuterium acetone exchange. 5 µL of sample or standard was reacted with 4 µL of 10N NaOH and 4 µL of 5% solution of acetone in acetonitrile for 24 hours. Acetone was extracted after addition of 500 mg of Na_2SO_4 and 600 µL of chloroform. After 2 min centrifugation at 3000 g, 80 µL was transferred in triplicate

into a GC-MS vial and plasma ^2H_2O enrichment was quantified from external standard curve on an Agilent DB-35MS column (30 m x 0.25 mm i.d. × 0.25 µm, Agilent J&W Scientific) installed in an Agilent 7890 A gas chromatograph (GC) interfaced with an Agilent 5975 C mass spectrometer (MS) with the following temperature program: 60 °C initial, increase by 20 °C/min to 100 °C, increase by 50 °C/min to 220 °C, and hold for 1 min.

De novo lipogenesis via ^2H_2O enrichment in various tissues was quantified by spiking 10-20 mg of frozen tissue or 10 µL of plasma with internal standards palmitate-d31 (Cambridge Isotope Laboratories) and coprostanol (Sigma, Cat# 7578) and homogenizing with 250 µL methanol and 250 µL water. Homogenate aliquot of 50 µL was taken to determine protein content using the BCA protein assay (Thermo Scientific). 500 µL chloroform was added to the remaining homogenate, then samples were vortexed for 5 min and centrifuged for 5 min at 4 ˚C and 15 000*g*. The chloroform phase was collected, dried, and resuspended with 500 µL 2% H_2SO_4 in methanol for 2 hours at 50 ˚C. 100 µL of saturated NaCl and 500 µL of hexane were added, sample were vortexed, and the upper hexane phase containing fatty acid methyl esters (FAMEs) was collected and transferred into a GC-MS vial. FAMES were analyzed using a Select FAME column (100 m × 0.25 mm i.d.) installed in an Agilent 7890 A GC interfaced with an Agilent 5975 C MS using the following temperature program: 80 °C initial, increase by 20 °C/min to 170 °C, increase by 1 °C/min to 204 °C, then 20 °C/min to 250 °C and hold for 10 min. The percent isotopologue distribution of each fatty acid was determined and corrected for natural abundance using in-house algorithms adapted from a previous report[123].

Long-chain base hydrolysis

10-20 mg of frozen tissue were spiked with internal standards sphinganine-d7 (Avanti Polar Lipids, Cat# 860658) and sphingosine-d7 (Avanti Polar Lipids, Cat# 860657) and tissues were homogenized or cells were scraped with 0.5 mL methanol. Homogenate aliquot of 50 µL was taken to determine protein content using the BCA protein assay (Thermo Scientific). Samples were placed on a mixer for 1 hr at 37°C and centrifuged at 2800g. Supernatant was transferred to a new Eppendorf tube and hydrolyzed for 16 hr at 65°C. 100 µL 10M KOH, 625 µL chloroform, 100 µL 2N NH_4OH, and 500 µL alkaline water were added to samples followed by vortexing for 5 min and centrifugation for 5 min at 16,000g. The lower organic phase was washed 3 times with alkaline water and dried under air. Quantification of hydrolyzed long chain bases was performed on an Agilent 6460 QQQ LC-MS/MS. Metabolite separation was achieved with a C18 column (Hypersil GOLD aQ C18 100 x 2.1 mm, 1.9 µm particle size, Thermo Scientific). Mobile phase A was composed of a 60:40 ratio of methanol:water containing 0.1% formic acid and 5 mM ammonium formate. Mobile phase B consisted of 100% methanol containing 0.1% formic acid and 5 mM ammonium formate. The gradient elution program consisted of holding at 40% B for 0.5 min, linearly increasing to 100% B over 15 min, and maintaining it for 9 min, followed by re-equilibration to the initial condition for 10 min. The capillary voltage was set to 3.5 kV, the drying gas temperature was 350 °C, the drying gas flow rate was 10 L/min, and the nebulizer pressure was 60 psi. Long chain bases were analyzed by multiple reaction monitoring (MRM) of the transition from precursor to product ions at associated optimized collision energies and fragmentor voltages (Table S3.1). Long chain bases were then quantified from spiked internal standards corresponding to respective long chain base class.

Targeted sphingolipid quantification

Frozen tissue (20-30 mg) or plasma were spiked with internal standards sphinganine-d7 (Avanti Polar Lipids, Cat# 860658), deoxysphinganine-d3 (Avanti Polar Lipids, Cat# 860474), d18:0-d7/13:0 dihydroceramide (Avanti Polar Lipids, Cat# 330726), d18:1-d7/15:0 ceramide (Avanti Polar Lipids, Cat# 860681), d18:1-d7/15:0 glucosylceramide (Avanti Polar Lipids, Cat# 330729), d18:1-d7/15:0 lactosylceramide (Avanti Polar Lipids, Cat# 330727), sphingosine-d7 (Avanti Polar Lipids, Cat# 860657), and d18:1/18:1-d9 sphingomyelin (Avanti Polar Lipids, Cat# 791649) or 18:1 sphingomyelin (d18:1/18:1)-d9 (Avanti Polar Lipids, Cat#860740). Tissue was homogenized and cells were scraped with 0.5 mL methanol and 0.5 mL H_2O. Homogenate aliquot of 100 µL was taken to determine protein content using the BCA protein assay (Thermo Scientific). The remaining homogenate was transferred to a new Eppendorf tube and 1 mL chloroform was added. For plasma, 0.5 mL methanol, 0.5 mL H_2O, and 1 mL chloroform were added directly. Samples were vortexed for 5 min and centrifuged for 5 min at 4 ˚C at 15,000*g*. The organic phase was collected and 2 µL of formic acid was added to the remaining polar phase which was re-extracted with 1 mL of chloroform. Combined organic phases were dried under nitrogen.

Quantification of sphingolipids was performed on an Agilent 6460 QQQ LC-MS/MS. Sphingolipid species were separated on a C8 column (Spectra 3 µm C8SR 150 × 3 mm inner diameter, Peeke Scientific). 5 µL of sample was injected. Mobile phase A was composed of 100% HPLC-grade water containing 2 mM ammonium formate and 0.2% formic acid, and mobile phase B consisted of 100% methanol containing 0.2% formic acid and 1 mM ammonium formate. The gradient elution program consisted of the following profile: 0 min, 82% B; 3 min, 82% B; 4 min, 90% B, 18 min, 99% B; 25 min, 99% B; 27 min; 82% B; 30 min, 82% B. Column re-equilibration followed each sample and lasted 10 min. The capillary voltage was set to 3.5 kV, the drying gas temperature was 350 °C, the drying gas flow rate was 10 L/min, and the nebulizer pressure was 60

psi. Sphingolipid species were analyzed by multiple reaction monitoring (MRM) of the transition from precursor to product ions at associated optimized collision energies and fragmentor voltages (Table S3.1). Sphingolipids were then quantified from spiked internal standards corresponding to respective sphingolipid class.

General lipidomics quantification

Frozen tissue or plasma was spiked with internal standards 18:1-d7 cholesteryl ester (Avanti Polar Lipids, Cat #791645), 15:0-18:1(d7) phosphatidylcholine (Avanti Polar Lipids, Cat #791637), 15:0-18:1(d7) phosphatidylethanolamine (Avanti Polar Lipids, Cat #791638), 18:1(d7) lysophosphatidylcholine (Avanti Polar Lipids, Cat#791643), 18:1(d7) lysophosphatidylethanolamine (Avanti Polar Lipids, Cat #791644), 15:0-18:1(d7) diacylglycerol (Avanti Polar Lipids, Cat #791647), 15:0-18:1(d7)-15:0 triacylglycerol (Avanti Polar Lipids, Cat #791648). Tissue was homogenized with 0.5 mL methanol and 0.5 mL H_2O. Homogenate aliquot of 100 µL was taken to determine protein content using the BCA protein assay (Thermo Scientific). The remaining homogenate was transferred to a new Eppendorf tube and 1 mL chloroform was added. For plasma, 0.5 mL methanol, 0.5 mL H_2O, and 1 mL chloroform were added directly. Samples were vortexed for 5 min, centrifuged for 5 min at 4 ˚C at 15,000*g*. The organic phase was collected and 2 µL of formic acid was added to the remaining polar phase which was re-extracted with 1 mL of chloroform. Combined organic phases were dried under nitrogen.

Chromatographic separation and lipid species identification was performed using Q Exactive orbitrap mass spectrometer with a Vanquish Flex Binary UHPLC system (Thermo Scientific) equipped with an Accucore C30, 150 × 2.1 mm, 2.6 µm particle (Thermo) column at 40 °C. 5 µL of sample was injected. Chromatography was performed using a gradient of 40:60 v/v

water: acetonitrile with 10 mM ammonium formate and 0.1% formic acid (mobile phase A) and 10:90 v/v acetonitrile: propan-2-ol with 10 mM ammonium formate and 0.1% formic acid (mobile phase B), both at a flow rate of 0.2 mL/min. The liquid chromatography gradient ran from 30% to 43% B from 3–8 min, then from 43% to 50% B from 8-9 min, then 50–90% B from 9–18 min, then 90–99% B from 18–26 min, then held at 99% B from 26–30 min, before returning to 30% B in 6 min and held for a further 4 min.

Lipids were analyzed in positive mode using spray voltage 3.2 kV. Sweep gas flow was 1 arbitrary units, auxiliary gas flow 2 arbitrary units and sheath gas flow 40 arbitrary units, with a capillary temperature of 325 °C. Full mass spectrometry (scan range 200–2,000 *m*/*z*) was used at 70,000 resolution with 106 automatic gain control and a maximum injection time of 100 ms. Data dependent MS2 (Top 6) mode at 17,500 resolution with automatic gain control set at 105 with a maximum injection time of 50 ms was used. Lipids were then quantified from spiked internal standards corresponding to respective lipid class. Lipid species specific fragments used for identification and quantification are presented in the Table S3.3.

RNA isolation and quantitative RT-PCR

RNA was extracted from 10-20 mgs liver using Direct-zol RNA kit (Direct-Zol RNA Miniprep Plus kit, Zymo Research). cDNA synthesis was performed using iScript Reverse Transcription Supermix for RT-PCR (iScript Reverse Transcription Supermix, Bio-Rad) with the following thermocycler protocol: 5 min at 25°C, 20 min 46°C, 1 min 95°C. PCR reactions were carried out using 96-well plates on an Applied Biosystems ViiA 7 Real-Time PCR System using the following parameters: 95°C for 20 s, 40 cycles of 95°C for 1 s, and 60°C for 20 s. The final volume (10 µL) of PCR SYBR-Green reaction consisted of 5 µL fast SYBR-Green Master Mix

(Applied Biosystems), 2 µL cDNA, 1 µL of 10 µM forward and reverse primers, and 2 µL of water. Primers are noted in Table S3.4.

Gene co-expression correlation analysis

Co-expression analysis of *SPTLC2* and *SPTLC3* in human liver was performed using the online tool CorrelationAnalyzeR[70]. *SPTLC2* and *SPTLC3* were selected to be analyzed in normal liver tissue in the gene versus gene comparison platform. The top 100 differentially correlated genes with *SPTLC2* and *SPTLC3*, as determined by their Pearson correlation coefficients (r), are listed in Table S3.5. These correlations coefficients against *SPTLC2* and *SPTLC3* for each gene are plotted in Figure 5J.

Statistical analysis

Data are presented as mean ± standard error of mean (SEM) of at least three biological replicates as indicated in figure legends. Statistical analysis was performed with GraphPad Prism 9.3.1 using two-tailed independent *t*-test to compare two groups, one-way ANOVA with Fisher's least significant difference (LSD) post hoc test to compare more than two groups, two-way ANOVA with Fisher's LSD post hoc test to compare two-factor study designs, and Pearson correlation coefficient (r) for gene co-expression correlation analysis. For all tests, $p<0.05$ was considered significant with $*p < 0.05$, $**p < 0.01$, or $*** p< 0.001$ unless otherwise noted.

3.6 Acknowledgements

We thank all members of the Metallo Lab for helpful discussions and thank J. Coker and C. Painter from the Gordts lab for their input in atherosclerosis and lipoprotein analysis, respectively. We additionally thank the Moores Cancer Center Histology Core and La Jolla

Institute for Immunology Histology Core for their help processing liver and aortic root samples, respectively. Chapter 3 has been submitted in the same publication as Chapter 2 and is under review. Jivani M. Gengatharan is the primary author of this manuscript. Michal K. Handzlik, Zoya Y. Chih, Maureen L. Ruchhoeft, Patrick Secrest, Ethan L. Ashley, Courtney R. Green, Martina Wallace, and Philip L.S.M. Gordts are co-authors of the paper. Christian M. Metallo is the corresponding author of this manuscript.

Chapter 4 Conclusions

4.1 Summary and significance

The studies in this dissertation establish metabolic flux through the sphingolipid biosynthesis pathway as critical to the progression of ASCVD. Specifically, sphingolipid biosynthetic flux coordinates trafficking of dietary fat through lipoprotein metabolism to initiate dissemination of lipids and atherosclerosis. While sphingolipids may not constitute a large percentage of circulating lipids compared to cholesterol, triglycerides, and phospholipids, the metabolic flux of these less abundant lipids is an important component of lipoprotein metabolism that drives atherosclerosis as demonstrated via dietary interventions with pharmacological inhibition of SPT, the rate-limiting enzyme of sphingolipid biosynthesis.

The first chapter, "Elucidating the role of sphingolipid metabolism in atherosclerotic cardiovascular disease using mass spectrometry," encompasses existing literature focused on the influence of dietary fat in ASCVD and the broader roles sphingolipids play in the pathogenesis of atherosclerosis. This work also delves into mass spectrometry approaches to measure lipid abundances and quantify lipid biosynthetic flux via stable isotope tracing.

The second chapter, "Unraveling the selective flux of CFAs versus TFAs through sphingolipid metabolism," combines stable isotope tracing and mass spectrometry *in vitro* to highlight differential incorporation of fatty acids into the LCB of sphingolipids via SPT promiscuity. We detected the preferential incorporation of TFAs versus CFAs by SPT into sphingolipids and characterized novel sphingolipids with the TFA elaidate in the LCB. This atypical sphingolipid flux was also exhibited in the increased secretion of TFA-derived sphingolipids from Huh7 cells. Overall, we identified a high affinity of TFAs to the sphingolipid biosynthetic pathway contributing to intracellular as well as extracellular flux of sphingolipids.

The third chapter, "Altered sphingolipid biosynthetic flux and lipoprotein trafficking contribute to trans fat-induced atherosclerosis," aims to discover the physiological role of TFA-derived sphingolipids in the liver steatosis and atherosclerosis induced by trans fat intake. We combined stable isotope tracing *in vivo*, dietary interventions, lipidomics, and histological measurements of the liver and aortic root to assess the intersection of sphingolipids and dietary trans fat *in vivo* metabolically and physiologically. Via myriocin, a pharmacological inhibitor of SPT, we demonstrated that SPT flux contributes to trans fat-induced hepatic steatosis and VLDL secretion, which supplies atherogenic lipids that initiate atherosclerosis.

These chapters comprehensively bridge analytical chemistry and physiology to highlight SPT flux and sphingolipid metabolism as a distinct node mediating the progression of ASCVD as a result of specific dietary fats. We have demonstrated that stable isotope tracing via mass spectrometry and quantitation of metabolic flux can elucidate changes in metabolism that are physiologically relevant to the pathogenesis of various diseases. Overall, these results should support the further study of metabolic flux in different disease states as these metabolic changes are intertwined in physiological responses that can initiate the progression of diseases.

4.2 Future outlook

We have demonstrated that sphingolipid metabolism and specifically SPT flux are linked with hepatic lipid homeostasis and secretion. While triglyceride loading via microsomal triglyceride transfer protein (MTTP) is the rate-limiting step for VLDL assembly and secretion[124], the biosynthetic flux and incorporation of sphingolipids also appear to influence VLDL secretion. Despite sphingolipids exhibiting low enrichment in VLDL compared to triglycerides and cholesterol, *in vivo* inhibition of SPT was sufficient to reduce VLDL secretion.

Therefore, aberrant SPT flux disrupts hepatic lipid homeostasis to alter VLDL secretion and contribute to an atherogenic circulating lipid profile.

We also noted SPT inhibition via myriocin shifted fatty acids towards phospholipids on Trans HFD. The Cis HFD did not induce the same diversion, indicating it only occurs in conditions with higher reliance on SPT flux. This lipid remodeling suggests an important interplay between sphingolipids and phospholipids. There are specific enzymes that connect the metabolic flux of both lipid classes. Sphingomyelin synthase (SMS) coordinates PC conversion to DAG with ceramide conversion to SM. Sphingolipid degradation via S1P lyase (SGPL1) also releases ethanolamine which can fuel the synthesis of PE via head group addition. Therefore, altered sphingolipid biosynthetic and degradation flux have direct links to influence homeostasis across the lipidome. This remodeling towards phospholipids is beneficial as mice fed Trans HFD + Myriocin demonstrated attenuated hepatic steatosis and *de novo* lipogenesis compared to Trans HFD feeding. While phospholipids appear to play a role in mediating lipid homeostasis, two major bioactive lipid classes that are thought to promote hepatic dysfunction and steatosis are DAGs and ceramides[125]–[128]. While the debate regarding the relative toxicity of DAGs and ceramides continues, our studies elucidate the need to consider compensation by other lipid classes in the presence of disrupted lipid homeostasis that causes accumulation in toxic intermediates such as DAGs and ceramides.

While hepatic lipids provide insight into aberrant metabolism that leads to disease states such as steatosis, we highlight the need to consider circulating lipids as part of hepatic lipid biosynthetic flux. For example, reducing VLDL secretion can enhance hepatic steatosis as intracellular lipids accumulate[129]. Our studies demonstrate that dietary trans fat intake elevated *de novo* lipogenesis and consequently drove hepatic steatosis while accelerating VLDL

secretion. Therefore, maintaining a balance between intracellular lipids and lipid secretion is critical in preventing the onset of liver steatosis and other hepatic disorders. In Huh7 cells, intracellular sphingomyelin did not appear to be drastically different among different fatty acid treatments. However, sphingomyelin efflux was significantly altered by trans fatty acid treatment. We observed a similar distinction between hepatic and circulating lipids *in vivo* as several hepatic sphingolipids were unchanged between both HFDs while specific circulating sphingolipids were altered following the Trans HFD. These differences were enhanced when considering the lipoprotein carrier such as VLDL-sphingolipids, further establishing the extension of hepatic lipid metabolism in circulating lipoproteins such as VLDL and importance of measuring both compartments. Further experiments should continue to measure media of hepatic-derived cell lines and compare both hepatic and circulating lipid profiles *in vivo* to capture the full picture of hepatic lipid biosynthetic flux. Models including primary hepatocytes or human liver organoids can provide a simpler but more representative view of this exchange between intracellular and secreted lipids into media compared to Huh7 or HepG2 hepatoma cells prior to expanding *in vivo*.

MUFAs such as oleic acid have been promoted as part of the healthy Mediterranean diet due to their propensity to reduce circulating atherogenic LDL-C[130]. Additionally, oleic acid has been demonstrated to reduce inflammation[131]–[133], non-metastatic tumor growth[134]–[136], and neurodegeneration[137]–[139]. Our studies support the benefit of dietary oleic acid as the 60% HFD enriched in oleic acid (Cis HFD) only induced glucose intolerance and obesity while the 60% HFD enriched in TFAs (Trans HFD) additionally enhanced hepatic steatosis and atherogenesis. These findings highlight a dichotomy in the processing of isomeric CFAs and TFAs to influence disease states. Just a change in double bond configuration can elicit different

physiological responses such that TFAs drive lipotoxic phenotypes such as hepatic steatosis atherosclerosis while CFAs induce weight gain. This increase in adiposity fueled by the Cis HFD is the expected and appropriate response to a fat overload, not accumulation in other tissues as found with the Trans HFD. Therefore, further studies modulating dietary oleic acid or preventing its endogenous synthesis via SCD1 can elucidate positive health effects of MUFAs while highlighting desaturase mechanisms such as SCD1 to convert toxic SFAs to MUFAs as critical to preventing the onset of lipotoxic disease states induced by dietary SFAs [83], [140], [141].

Sphingolipid metabolism is one of the only lipid metabolic pathways that canonically requires a particular acyl-CoA substrate – palmitoyl-CoA. The promiscuity with regards to acyl-CoA substrate maintains selectivity towards saturated substrates [67]. Our findings highlight that atypical trans unsaturated fatty acid substrates are highly utilized by SPT due to their structural mimicry of the canonical saturated substrate. This structural preference in substrate makes sphingolipid metabolism a distinct node that can be directly influenced by dietary fat composition. We highlight that a diet consisting of TFAs, which are structurally similar to SFAs, drives sphingolipid metabolism partially due to increased substrate availability and in turn promotes hepatic VLDL secretion. Therefore, dietary fatty acid composition influences sphingolipid metabolism to make it a critical metabolic vulnerability in diet-induced obesity and co-morbidities such as liver steatosis and ASCVD. Further studies focused on the relative contributions of various lipid biosynthetic pathways depending on dietary fat composition are warranted to determine novel therapeutic targets and identify precision nutrition-based treatments. SFAs are still present in various fat sources and their reliance on sphingolipid metabolism *in vivo* has not been thoroughly characterized by sufficient studies[142], [143] despite their preferential usage as acyl-CoA substrates of SPT[67]. Administering HFDs

enriched in SFAs while modulating SPT genetically or via myriocin can elucidate the importance of sphingolipid metabolism in processing excess SFAs, which is relevant in current Western diets.

While the World Health Organization (WHO) announced in 2018 a global plan to eliminate TFAs from food supplies by the end of 2023, several countries have yet to establish policies to eliminate TFAs from processed fat sources. WHO reported more than 100 countries have still failed to remove trans fats in their food supplies, which puts approximately 5 billion people at risk for the atherogenic effects of dietary trans fats [144]. TFAs are also still acceptable below 0.5 g per serving in the USA with the ban and are naturally present in dairy and meat. The progressive ban has reduced cardiovascular incidents in the USA [145]. However, chronic intake of these alternate sources with low TFAs may induce long-term perturbations to hepatic and circulating lipid homeostasis that can still promote ASCVD. Given the high percentage of the global population still at risk for the atherogenicity of trans fats, our study and others are required to highlight new mechanisms of atherogenicity beyond major drivers such as cholesterol to identify alternative therapeutic targets. While clinical studies primarily focus on circulating lipid profiles, rodent models can continue to reveal insight into hepatic and local endothelial contribution to atherogenic lipids.

Myriocin has been used for several years to inhibit SPT through intraperitoneal or oral administration. It can induce gastrointestinal dysfunction[121] and exhibits immunosuppressive potential [146]. Therefore, alternative approaches to modulating SPT activity should be considered. Novel pharmacological inhibitors have been designed to target SPT without gut toxicity [147]. AAV-mediated genetic knockout of SPTLC1 can also bypass certain side effects and target SPT in a tissue-specific manner to modulate local sphingolipid biosynthesis [148]. In

the context of our study, AAV8-mediated depletion of SPTLC1 in the liver may directly support the link between SPT flux and hepatic VLDL secretion found with myriocin.

Polyunsaturated SM were elevated upon TFA treatment *in vitro* and Trans HFD administration *in vivo*. These species may serve as biomarkers of aberrant TFA flux through SPT and sphingolipid metabolism. Stable isotope tracing with the ^{2}H-labeled TFA elaidate revealed the polyunsaturated SM were derived from elaidate. However, this distinction cannot be clearly made *in vivo* due to the cost of administering tracers long-term to obtain sufficient enrichment in sphingolipids. Additionally, SM can only be identified by the sum of their acyl chains as the MRM only captures the loss of the phosphocholine head group. Therefore, SM can be denoted by the number of their double bonds without positional information *in vivo*. However, *in vitro* results suggest that while the number of double bonds may be the same between different SM species, the double bond position and configuration may be different. Canonical SM will have typically have a trans double bond (4E) via DEGS and can have an additional cis double bond (14Z) via FADS3. TFA-derived SM will have the canonical trans double bond (4E) via DEGS as well as the trans double bond derived from the original TFA. Therefore, the presence of various isobaric SM species complicates the interpretation of elevated levels of polyunsaturated SM. MS^{n} with further fragmentation of the molecule may provide insight into double bond position and configuration to confirm incorporation of TFAs into the LCB. Revealing structural information through this advanced mass spectrometry can enhance the accuracy of identifying these complex, redundant lipids and further advance the field of lipidomics to identify novel biomarkers.

S1P is an important signaling sphingolipid involved in mediating various cellular processes and the progression of several diseases including cancer[19]–[21], inflammation[22]–

[24], atherosclerosis[25]–[27], angiogenesis[28]–[30], and cell growth[31], [32]. Canonically, S1P is derived from a palmitoyl-CoA substrate for SPT to form S1P d18:1. We expect the TFA elaidate to similarly form S1P d20:2 (E) with an additional trans double bond derived from elaidate itself. While we were not able to use our methods to detect S1P, the presence of TFA-derived S1P may prevent expected S1P signaling with its structural differences. Alternatively, synthesis of TFA-derived S1P may reduce production of canonical S1P, thereby diminishing its ability to initiate specific cellular processes or mediate disease progression. Therefore, further studies in the degradation of TFA-derived sphingolipids will provide more insight on the altered sphingolipid flux induced by TFAs and whether it is due to improper degradation or truly elevated biosynthetic flux.

Long-term myriocin treatment *in vivo* exhibited a distinct regulation of SPT subunits with a dramatic reduction in *Sptlc3* mRNA expression. *SPTLC3* has been correlated to cardiovascular risk factors and events such as dyslipidemia[78], LDL-C[76], and myocardial infarction[77]. This unfavorable plasma lipid profile correlated to *SPTLC3* may be derived from the perturbed hepatic VLDL secretion as evidenced with myriocin with Trans HFD in our studies. From publicly available transcriptional databases, we also identified a strong correlation of *SPTLC3* to VLDL secretion genes *MTTP* and various *APO* genes. Therefore, these correlations establish a specific SPT subunit as a coordinator of hepatic lipid secretion that influences cardiovascular risk. SPTLC3 may prove to be a promising candidate as a therapeutic target for ASVCD. AAV-mediated overexpression of *Sptlc3* in mice upon HFD administration can mechanistically elucidate the link between this specific SPT subunit and hepatic VLDL secretion *in vivo* through inhibition of lipoprotein lipases. In addition, CRISPR-Cas9-mediated KO of *SPTLC3* in a human hepatocarcinoma cell line such as Huh7 cells treated with exogenous fatty acids can reveal the

connection between SPT flux and VLDL secretion that corresponds to human genetic correlations[78], [77], [76].

SPTLC3 is also highly expressed in tissues with high lipid processing and secretory functions. These tissues include skin, intestine, hepatocytes, and macrophages, which actively secrete lipids as lamellar bodies, chylomicrons, VLDL, and HDL, respectively. SPTLC3 has been shown to promote LCB diversity through the incorporation of atypical fatty acid substrates[70], [73]. This diversity has been thought to aid in barrier function of specialized tissues such as skin and intestine with high SPTLC3 expression. Given the secretory capabilities of these cells, SPTLC3-induced LCB diversity may also be required to facilitate lipid secretion, thereby maintaining lipid homeostasis and cell function. Therefore, investigating SPTLC3 in diverse cell types can uncover the role of sphingolipids in various diseases as cells with high *SPTLC3* expression may contribute to the pathogenesis.

Overall, there are gaps in our understanding of the role of sphingolipids in various diseases including ASCVD and there is much to be learned about the mechanisms by which they disrupt lipid homeostasis and cell function in these disease states. Progress in advanced mass spectrometry technology will enable accurate quantitation of lipid metabolism to uncover critical links to physiological perturbations. These new tools and analytical techniques should be utilized to identify metabolic vulnerabilities and develop novel therapeutic targets for any disease of interest including ASCVD.

Chapter S1 Supplement to Chapter 2

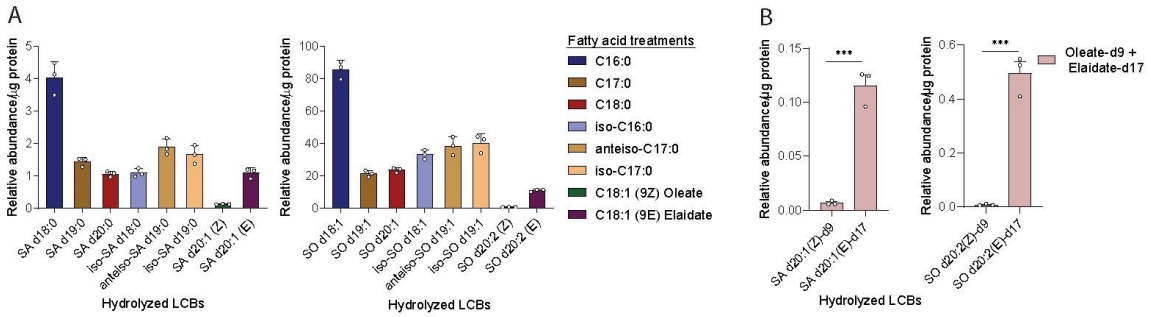

Figure S1.1 TFAs are preferentially metabolized by SPT over CFAs.

(**A**) Hydrolyzed LCBs synthesized from supplemented fatty acid treatments in Huh7 cells (n=3 per group). (**B**) Hydrolyzed SA and SO LCBs synthesized from co-treatment of 50 µM oleate-d9 and 50 µM elaidate-d17 in Huh7 cells (n=3 per group). Data are mean ± standard error of mean (SEM) were analyzed using an independent t-test (B). *p < 0.05, **p < 0.01, or *** p< 0.001 unless otherwise noted.

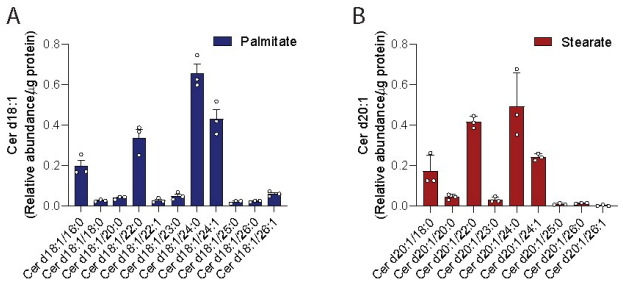

Figure S1.2 Molecular partitioning of CFAs and TFAs through sphingolipid metabolism.

(**A**) Ceramide d18:1 profile following 100 µM palmitate supplementation in Huh7 cells (n=3 per group). (**B**) Ceramide d20:1 profile following 100 µM stearate supplementation in Huh7 cells (n=3 per group). Data are presented as mean ± standard error of mean (SEM). *p < 0.05, **p < 0.01, or *** p< 0.001 unless otherwise noted.

Figure S1.3 TFAs drive aberrant sphingomyelin secretion.

(**A**) Profile of lysophosphatidylcholine (LPC) species with 2H labeling from oleate-d9 or elaidate-d17 in Huh7 cells (n=3 per group). (**B**) Profile of lysophosphatidylethanolamine(LPE) species with 2H labeling from oleate-d9 or elaidate-d17 in Huh7 cells (n=3 per group). (**C**) Profile of phosphatidylcholine (PC) species with 2H labeling from oleate-d9 or elaidate-d17 in Huh7 cells (n=3 per group). (**D**) Profile of phosphatidylethanolamine (PE) species with 2H labeling from oleate-d9 or elaidate-d17 in Huh7 cells (n=3 per group). (**E**) Profile of diacylglycerol (DAG) species with 2H labeling from oleate-d9 or elaidate-d17 in Huh7 cells (n=3 per group). (**F**) Profile of triacylglycerol (TAG) species with 2H labeling from oleate-d9 or elaidate-d17 in Huh7 cells (n=3 per group). (**G**) Hydrolyzed SA and SO LCBs synthesized from oleate-d9 or elaidate-d17, respectively, in Huh7 cells treated with elaidate or elaidate and myriocin (n=3 per group). (**H**) LCB 2H labeling from elaidate-d17 producing a d20:2-d17 LCB in glucosyl/galactosy-ceramides (Gluc/Gal-Cer) in Huh7 cells treated with elaidate-d17 or elaidate-d17 and myriocin (n=3 per group). (**I**) LCB 2H labeling from elaidate-d17 producing a d20:2-d17 LCB in lactosyl-ceramides (Lact-Cer) in Huh7 cells treated with elaidate-d17 or elaidate-d17 and myriocin (n=3 per group). (**J**) 2H labeling on sphingomyelin from oleate-d9 or elaidate-d17 in Huh7 cells treated with elaidate-d17 or elaidate-d17 and myriocin (n=3 per group). Data are mean ± standard error of mean (SEM) were analyzed using an independent t-test (H-I) or two-way ANOVA with Fisher's LSD post hoc test (G,J). *$p < 0.05$, **$p < 0.01$, or *** $p< 0.001$ unless otherwise noted.

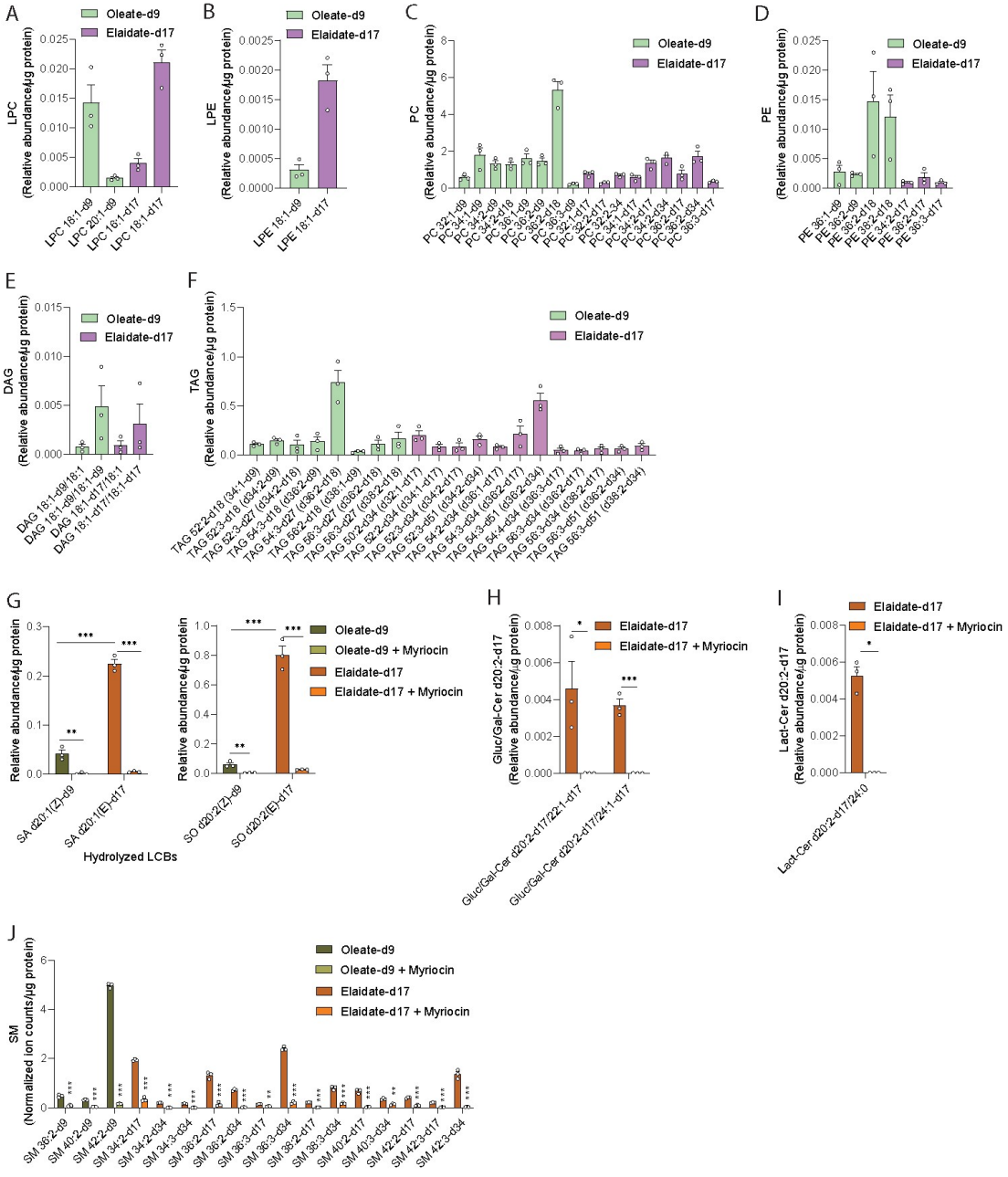
A
LPC
(Relative abundance/µg protein)
Oleate-d9
Elaidate-d17
LPC 18:1-d9
LPC 20:1-d9
LPC 18:1-d17
LPC 18:1-d17
B
LPE
LPE 18:1-d9
LPE 18:1-d17
C
PC
PC 32:1-d9
PC 34:1-d9
PC 34:2-d9
PC 34:2-d18
PC 36:1-d9
PC 36:2-d9
PC 36:2-d18
PC 36:3-d9
PC 32:1-d17
PC 32:2-34
PC 34:1-d17
PC 34:2-d17
PC 34:2-d34
PC 36:2-d17
PC 36:2-d34
PC 36:3-d17
D
PE
PE 36:1-d9
PE 36:2-d9
PE 36:2-d18
PE 36:3-d18
PE 34:2-d17
PE 36:2-d17
PE 36:3-d17
E
DAG
(Relative abundance/µg protein)
DAG 18:1-d9/18:1
DAG 18:1-d9/18:1-d9
DAG 18:1-d17/18:1
DAG 18:1-d17/18:1-d17
F
TAG
(Relative abundance/µg protein)
TAG 52:2-d18 (34:1-d9)
TAG 52:3-d18 (d34:2-d9)
TAG 52:3-d27 (d34:2-d18)
TAG 54:3-d18 (d36:2-d9)
TAG 54:3-d27 (d36:2-d18)
TAG 56:2-d18 (d36:1-d9)
TAG 56:3-d27 (d36:2-d18)
TAG 56:3-d27 (d38:2-d18)
TAG 60:2-d34 (d32:1-d17)
TAG 52:2-d34 (d34:1-d17)
TAG 52:3-d34 (d34:2-d17)
TAG 52:3-d51 (d34:2-d34)
TAG 54:2-d34 (d36:1-d17)
TAG 54:3-d34 (d36:2-d17)
TAG 54:3-d51 (d36:2-d34)
TAG 54:4-d34 (d36:3-d17)
TAG 56:3-d34 (d36:3-d34)
TAG 56:3-d34 (d38:2-d17)
TAG 56:3-d51 (d38:2-d34)
TAG 56:3-d51 (d38:2-d34)
G
Relative abundance/µg protein
Oleate-d9
Oleate-d9 + Myriocin
Elaidate-d17
Elaidate-d17 + Myriocin
SA d20:1(Z)-d9
SA d20:1(E)-d17
SO d20:2(Z)-d9
SO d20:2(E)-d17
Hydrolyzed LCBs
H
Gluc/Gal-Cer d20:2-d17
(Relative abundance/µg protein)
Elaidate-d17
Elaidate-d17 + Myriocin
Gluc/Gal-Cer d20:2-d17/22:1-d17
Gluc/Gal-Cer d20:2-d17/24:1-d17
I
Lact-Cer d20:2-d17
(Relative abundance/µg protein)
Elaidate-d17
Elaidate-d17 + Myriocin
Lact-Cer d20:2-d17/24:0
J
SM
(Normalized ion counts/µg protein)
Oleate-d9
Oleate-d9 + Myriocin
Elaidate-d17
Elaidate-d17 + Myriocin
SM 36:2-d9
SM 40:2-d9
SM 42:2-d9
SM 34:2-d17
SM 34:2-d34
SM 34:3-d34
SM 36:2-d17
SM 36:2-d34
SM 36:3-d17
SM 36:3-d34
SM 38:2-d17
SM 38:3-d34
SM 40:2-d17
SM 40:3-d34
SM 42:2-d17
SM 42:3-d17
SM 42:3-d34

Chapter S2 Supplement to Chapter 3

Figure S2.1 Inhibition of sphingolipid biosynthesis mitigates trans fat-induced atherosclerosis.

(**A**) Food intake over course of 16 weeks in mice fed Cis HFD, Cis HFD + Myriocin, Trans HFD, Trans HFD + Myriocin (n=15 per group). (**B**) Epididymal adipose tissue (eWAT) weight in mice fed Cis HFD, Cis HFD + Myriocin, Trans HFD, or Trans HFD + Myriocin (n=15 per group) (**C**) Fasting blood glucose concentration over the course of 16 weeks in mice fed Cis HFD, Cis HFD + Myriocin, Trans HFD, Trans HFD + Myriocin (n=10 per group). (**D**) I.P. glucose tolerance test after 15 weeks of feeding mice Cis HFD, Cis HFD + Myriocin, Trans HFD, or Trans HFD + Myriocin (n=10 per group). (**E**) Hepatic mRNA expression of *Col1a1* in mice fed Cis HFD, Cis HFD + Myriocin, Trans HFD, Trans HFD + Myriocin (n=7-10 per group). (**F**) Hepatic total fatty acid abundance in mice fed Cis HFD, Cis HFD + Myriocin, Trans HFD, or Trans HFD + Myriocin (n=5 per group). (**G**) Hepatic triacylglycerol (TAG) abundance in mice fed Cis HFD, Cis HFD + Myriocin, Trans HFD, or Trans HFD + Myriocin (n=10 per group). (**H**) Hepatic cholesteryl ester (ChE) abundance in mice fed Cis HFD, Cis HFD + Myriocin, Trans HFD, or Trans HFD + Myriocin (n=10 per group). (**I**) Hepatic lysophosphatidylcholine (LPC) abundance in mice fed Cis HFD, Cis HFD + Myriocin, Trans HFD, or Trans HFD + Myriocin (n=10 per group). (**J**) Hepatic lysophosphatidylethanolamine (LPE) abundance in mice fed Cis HFD, Cis HFD + Myriocin, Trans HFD, or Trans HFD + Myriocin (n=10 per group). (**K**) Hepatic total sphingolipid class abundances in mice fed Cis HFD, Cis HFD + Myriocin, Trans HFD, or Trans HFD + Myriocin (n=9-10 per group). Data are mean ± standard error of mean (SEM) were analyzed using a two-way ANOVA with Fisher's LSD post hoc test (A-K). *$p < 0.05$, **$p < 0.01$, or *** $p< 0.001$ unless otherwise noted.

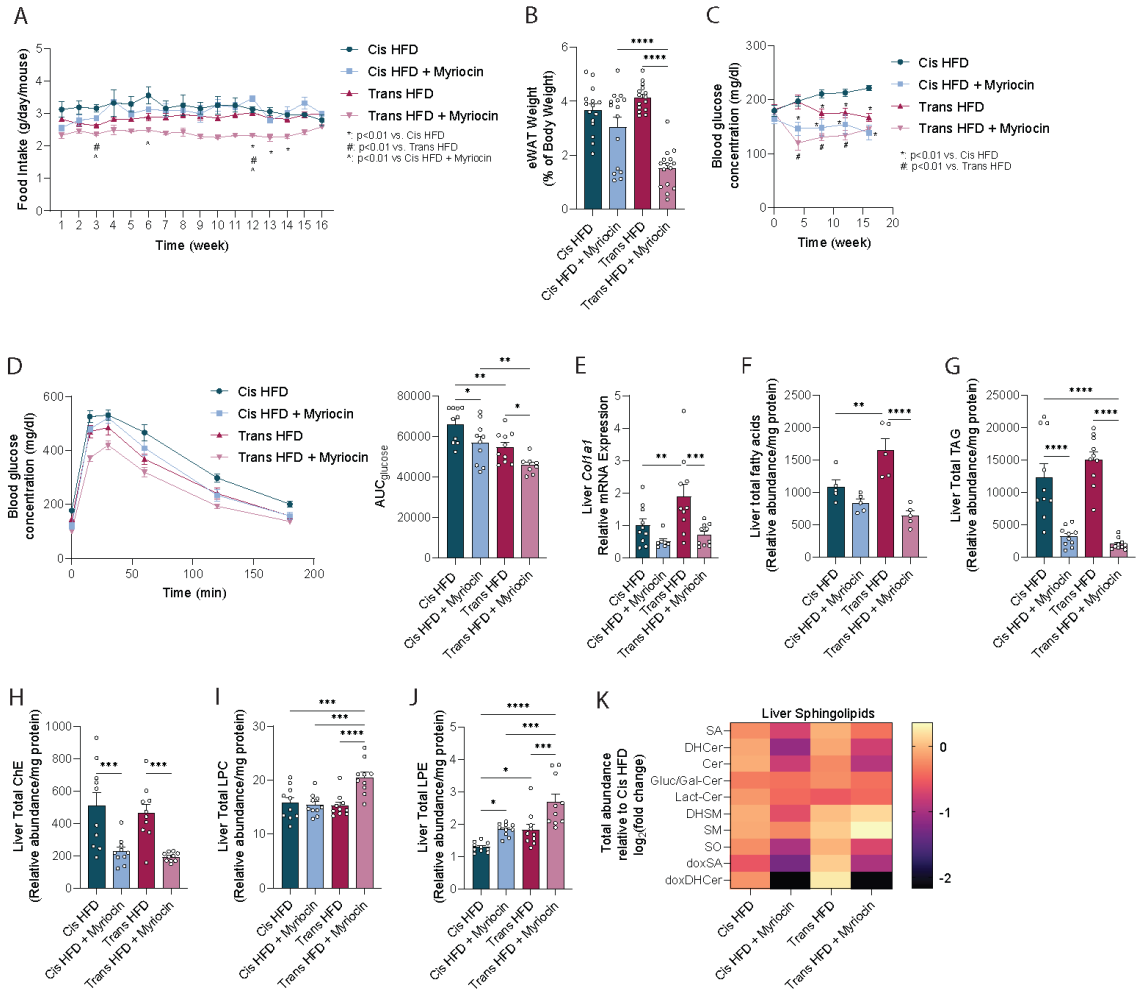
A
Food intake (g/day/mouse)
Time (week)
Cis HFD
Cis HFD + Myriocin
Trans HFD
Trans HFD + Myriocin
*: p<0.01 vs. Cis HFD
#: p<0.01 vs. Trans HFD
^: p<0.01 vs Cis HFD + Myriocin
B
eWAT Weight (% of Body Weight)
C
Blood glucose concentration (mg/dl)
Time (week)
*: p<0.01 vs. Cis HFD
# p<0.01 vs. Trans HFD
D
Blood glucose concentration (mg/dl)
Time (min)
AUCglucose
E
Liver Col1a1 Relative mRNA Expression
F
Liver total fatty acids (Relative abundance/mg protein)
G
Liver Total TAG (Relative abundance/mg protein)
H
Liver Total ChE (Relative abundance/mg protein)
I
Liver Total LPC (Relative abundance/mg protein)
J
Liver Total LPE (Relative abundance/mg protein)
K
Liver Sphingolipids
Total abundance relative to Cis HFD log2(fold change)
SA
DHCer
Cer
Gluc/Gal-Cer
Lact-Cer
DHSM
SM
SO
doxSA
doxDHCer

Figure S2.2 Inhibition of sphingolipid biosynthesis mitigates trans fat-induced atherosclerosis.

(**A**) Lipoprotein analysis of plasma triglycerides from mice fed Cis HFD, Cis HFD + Myriocin, Trans HFD, Trans HFD + Myriocin (3 pooled plasma per group from n=3 each). CR: chylomicron remnant, VLDL: very-low-density lipoprotein, IDL: intermediate-density lipoprotein, LDL: low-density lipoprotein, HDL: high-density lipoprotein (**B**) Baseline triglyceride concentration prior to administering Tyloxapol to measure hepatic VLDL secretion (n=5 per group). (**C**) Newly synthesized palmitate in plasma of mice fed Cis HFD, Cis HFD + Myriocin, Trans HFD, Trans HFD + Myriocin (n=5 per group). (**D**) Plasma lipidomics of mice fed Cis HFD, Cis HFD + Myriocin, Trans HFD, Trans HFD + Myriocin (n=10 per group). (**E**) Profile of plasma di- and poly-unsaturated sphingomyelin (SM) containing >2 double bonds in mice fed Cis HFD, Cis HFD + Myriocin, Trans HFD, Trans HFD + Myriocin (n=10 per group). (**F**) Plasma abundance of dihydrosphingomyelin (SM) containing 0 double bonds in mice fed Cis HFD, Cis HFD + Myriocin, Trans HFD, Trans HFD + Myriocin (n=10 per group). (**G**) Plasma abundance of monounsaturated sphingomyelin (SM) containing 1 double bonds in mice fed Cis HFD, Cis HFD + Myriocin, Trans HFD, Trans HFD + Myriocin (n=10 per group). (**H**) Plasma abundance of diunsaturated sphingomyelin (SM) containing 2 double bonds in mice fed Cis HFD, Cis HFD + Myriocin, Trans HFD, Trans HFD + Myriocin (n=10 per group). (**I**) Lipoprotein analysis of plasma sphingomyelin from mice fed Cis HFD, CIs HFD + Myriocin, Trans HFD, Trans HFD + Myriocin (3 pooled plasma per group from n=3 each). CR: chylomicron remnant, VLDL: very-low-density lipoprotein, IDL: intermediate-density lipoprotein, LDL: low-density lipoprotein, HDL: high-density lipoprotein. Data are mean ± standard error of mean (SEM) were analyzed using a two-way ANOVA with Fisher's LSD post hoc test (B-H). *$p < 0.05$, **$p < 0.01$, or *** $p< 0.001$ unless otherwise noted.

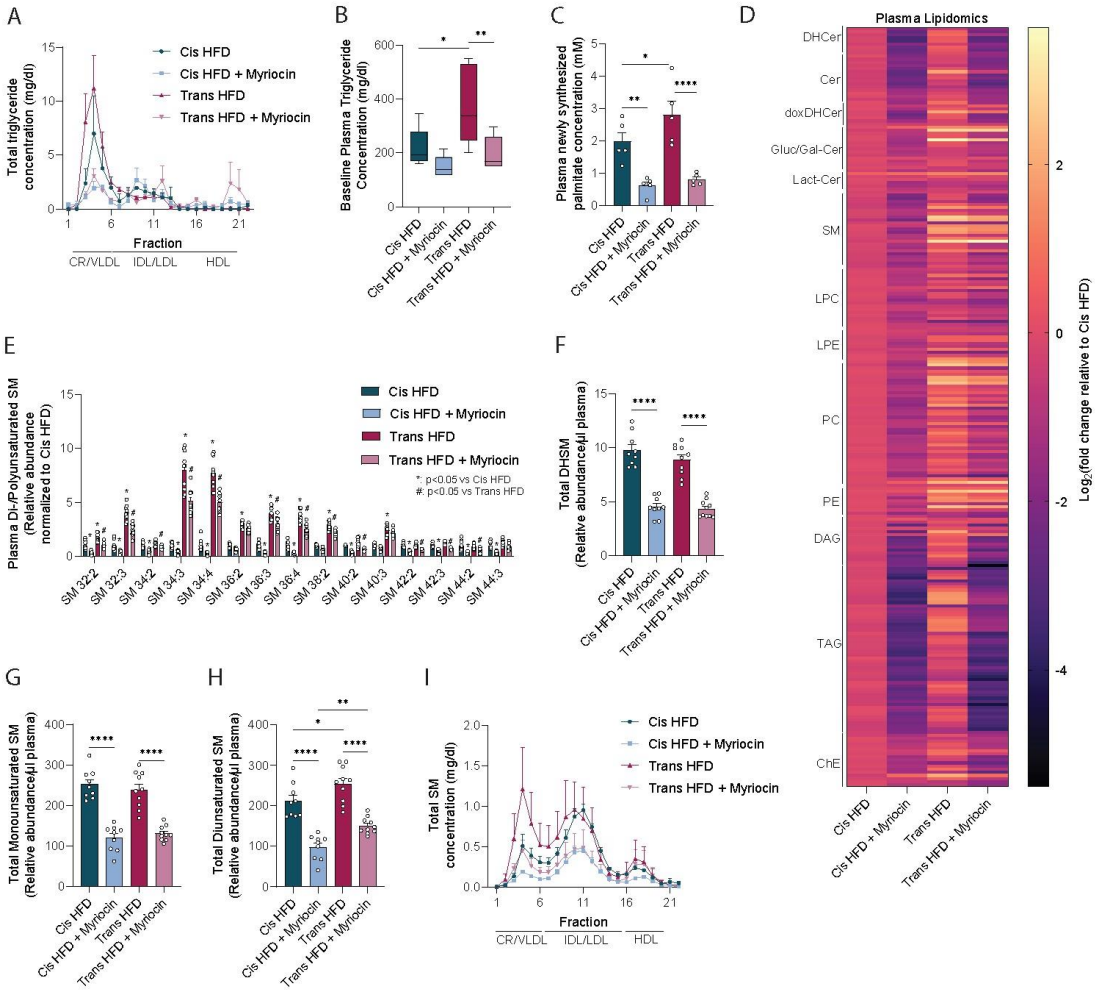
A
Total triglyceride concentration (mg/dl)
Cis HFD
Cis HFD + Myriocin
Trans HFD
Trans HFD + Myriocin
Fraction
CR/VLDL
IDL/LDL
HDL
B
Baseline Plasma Triglyceride Concentration (mg/dl)
C
Plasma newly synthesized palmitate concentration (mM)
D
Plasma Lipidomics
DHCer
Cer
doxDHCer
Gluc/Gal-Cer
Lact-Cer
SM
LPC
LPE
PC
PE
DAG
TAG
ChE
Log2(fold change relative to Cis HFD)
E
Plasma Di-/Polyunsaturated SM (Relative abundance normalized to Cis HFD)
*: p<0.05 vs Cis HFD
#: p<0.05 vs Trans HFD
F
Total DHSM (Relative abundance/µl plasma)
G
Total Monounsaturated SM (Relative abundance/µl plasma)
H
Total Diunsaturated SM (Relative abundance/µl plasma)
I
Total SM concentration (mg/dl)

Chapter S3 Supplemental tables to Chapters 2 and 3

Table S3.1 Lipid multiple reaction monitoring (MRMs), collision energies, and fragmentor voltages for LC-MS.

Lipid Species	Precursor Ion	Product Ion	Fragmentor (V)	CE (V)
SA d18:0 d7	309.4	291.4	120	9
SA d12:0	218.4	200.4	120	9
SA d14:0	246.4	228.4	120	9
SA d16:0	274.4	256.4	120	9
SA d17:0	288.4	270.4	120	9
SA d18:0	302.4	284.4	120	9
SA d18:1	300.4	282.4	120	9
SA d18:1-d17	317.4	299.4	120	9
SA d18:1-d9	309.4	291.4	120	9
SA d19:0	316.4	298.4	120	9
SA d20:0	330.4	312.4	120	9
SA d20:1	328.4	310.4	120	9
SA d20:1-d17	345.4	327.4	120	9
SA d20:1-d9	337.4	319.4	120	9
SA d22:0	358.4	340.4	120	9
SA d22:1	356.4	338.4	120	9
SA d22:1-d17	373.4	355.4	120	9
SA d22:1-d9	365.4	347.4	120	9
SA d24:0	386.4	368.4	120	9
SA d24:1	384.4	366.4	120	9
SA d24:1-d17	401.4	383.4	120	9
SA d24:1-d9	393.4	375.4	120	9
DHCer d18:0-d7/13:0	505.5	273.4	100	17
DHCer d18:0/12:0	484.5	266.4	100	17

Table S3.1 Lipid multiple reaction monitoring (MRMs), collision energies, and fragmentor voltages for LC-MS.

Lipid Species	Precursor Ion	Product Ion	Fragmentor (V)	CE (V)
DHCer d18:0/14:0	512.5	266.4	100	17
DHCer d18:0/15:0	526.5	266.4	100	17
DHCer d18:0/16:0	540.5	266.4	100	17
DHCer d18:0/16:0	540.5	266.4	100	17
DHCer d18:0/16:1	538.5	266.4	100	17
DHCer d18:0/16:1-d17	555.5	266.4	100	17
DHCer d18:0/16:1-d9	547.5	266.4	100	17
DHCer d18:0/17:0	554.6	266.4	100	17
DHCer d18:0/18:0	568.6	266.4	100	17
DHCer d18:0/18:1	566.6	266.4	100	17
DHCer d18:0/18:1-d17	583.6	266.4	100	17
DHCer d18:0/18:1-d9	575.6	266.4	100	17
DHCer d18:0/19:0	582.6	266.4	100	17
DHCer d18:0/20:0	596.6	266.4	100	17
DHCer d18:0/20:1	594.6	266.4	100	17
DHCer d18:0/20:1-d17	611.6	266.4	100	17
DHCer d18:0/20:1-d9	603.6	266.4	100	17
DHCer d18:0/21:0	610.6	266.4	100	17
DHCer d18:0/22:0	624.6	266.4	100	17
DHCer d18:0/22:1	622.6	266.4	100	17
DHCer d18:0/22:1-d17	639.6	266.4	100	17
DHCer d18:0/22:1-d9	631.6	266.4	100	17
DHCer d18:0/23:0	638.6	266.4	100	17
DHCer d18:0/24:0	652.7	266.4	100	17
DHCer d18:0/24:0	652.7	266.4	100	17
DHCer d18:0/24:1	650.6	266.4	100	17

Table S3.1 Lipid multiple reaction monitoring (MRMs), collision energies, and fragmentor voltages for LC-MS.

Lipid Species	Precursor Ion	Product Ion	Fragmentor (V)	CE (V)
DHCer d18:0/24:1-d17	667.6	266.4	100	17
DHCer d18:0/24:1-d9	659.6	266.4	100	17
DHCer d18:0/25:0	666.7	266.4	100	17
DHCer d18:0/26:0	680.7	266.4	100	17
DHCer d18:0/26:1	678.7	266.4	100	17
DHCer d18:0/26:1-d17	695.7	266.4	100	17
DHCer d18:0/26:1-d9	687.7	266.4	100	17
DHCer d20:0/12:0	512.5	294.4	100	17
DHCer d20:0/14:0	540.5	294.4	100	17
DHCer d20:0/15:0	554.6	294.4	100	17
DHCer d20:0/16:0	568.6	294.4	100	17
DHCer d20:0/16:1	566.6	294.4	100	17
DHCer d20:0/16:1-d17	583.6	294.4	100	17
DHCer d20:0/16:1-d9	575.6	294.4	100	17
DHCer d20:0/17:0	582.6	294.4	100	17
DHCer d20:0/18:0	596.6	294.4	100	17
DHCer d20:0/18:0	596.6	294.4	100	17
DHCer d20:0/18:0	596.6	294.4	100	17
DHCer d20:0/18:1	594.6	294.4	100	17
DHCer d20:0/18:1-d17	611.6	294.4	100	17
DHCer d20:0/18:1-d9	603.6	294.4	100	17
DHCer d20:0/19:0	610.6	294.4	100	17
DHCer d20:0/20:0	624.6	294.4	100	17
DHCer d20:0/20:1	622.6	294.4	100	17
DHCer d20:0/20:1-d17	639.6	294.4	100	17
DHCer d20:0/20:1-d9	631.6	294.4	100	17

Table S3.1 Lipid multiple reaction monitoring (MRMs), collision energies, and fragmentor voltages for LC-MS.

Lipid Species	Precursor Ion	Product Ion	Fragmentor (V)	CE (V)
DHCer d20:0/21:0	638.6	294.4	100	17
DHCer d20:0/22:0	652.7	294.4	100	17
DHCer d20:0/22:1	650.6	294.4	100	17
DHCer d20:0/22:1-d17	667.6	294.4	100	17
DHCer d20:0/22:1-d9	659.6	294.4	100	17
DHCer d20:0/23:0	666.7	294.4	100	17
DHCer d20:0/24:0	680.7	294.4	100	17
DHCer d20:0/24:0	680.7	294.4	100	17
DHCer d20:0/24:0	680.7	294.4	100	17
DHCer d20:0/24:1	678.7	294.4	100	17
DHCer d20:0/24:1-d17	695.7	294.4	100	17
DHCer d20:0/24:1-d9	687.7	294.4	100	17
DHCer d20:0/25:0	694.7	294.4	100	17
DHCer d20:0/26:0	708.7	294.4	100	17
DHCer d20:0/26:1	706.7	294.4	100	17
DHCer d20:0/26:1-d17	723.7	294.4	100	17
DHCer d20:0/26:1-d9	715.7	294.4	100	17
DHCer d20:1-d17/12:0	527.5	309.4	100	17
DHCer d20:1-d17/14:0	555.5	309.4	100	17
DHCer d20:1-d17/15:0	569.5	309.4	100	17
DHCer d20:1-d17/16:0	583.5	309.4	100	17
DHCer d20:1-d17/16:1	581.5	309.4	100	17
DHCer d20:1-d17/16:1-d17	598.5	309.4	100	17
DHCer d20:1-d17/17:0	597.5	309.4	100	17
DHCer d20:1-d17/18:0	611.5	309.4	100	17
DHCer d20:1-d17/18:1	609.5	309.4	100	17

Table S3.1 Lipid multiple reaction monitoring (MRMs), collision energies, and fragmentor voltages for LC-MS.

Lipid Species	Precursor Ion	Product Ion	Fragmentor (V)	CE (V)
DHCer d20:1-d17/18:1-d17	626.5	309.4	100	17
DHCer d20:1-d17/19:0	625.5	309.4	100	17
DHCer d20:1-d17/20:0	639.5	309.4	100	17
DHCer d20:1-d17/20:1	637.5	309.4	100	17
DHCer d20:1-d17/20:1-d17	654.5	309.4	100	17
DHCer d20:1-d17/21:0	653.5	309.4	100	17
DHCer d20:1-d17/22:0	667.5	309.4	100	17
DHCer d20:1-d17/22:1	665.5	309.4	100	17
DHCer d20:1-d17/22:1-d17	682.5	309.4	100	17
DHCer d20:1-d17/23:0	681.5	309.4	100	17
DHCer d20:1-d17/24:0	695.5	309.4	100	17
DHCer d20:1-d17/24:1	693.5	309.4	100	17
DHCer d20:1-d17/24:1-d17	710.5	309.4	100	17
DHCer d20:1-d17/25:0	709.5	309.4	100	17
DHCer d20:1-d17/26:0	723.5	309.4	100	17
DHCer d20:1-d17/26:1	721.5	309.4	100	17
DHCer d20:1-d17/26:1-d17	738.5	309.4	100	17
DHCer d20:1-d9/12:0	519.5	301.4	100	17
DHCer d20:1-d9/14:0	547.5	301.4	100	17
DHCer d20:1-d9/15:0	561.5	301.4	100	17
DHCer d20:1-d9/16:0	575.5	301.4	100	17
DHCer d20:1-d9/16:1	573.5	301.4	100	17
DHCer d20:1-d9/16:1-d9	582.5	301.4	100	17
DHCer d20:1-d9/17:0	589.5	301.4	100	17
DHCer d20:1-d9/18:0	603.5	301.4	100	17
DHCer d20:1-d9/18:1	601.5	301.4	100	17

Table S3.1 Lipid multiple reaction monitoring (MRMs), collision energies, and fragmentor voltages for LC-MS.

Lipid Species	Precursor Ion	Product Ion	Fragmentor (V)	CE (V)
DHCer d20:1-d9/18:1-d9	610.5	301.4	100	17
DHCer d20:1-d9/19:0	617.5	301.4	100	17
DHCer d20:1-d9/20:0	631.5	301.4	100	17
DHCer d20:1-d9/20:1	629.5	301.4	100	17
DHCer d20:1-d9/20:1-d9	638.5	301.4	100	17
DHCer d20:1-d9/21:0	645.5	301.4	100	17
DHCer d20:1-d9/22:0	659.5	301.4	100	17
DHCer d20:1-d9/22:1	657.5	301.4	100	17
DHCer d20:1-d9/22:1-d9	666.5	301.4	100	17
DHCer d20:1-d9/23:0	673.5	301.4	100	17
DHCer d20:1-d9/24:0	687.5	301.4	100	17
DHCer d20:1-d9/24:1	685.5	301.4	100	17
DHCer d20:1-d9/24:1-d9	694.5	301.4	100	17
DHCer d20:1-d9/25:0	701.5	301.4	100	17
DHCer d20:1-d9/26:0	715.5	301.4	100	17
DHCer d20:1-d9/26:1	713.5	301.4	100	17
DHCer d20:1-d9/26:1-d9	722.5	301.4	100	17
Cer d18:1-d7/15:0	531.5	271.4	110	25
Cer d18:1/12:0	482.5	264.4	110	25
Cer d18:1/14:0	510.5	264.4	110	25
Cer d18:1/15:0	524.5	264.4	110	25
Cer d18:1/16:0	538.5	264.4	110	25
Cer d18:1/16:1	536.5	264.4	110	25
Cer d18:1/16:1-d17	553.5	264.4	110	25
Cer d18:1/16:1-d9	545.5	264.4	110	25
Cer d18:1/17:0	552.5	264.4	110	25

Table S3.1 Lipid multiple reaction monitoring (MRMs), collision energies, and fragmentor voltages for LC-MS.

Lipid Species	Precursor Ion	Product Ion	Fragmentor (V)	CE (V)
Cer d18:1/18:0	566.6	264.4	110	25
Cer d18:1/18:1	564.5	264.4	110	25
Cer d18:1/18:1-d17	581.5	264.4	110	25
Cer d18:1/18:1-d9	573.5	264.4	110	25
Cer d18:1/18:1-d9	571.5	264.4	110	25
Cer d18:1/19:0	580.6	264.4	110	25
Cer d18:1/20:0	594.6	264.4	110	25
Cer d18:1/20:1	592.6	264.4	110	25
Cer d18:1/20:1-d17	609.6	264.4	110	25
Cer d18:1/20:1-d9	601.6	264.4	110	25
Cer d18:1/21:0	608.6	264.4	110	25
Cer d18:1/22:0	622.6	264.4	110	25
Cer d18:1/22:1	620.6	264.4	110	25
Cer d18:1/22:1-d17	637.6	264.4	110	25
Cer d18:1/22:1-d9	629.6	264.4	110	25
Cer d18:1/23:0	636.6	264.4	110	25
Cer d18:1/24:0	650.6	264.4	110	25
Cer d18:1/24:1	648.6	264.4	110	25
Cer d18:1/24:1-d17	665.6	264.4	110	25
Cer d18:1/24:1-d9	657.6	264.4	110	25
Cer d18:1/25:0	664.7	264.4	110	25
Cer d18:1/26:0	678.7	264.4	110	25
Cer d18:1/26:1	676.7	264.4	110	25
Cer d18:1/26:1-d17	693.7	264.4	110	25
Cer d18:1/26:1-d9	685.7	264.4	110	25
Cer d20:1/12:0	510.5	292.4	110	25

Table S3.1 Lipid multiple reaction monitoring (MRMs), collision energies, and fragmentor voltages for LC-MS.

Lipid Species	Precursor Ion	Product Ion	Fragmentor (V)	CE (V)
Cer d20:1/14:0	538.5	292.4	110	25
Cer d20:1/15:0	552.5	292.4	110	25
Cer d20:1/16:0	566.6	292.4	110	25
Cer d20:1/16:1	564.6	292.4	110	25
Cer d20:1/16:1-d17	581.6	292.4	110	25
Cer d20:1/16:1-d9	573.6	292.4	110	25
Cer d20:1/17:0	580.6	292.4	110	25
Cer d20:1/18:0	594.6	292.4	110	25
Cer d20:1/18:1	592.6	292.4	110	25
Cer d20:1/18:1-d17	609.6	292.4	110	25
Cer d20:1/18:1-d9	601.6	292.4	110	25
Cer d20:1/19:0	608.6	292.4	110	25
Cer d20:1/20:0	622.6	292.4	110	25
Cer d20:1/20:1	620.6	292.4	110	25
Cer d20:1/20:1-d17	637.6	292.4	110	25
Cer d20:1/20:1-d9	629.6	292.4	110	25
Cer d20:1/21:0	636.6	292.4	110	25
Cer d20:1/22:0	650.6	292.4	110	25
Cer d20:1/22:1	648.6	292.4	110	25
Cer d20:1/22:1-d17	665.6	292.4	110	25
Cer d20:1/22:1-d9	657.6	292.4	110	25
Cer d20:1/23:0	664.7	292.4	110	25
Cer d20:1/24:0	678.7	292.4	110	25
Cer d20:1/24:1	676.7	292.4	110	25
Cer d20:1/24:1-d17	693.7	292.4	110	25
Cer d20:1/24:1-d9	685.7	292.4	110	25

Table S3.1 Lipid multiple reaction monitoring (MRMs), collision energies, and fragmentor voltages for LC-MS.

Lipid Species	Precursor Ion	Product Ion	Fragmentor (V)	CE (V)
Cer d20:1/25:0	692.7	292.4	110	25
Cer d20:1/26:0	706.7	292.4	110	25
Cer d20:1/26:1	704.7	292.4	110	25
Cer d20:1/26:1-d17	721.7	292.4	110	25
Cer d20:1/26:1-d9	713.7	292.4	110	25
Cer d20:2/12:0	508.5	290.4	110	25
Cer d20:2/14:0	536.5	290.4	110	25
Cer d20:2/15:0	550.5	290.4	110	25
Cer d20:2/16:0	564.5	290.4	110	25
Cer d20:2/16:1	562.5	290.4	110	25
Cer d20:2/17:0	578.6	290.4	110	25
Cer d20:2/18:0	592.6	290.4	110	25
Cer d20:2/18:1	590.6	290.4	110	25
Cer d20:2/19:0	606.6	290.4	110	25
Cer d20:2/20:0	620.6	290.4	110	25
Cer d20:2/20:1	618.6	290.4	110	25
Cer d20:2/21:0	634.6	290.4	110	25
Cer d20:2/22:0	648.6	290.4	110	25
Cer d20:2/22:1	646.6	290.4	110	25
Cer d20:2/23:0	662.6	290.4	110	25
Cer d20:2/24:0	676.7	290.4	110	25
Cer d20:2/24:1	674.6	290.4	110	25
Cer d20:2/25:0	690.7	290.4	110	25
Cer d20:2/26:0	704.7	290.4	110	25
Cer d20:2/26:0	702.7	290.4	110	25
Cer d20:2-d17/12:0	525.5	307.4	110	25

Table S3.1 Lipid multiple reaction monitoring (MRMs), collision energies, and fragmentor voltages for LC-MS.

Lipid Species	Precursor Ion	Product Ion	Fragmentor (V)	CE (V)
Cer d20:2-d17/14:0	553.5	307.4	110	25
Cer d20:2-d17/15:0	567.5	307.4	110	25
Cer d20:2-d17/16:0	581.5	307.4	110	25
Cer d20:2-d17/16:1	579.5	307.4	110	25
Cer d20:2-d17/16:1-d17	596.5	307.4	110	25
Cer d20:2-d17/17:0	595.6	307.4	110	25
Cer d20:2-d17/18:0	609.6	307.4	110	25
Cer d20:2-d17/18:1	607.6	307.4	110	25
Cer d20:2-d17/18:1-d17	624.6	307.4	110	25
Cer d20:2-d17/19:0	623.6	307.4	110	25
Cer d20:2-d17/20:0	637.6	307.4	110	25
Cer d20:2-d17/20:1	635.6	307.4	110	25
Cer d20:2-d17/20:1-d17	652.6	307.4	110	25
Cer d20:2-d17/21:0	651.6	307.4	110	25
Cer d20:2-d17/22:0	665.6	307.4	110	25
Cer d20:2-d17/22:1	663.6	307.4	110	25
Cer d20:2-d17/22:1-d17	680.6	307.4	110	25
Cer d20:2-d17/23:0	679.6	307.4	110	25
Cer d20:2-d17/24:0	693.6	307.4	110	25
Cer d20:2-d17/24:1	691.6	307.4	110	25
Cer d20:2-d17/24:1-d17	708.6	307.4	110	25
Cer d20:2-d17/25:0	707.6	307.4	110	25
Cer d20:2-d17/26:0	721.6	307.4	110	25
Cer d20:2-d17/26:1	719.6	307.4	110	25
Cer d20:2-d17/26:1-d17	736.6	307.4	110	25
Cer d20:2-d9/12:0	517.5	299.4	110	25

Table S3.1 Lipid multiple reaction monitoring (MRMs), collision energies, and fragmentor voltages for LC-MS.

Lipid Species	Precursor Ion	Product Ion	Fragmentor (V)	CE (V)
Cer d20:2-d9/14:0	545.5	299.4	110	25
Cer d20:2-d9/15:0	559.5	299.4	110	25
Cer d20:2-d9/16:0	573.5	299.4	110	25
Cer d20:2-d9/16:1	571.5	299.4	110	25
Cer d20:2-d9/16:1-d9	580.5	299.4	110	25
Cer d20:2-d9/17:0	587.5	299.4	110	25
Cer d20:2-d9/18:0	601.6	299.4	110	25
Cer d20:2-d9/18:1	599.6	299.4	110	25
Cer d20:2-d9/18:1-d9	608.6	299.4	110	25
Cer d20:2-d9/19:0	615.6	299.4	110	25
Cer d20:2-d9/20:0	629.6	299.4	110	25
Cer d20:2-d9/20:1	627.6	299.4	110	25
Cer d20:2-d9/20:1-d9	636.6	299.4	110	25
Cer d20:2-d9/21:0	643.6	299.4	110	25
Cer d20:2-d9/22:0	657.6	299.4	110	25
Cer d20:2-d9/22:1	655.6	299.4	110	25
Cer d20:2-d9/22:1-d9	664.6	299.4	110	25
Cer d20:2-d9/23:0	671.6	299.4	110	25
Cer d20:2-d9/24:0	685.6	299.4	110	25
Cer d20:2-d9/24:1	683.6	299.4	110	25
Cer d20:2-d9/24:1-d9	692.6	299.4	110	25
Cer d20:2-d9/25:0	699.6	299.4	110	25
Cer d20:2-d9/26:0	713.6	299.4	110	25
Cer d20:2-d9/26:1	711.6	299.4	110	25
Cer d20:2-d9/26:1-d9	720.6	299.4	110	25
SDiene d18:2/12:0	480.5	262.4	110	25

Table S3.1 Lipid multiple reaction monitoring (MRMs), collision energies, and fragmentor voltages for LC-MS.

Lipid Species	Precursor Ion	Product Ion	Fragmentor (V)	CE (V)
SDiene d18:2/14:0	508.5	262.4	110	25
SDiene d18:2/15:0	522.5	262.4	110	25
SDiene d18:2/16:0	536.5	262.4	110	25
SDiene d18:2/16:1	534.5	262.4	110	25
SDiene d18:2/16:1-d17	551.5	262.4	110	25
SDiene d18:2/16:1-d9	543.5	262.4	110	25
SDiene d18:2/17:0	550.5	262.4	110	25
SDiene d18:2/18:0	564.6	262.4	110	25
SDiene d18:2/18:1	562.5	262.4	110	25
SDiene d18:2/18:1-d17	579.5	262.4	110	25
SDiene d18:2/18:1-d9	571.5	262.4	110	25
SDiene d18:2/19:0	578.6	262.4	110	25
SDiene d18:2/20:0	592.6	262.4	110	25
SDiene d18:2/20:1	590.6	262.4	110	25
SDiene d18:2/20:1-d17	607.6	262.4	110	25
SDiene d18:2/20:1-d9	599.6	262.4	110	25
SDiene d18:2/21:0	606.6	262.4	110	25
SDiene d18:2/22:0	620.6	262.4	110	25
SDiene d18:2/22:1	618.6	262.4	110	25
SDiene d18:2/22:1-d17	635.6	262.4	110	25
SDiene d18:2/22:1-d9	627.6	262.4	110	25
SDiene d18:2/23:0	634.6	262.4	110	25
SDiene d18:2/24:0	648.6	262.4	110	25
SDiene d18:2/24:1	646.6	262.4	110	25
SDiene d18:2/24:1-d17	663.6	262.4	110	25
SDiene d18:2/24:1-d9	655.6	262.4	110	25

Table S3.1 Lipid multiple reaction monitoring (MRMs), collision energies, and fragmentor voltages for LC-MS.

Lipid Species	Precursor Ion	Product Ion	Fragmentor (V)	CE (V)
SDiene d18:2/25:0	662.7	262.4	110	25
SDiene d18:2/26:0	676.7	262.4	110	25
SDiene d18:2/26:1	674.7	262.4	110	25
SDiene d18:2/26:1-d17	691.7	262.4	110	25
SDiene d18:2/26:1-d9	683.7	262.4	110	25
Gluc/Gal-Cer d18:1-d7/15:0	693.6	271.2	123	37
Gluc/Gal-Cer d18:1/12:0	644.5	264.4	123	37
Gluc/Gal-Cer d18:1/14:0	672.5	264.4	123	37
Gluc/Gal-Cer d18:1/15:0	686.6	264.4	123	37
Gluc/Gal-Cer d18:1/16:0	700.6	264.4	123	37
Gluc/Gal-Cer d18:1/16:1	698.6	264.4	123	37
Gluc/Gal-Cer d18:1/16:1-d17	715.6	264.4	123	37
Gluc/Gal-Cer d18:1/16:1-d9	707.6	264.4	123	37
Gluc/Gal-Cer d18:1/17:0	714.6	264.4	123	37
Gluc/Gal-Cer d18:1/18:0	728.6	264.4	123	37
Gluc/Gal-Cer d18:1/18:1	726.6	264.4	123	37
Gluc/Gal-Cer d18:1/18:1-d17	743.6	264.4	123	37
Gluc/Gal-Cer d18:1/18:1-d9	735.6	264.4	123	37
Gluc/Gal-Cer d18:1/19:0	742.6	264.4	123	37
Gluc/Gal-Cer d18:1/20:0	756.6	264.4	123	37
Gluc/Gal-Cer d18:1/20:1	754.6	264.4	123	37
Gluc/Gal-Cer d18:1/20:1-d17	771.6	264.4	123	37
Gluc/Gal-Cer d18:1/20:1-d9	763.6	264.4	123	37
Gluc/Gal-Cer d18:1/21:0	770.7	264.4	123	37
Gluc/Gal-Cer d18:1/22:0	784.7	264.4	123	37
Gluc/Gal-Cer d18:1/22:1	782.7	264.4	123	37

Table S3.1 Lipid multiple reaction monitoring (MRMs), collision energies, and fragmentor voltages for LC-MS.

Lipid Species	Precursor Ion	Product Ion	Fragmentor (V)	CE (V)
Gluc/Gal-Cer d18:1/22:1-d17	799.7	264.4	123	37
Gluc/Gal-Cer d18:1/22:1-d9	791.7	264.4	123	37
Gluc/Gal-Cer d18:1/23:0	798.7	264.4	123	37
Gluc/Gal-Cer d18:1/24:0	812.7	264.4	123	37
Gluc/Gal-Cer d18:1/24:1	810.7	264.4	123	37
Gluc/Gal-Cer d18:1/24:1-d17	827.7	264.4	123	37
Gluc/Gal-Cer d18:1/24:1-d9	819.7	264.4	123	37
Gluc/Gal-Cer d18:1/25:0	826.7	264.4	123	37
Gluc/Gal-Cer d18:1/26:0	840.7	264.4	123	37
Gluc/Gal-Cer d18:1/26:1	838.7	264.4	123	37
Gluc/Gal-Cer d18:1/26:1-d17	855.7	264.4	123	37
Gluc/Gal-Cer d18:1/26:1-d9	847.7	264.4	123	37
Gluc/Gal-Cer d20:1/12:0	672.5	292.4	123	37
Gluc/Gal-Cer d20:1/14:0	700.6	292.4	123	37
Gluc/Gal-Cer d20:1/15:0	714.6	292.4	123	37
Gluc/Gal-Cer d20:1/16:0	728.6	292.4	123	37
Gluc/Gal-Cer d20:1/16:1	726.6	292.4	123	37
Gluc/Gal-Cer d20:1/16:1-d17	743.6	292.4	123	37
Gluc/Gal-Cer d20:1/16:1-d9	735.6	292.4	123	37
Gluc/Gal-Cer d20:1/17:0	742.6	292.4	123	37
Gluc/Gal-Cer d20:1/18:0	756.6	292.4	123	37
Gluc/Gal-Cer d20:1/18:1	754.6	292.4	123	37
Gluc/Gal-Cer d20:1/18:1-d17	771.6	292.4	123	37
Gluc/Gal-Cer d20:1/18:1-d9	763.6	292.4	123	37
Gluc/Gal-Cer d20:1/19:0	770.7	292.4	123	37
Gluc/Gal-Cer d20:1/20:0	784.7	292.4	123	37

Table S3.1 Lipid multiple reaction monitoring (MRMs), collision energies, and fragmentor voltages for LC-MS.

Lipid Species	Precursor Ion	Product Ion	Fragmentor (V)	CE (V)
Gluc/Gal-Cer d20:1/20:1	782.7	292.4	123	37
Gluc/Gal-Cer d20:1/20:1-d17	799.7	292.4	123	37
Gluc/Gal-Cer d20:1/20:1-d9	791.7	292.4	123	37
Gluc/Gal-Cer d20:1/21:0	798.7	292.4	123	37
Gluc/Gal-Cer d20:1/22:0	812.7	292.4	123	37
Gluc/Gal-Cer d20:1/22:1	810.7	292.4	123	37
Gluc/Gal-Cer d20:1/22:1-d17	827.7	292.4	123	37
Gluc/Gal-Cer d20:1/22:1-d9	819.7	292.4	123	37
Gluc/Gal-Cer d20:1/23:0	826.7	292.4	123	37
Gluc/Gal-Cer d20:1/24:0	840.7	292.4	123	37
Gluc/Gal-Cer d20:1/24:1	838.7	292.4	123	37
Gluc/Gal-Cer d20:1/24:1-d17	855.7	292.4	123	37
Gluc/Gal-Cer d20:1/24:1-d9	847.7	292.4	123	37
Gluc/Gal-Cer d20:1/25:0	854.7	292.4	123	37
Gluc/Gal-Cer d20:1/26:0	868.8	292.4	123	37
Gluc/Gal-Cer d20:1/26:1	866.7	292.4	123	37
Gluc/Gal-Cer d20:1/26:1-d17	883.7	292.4	123	37
Gluc/Gal-Cer d20:1/26:1-d9	875.7	292.4	123	37
Gluc/Gal-Cer d20:2/12:0	670.5	290.4	123	37
Gluc/Gal-Cer d20:2/14:0	698.6	290.4	123	37
Gluc/Gal-Cer d20:2/15:0	712.6	290.4	123	37
Gluc/Gal-Cer d20:2/16:0	726.6	290.4	123	37
Gluc/Gal-Cer d20:2/16:1	724.6	290.4	123	37
Gluc/Gal-Cer d20:2/17:0	740.6	290.4	123	37
Gluc/Gal-Cer d20:2/18:0	754.6	290.4	123	37
Gluc/Gal-Cer d20:2/18:1	752.6	290.4	123	37

Table S3.1 Lipid multiple reaction monitoring (MRMs), collision energies, and fragmentor voltages for LC-MS.

Lipid Species	Precursor Ion	Product Ion	Fragmentor (V)	CE (V)
Gluc/Gal-Cer d20:2/19:0	768.6	290.4	123	37
Gluc/Gal-Cer d20:2/20:0	782.7	290.4	123	37
Gluc/Gal-Cer d20:2/20:1	780.6	290.4	123	37
Gluc/Gal-Cer d20:2/21:0	796.7	290.4	123	37
Gluc/Gal-Cer d20:2/22:0	810.7	290.4	123	37
Gluc/Gal-Cer d20:2/22:1	808.7	290.4	123	37
Gluc/Gal-Cer d20:2/23:0	824.7	290.4	123	37
Gluc/Gal-Cer d20:2/24:0	838.7	290.4	123	37
Gluc/Gal-Cer d20:2/24:1	836.7	290.4	123	37
Gluc/Gal-Cer d20:2/25:0	852.7	290.4	123	37
Gluc/Gal-Cer d20:2/26:0	866.7	290.4	123	37
Gluc/Gal-Cer d20:2/26:1	864.7	290.4	123	37
Gluc/Gal-Cer d20:2-d17/12:0	687.5	307.4	123	37
Gluc/Gal-Cer d20:2-d17/14:0	715.5	307.4	123	37
Gluc/Gal-Cer d20:2-d17/15:0	729.6	307.4	123	37
Gluc/Gal-Cer d20:2-d17/16:0	743.6	307.4	123	37
Gluc/Gal-Cer d20:2-d17/16:1	741.6	307.4	123	37
Gluc/Gal-Cer d20:2-d17/16:1-d17	758.6	307.4	123	37
Gluc/Gal-Cer d20:2-d17/17:0	757.6	307.4	123	37
Gluc/Gal-Cer d20:2-d17/18:0	771.6	307.4	123	37
Gluc/Gal-Cer d20:2-d17/18:1	769.6	307.4	123	37
Gluc/Gal-Cer d20:2-d17/18:1-d17	786.6	307.4	123	37
Gluc/Gal-Cer d20:2-d17/19:0	785.6	307.4	123	37
Gluc/Gal-Cer d20:2-d17/20:0	799.6	307.4	123	37
Gluc/Gal-Cer d20:2-d17/20:1	797.6	307.4	123	37

Table S3.1 Lipid multiple reaction monitoring (MRMs), collision energies, and fragmentor voltages for LC-MS.

Lipid Species	Precursor Ion	Product Ion	Fragmentor (V)	CE (V)
Gluc/Gal-Cer d20:2-d17/20:1-d17	814.6	307.4	123	37
Gluc/Gal-Cer d20:2-d17/21:0	813.6	307.4	123	37
Gluc/Gal-Cer d20:2-d17/22:0	827.7	307.4	123	37
Gluc/Gal-Cer d20:2-d17/22:1	825.6	307.4	123	37
Gluc/Gal-Cer d20:2-d17/22:1-d17	842.7	307.4	123	37
Gluc/Gal-Cer d20:2-d17/23:0	841.7	307.4	123	37
Gluc/Gal-Cer d20:2-d17/24:0	855.7	307.4	123	37
Gluc/Gal-Cer d20:2-d17/24:1	853.7	307.4	123	37
Gluc/Gal-Cer d20:2-d17/24:1-d17	870.7	307.4	123	37
Gluc/Gal-Cer d20:2-d17/25:0	869.7	307.4	123	37
Gluc/Gal-Cer d20:2-d17/26:0	883.7	307.4	123	37
Gluc/Gal-Cer d20:2-d17/26:1	881.7	307.4	123	37
Gluc/Gal-Cer d20:2-d17/26:1-d17	898.7	307.4	123	37
Gluc/Gal-Cer d20:2-d9/12:0	679.5	299.4	123	37
Gluc/Gal-Cer d20:2-d9/14:0	707.5	299.4	123	37
Gluc/Gal-Cer d20:2-d9/15:0	721.5	299.4	123	37
Gluc/Gal-Cer d20:2-d9/16:0	735.6	299.4	123	37
Gluc/Gal-Cer d20:2-d9/16:1	733.6	299.4	123	37
Gluc/Gal-Cer d20:2-d9/16:1-d9	742.6	299.4	123	37
Gluc/Gal-Cer d20:2-d9/17:0	749.6	299.4	123	37
Gluc/Gal-Cer d20:2-d9/18:0	763.6	299.4	123	37
Gluc/Gal-Cer d20:2-d9/18:1	761.6	299.4	123	37
Gluc/Gal-Cer d20:2-d9/18:1-d9	770.6	299.4	123	37
Gluc/Gal-Cer d20:2-d9/19:0	777.6	299.4	123	37
Gluc/Gal-Cer d20:2-d9/20:0	791.6	299.4	123	37

Table S3.1 Lipid multiple reaction monitoring (MRMs), collision energies, and fragmentor voltages for LC-MS.

Lipid Species	Precursor Ion	Product Ion	Fragmentor (V)	CE (V)
Gluc/Gal-Cer d20:2-d9/20:1	789.6	299.4	123	37
Gluc/Gal-Cer d20:2-d9/20:1-d9	798.6	299.4	123	37
Gluc/Gal-Cer d20:2-d9/21:0	805.7	299.4	123	37
Gluc/Gal-Cer d20:2-d9/22:0	819.7	299.4	123	37
Gluc/Gal-Cer d20:2-d9/22:1	817.7	299.4	123	37
Gluc/Gal-Cer d20:2-d9/22:1-d9	826.7	299.4	123	37
Gluc/Gal-Cer d20:2-d9/23:0	833.7	299.4	123	37
Gluc/Gal-Cer d20:2-d9/24:0	847.7	299.4	123	37
Gluc/Gal-Cer d20:2-d9/24:1	845.7	299.4	123	37
Gluc/Gal-Cer d20:2-d9/24:1-d9	854.7	299.4	123	37
Gluc/Gal-Cer d20:2-d9/25:0	861.7	299.4	123	37
Gluc/Gal-Cer d20:2-d9/26:0	875.7	299.4	123	37
Gluc/Gal-Cer d20:2-d9/26:1	873.7	299.4	123	37
Gluc/Gal-Cer d20:2-d9/26:1-d9	882.7	299.4	123	37
Lact-Cer d18:1-d7/15:0	855.7	271.2	88	41
Lact-Cer d18:1/12:0	806.6	264.4	88	41
Lact-Cer d18:1/14:0	834.6	264.4	88	41
Lact-Cer d18:1/15:0	848.6	264.4	88	41
Lact-Cer d18:1/16:0	862.6	264.4	88	41
Lact-Cer d18:1/16:1	860.6	264.4	88	41
Lact-Cer d18:1/16:1-d17	877.6	264.4	88	41
Lact-Cer d18:1/16:1-d9	869.6	264.4	88	41
Lact-Cer d18:1/17:0	876.6	264.4	88	41
Lact-Cer d18:1/18:0	890.7	264.4	88	41
Lact-Cer d18:1/18:1	888.6	264.4	88	41
Lact-Cer d18:1/18:1-d17	905.6	264.4	88	41

Table S3.1 Lipid multiple reaction monitoring (MRMs), collision energies, and fragmentor voltages for LC-MS.

Lipid Species	Precursor Ion	Product Ion	Fragmentor (V)	CE (V)
Lact-Cer d18:1/18:1-d9	897.6	264.4	88	41
Lact-Cer d18:1/19:0	904.7	264.4	88	41
Lact-Cer d18:1/20:0	918.7	264.4	88	41
Lact-Cer d18:1/20:1	916.7	264.4	88	41
Lact-Cer d18:1/20:1-d17	933.7	264.4	88	41
Lact-Cer d18:1/20:1-d9	925.7	264.4	88	41
Lact-Cer d18:1/21:0	932.7	264.4	88	41
Lact-Cer d18:1/22:0	946.7	264.4	88	41
Lact-Cer d18:1/22:1	944.7	264.4	88	41
Lact-Cer d18:1/22:1-d17	961.7	264.4	88	41
Lact-Cer d18:1/22:1-d9	953.7	264.4	88	41
Lact-Cer d18:1/23:0	960.7	264.4	88	41
Lact-Cer d18:1/24:0	974.8	264.4	88	41
Lact-Cer d18:1/24:1	972.7	264.4	88	41
Lact-Cer d18:1/24:1-d17	989.7	264.4	88	41
Lact-Cer d18:1/24:1-d9	981.7	264.4	88	41
Lact-Cer d18:1/25:0	988.8	264.4	88	41
Lact-Cer d18:1/26:0	1002.8	264.4	88	41
Lact-Cer d18:1/26:1	1000.8	264.4	88	41
Lact-Cer d18:1/26:1-d17	1017.8	264.4	88	41
Lact-Cer d18:1/26:1-d9	1009.8	264.4	88	41
Lact-Cer d20:1/12:0	834.6	292.4	88	41
Lact-Cer d20:1/14:0	862.6	292.4	88	41
Lact-Cer d20:1/15:0	876.6	292.4	88	41
Lact-Cer d20:1/16:0	890.7	292.4	88	41
Lact-Cer d20:1/16:1	888.6	292.4	88	41

Table S3.1 Lipid multiple reaction monitoring (MRMs), collision energies, and fragmentor voltages for LC-MS.

Lipid Species	Precursor Ion	Product Ion	Fragmentor (V)	CE (V)
Lact-Cer d20:1/16:1-d17	905.6	292.4	88	41
Lact-Cer d20:1/16:1-d9	897.6	292.4	88	41
Lact-Cer d20:1/17:0	904.7	292.4	88	41
Lact-Cer d20:1/18:0	918.7	292.4	88	41
Lact-Cer d20:1/18:1	916.7	292.4	88	41
Lact-Cer d20:1/18:1-d17	933.7	292.4	88	41
Lact-Cer d20:1/18:1-d9	925.7	292.4	88	41
Lact-Cer d20:1/19:0	932.7	292.4	88	41
Lact-Cer d20:1/20:0	946.7	292.4	88	41
Lact-Cer d20:1/20:1	944.7	292.4	88	41
Lact-Cer d20:1/20:1-d17	961.7	292.4	88	41
Lact-Cer d20:1/20:1-d9	953.7	292.4	88	41
Lact-Cer d20:1/21:0	960.7	292.4	88	41
Lact-Cer d20:1/22:0	974.8	292.4	88	41
Lact-Cer d20:1/22:1	972.7	292.4	88	41
Lact-Cer d20:1/22:1-d17	989.7	292.4	88	41
Lact-Cer d20:1/22:1-d9	981.7	292.4	88	41
Lact-Cer d20:1/23:0	988.8	292.4	88	41
Lact-Cer d20:1/24:0	1002.8	292.4	88	41
Lact-Cer d20:1/24:1	1000.8	292.4	88	41
Lact-Cer d20:1/24:1-d17	1017.8	292.4	88	41
Lact-Cer d20:1/24:1-d9	1009.8	292.4	88	41
Lact-Cer d20:1/25:0	1016.8	292.4	88	41
Lact-Cer d20:1/26:0	1030.8	292.4	88	41
Lact-Cer d20:1/26:1	1028.8	292.4	88	41
Lact-Cer d20:1/26:1-d17	1045.8	292.4	88	41

Table S3.1 Lipid multiple reaction monitoring (MRMs), collision energies, and fragmentor voltages for LC-MS.

Lipid Species	Precursor Ion	Product Ion	Fragmentor (V)	CE (V)
Lact-Cer d20:1/26:1-d9	1037.8	292.4	88	41
Lact-Cer d20:2/12:0	832.6	290.4	88	41
Lact-Cer d20:2/14:0	860.6	290.4	88	41
Lact-Cer d20:2/15:0	874.6	290.4	88	41
Lact-Cer d20:2/16:0	888.6	290.4	88	41
Lact-Cer d20:2/16:1	886.6	290.4	88	41
Lact-Cer d20:2/17:0	902.7	290.4	88	41
Lact-Cer d20:2/18:0	916.7	290.4	88	41
Lact-Cer d20:2/18:1	914.7	290.4	88	41
Lact-Cer d20:2/19:0	930.7	290.4	88	41
Lact-Cer d20:2/20:0	944.7	290.4	88	41
Lact-Cer d20:2/20:1	942.7	290.4	88	41
Lact-Cer d20:2/21:0	958.7	290.4	88	41
Lact-Cer d20:2/22:0	972.7	290.4	88	41
Lact-Cer d20:2/22:1	970.7	290.4	88	41
Lact-Cer d20:2/23:0	986.8	290.4	88	41
Lact-Cer d20:2/24:0	1000.8	290.4	88	41
Lact-Cer d20:2/24:1	998.8	290.4	88	41
Lact-Cer d20:2/25:0	1014.8	290.4	88	41
Lact-Cer d20:2/26:0	1028.8	290.4	88	41
Lact-Cer d20:2/26:1	1026.8	290.4	88	41
Lact-Cer d20:2-d17/12:0	849.6	307.4	88	41
Lact-Cer d20:2-d17/14:0	877.6	307.4	88	41
Lact-Cer d20:2-d17/15:0	891.6	307.4	88	41
Lact-Cer d20:2-d17/16:0	905.6	307.4	88	41
Lact-Cer d20:2-d17/16:1	903.6	307.4	88	41

Table S3.1 Lipid multiple reaction monitoring (MRMs), collision energies, and fragmentor voltages for LC-MS.

Lipid Species	Precursor Ion	Product Ion	Fragmentor (V)	CE (V)
Lact-Cer d20:2-d17/16:1-d17	920.6	307.4	88	41
Lact-Cer d20:2-d17/17:0	919.6	307.4	88	41
Lact-Cer d20:2-d17/18:0	933.7	307.4	88	41
Lact-Cer d20:2-d17/18:1	931.7	307.4	88	41
Lact-Cer d20:2-d17/18:1-d17	948.7	307.4	88	41
Lact-Cer d20:2-d17/19:0	947.7	307.4	88	41
Lact-Cer d20:2-d17/20:0	961.7	307.4	88	41
Lact-Cer d20:2-d17/20:1	959.7	307.4	88	41
Lact-Cer d20:2-d17/20:1-d17	976.7	307.4	88	41
Lact-Cer d20:2-d17/21:0	975.7	307.4	88	41
Lact-Cer d20:2-d17/22:0	989.7	307.4	88	41
Lact-Cer d20:2-d17/22:1	987.7	307.4	88	41
Lact-Cer d20:2-d17/22:1-d17	1004.7	307.4	88	41
Lact-Cer d20:2-d17/23:0	1003.7	307.4	88	41
Lact-Cer d20:2-d17/24:0	1017.7	307.4	88	41
Lact-Cer d20:2-d17/24:1	1015.7	307.4	88	41
Lact-Cer d20:2-d17/24:1-d17	1032.7	307.4	88	41
Lact-Cer d20:2-d17/25:0	1031.8	307.4	88	41
Lact-Cer d20:2-d17/26:0	1045.8	307.4	88	41
Lact-Cer d20:2-d17/26:1	1043.8	307.4	88	41
Lact-Cer d20:2-d17/26:1-d17	1060.8	307.4	88	41
Lact-Cer d20:2-d9/12:0	841.6	299.4	88	41
Lact-Cer d20:2-d9/14:0	869.6	299.4	88	41
Lact-Cer d20:2-d9/15:0	883.6	299.4	88	41
Lact-Cer d20:2-d9/16:0	897.6	299.4	88	41
Lact-Cer d20:2-d9/16:1	895.6	299.4	88	41

Table S3.1 Lipid multiple reaction monitoring (MRMs), collision energies, and fragmentor voltages for LC-MS.

Lipid Species	Precursor Ion	Product Ion	Fragmentor (V)	CE (V)
Lact-Cer d20:2-d9/16:1-d9	904.6	299.4	88	41
Lact-Cer d20:2-d9/17:0	911.7	299.4	88	41
Lact-Cer d20:2-d9/18:0	925.7	299.4	88	41
Lact-Cer d20:2-d9/18:1	923.7	299.4	88	41
Lact-Cer d20:2-d9/18:1-d9	932.7	299.4	88	41
Lact-Cer d20:2-d9/19:0	939.7	299.4	88	41
Lact-Cer d20:2-d9/20:0	953.7	299.4	88	41
Lact-Cer d20:2-d9/20:1	951.7	299.4	88	41
Lact-Cer d20:2-d9/20:1-d9	960.7	299.4	88	41
Lact-Cer d20:2-d9/21:0	967.7	299.4	88	41
Lact-Cer d20:2-d9/22:0	981.7	299.4	88	41
Lact-Cer d20:2-d9/22:1	979.7	299.4	88	41
Lact-Cer d20:2-d9/22:1-d9	988.7	299.4	88	41
Lact-Cer d20:2-d9/23:0	995.8	299.4	88	41
Lact-Cer d20:2-d9/24:0	1009.8	299.4	88	41
Lact-Cer d20:2-d9/24:1	1007.8	299.4	88	41
Lact-Cer d20:2-d9/24:1-d9	1016.8	299.4	88	41
Lact-Cer d20:2-d9/25:0	1023.8	299.4	88	41
Lact-Cer d20:2-d9/26:0	1037.8	299.4	88	41
Lact-Cer d20:2-d9/26:1	1035.8	299.4	88	41
Lact-Cer d20:2-d9/26:1-d9	1044.8	299.4	88	41
SM (d18:1/18:1)-d9	738.6	193	82	25
SM d18:1/18:1-d9	738.6	184	82	25
SM 30:0	649.5	184	82	25
SM 30:1	647.5	184	82	25
SM 30:1-d17	664.5	184	82	25

Table S3.1 Lipid multiple reaction monitoring (MRMs), collision energies, and fragmentor voltages for LC-MS.

Lipid Species	Precursor Ion	Product Ion	Fragmentor (V)	CE (V)
SM 30:1-d9	656.5	184	82	25
SM 32:0	677.6	184	82	25
SM 32:1	675.5	184	82	25
SM 32:1-d17	692.5	184	82	25
SM 32:1-d9	684.5	184	82	25
SM 32:2	673.5	184	82	25
SM 32:2-d17	690.5	184	82	25
SM 32:2-d18	691.5	184	82	25
SM 32:2-d34	707.5	184	82	25
SM 32:2-d9	682.5	184	82	25
SM 32:3	671.5	184	82	25
SM 32:3-d17	688.5	184	82	25
SM 32:3-d18	689.5	184	82	25
SM 32:3-d34	705.5	184	82	25
SM 32:3-d9	680.5	184	82	25
SM 34:0	705.6	184	82	25
SM 34:1	703.6	184	82	25
SM 34:1-d17	720.6	184	82	25
SM 34:1-d9	712.6	184	82	25
SM 34:2	701.6	184	82	25
SM 34:2-d17	718.6	184	82	25
SM 34:2-d18	719.6	184	82	25
SM 34:2-d34	735.6	184	82	25
SM 34:2-d9	710.6	184	82	25
SM 34:3	699.5	184	82	25
SM 34:3-d17	716.5	184	82	25

Table S3.1 Lipid multiple reaction monitoring (MRMs), collision energies, and fragmentor voltages for LC-MS.

Lipid Species	Precursor Ion	Product Ion	Fragmentor (V)	CE (V)
SM 34:3-d18	717.5	184	82	25
SM 34:3-d34	733.5	184	82	25
SM 34:3-d9	708.5	184	82	25
SM 34:4	697.5	184	82	25
SM 36:0	733.6	184	82	25
SM 36:1	731.6	184	82	25
SM 36:1-d17	748.6	184	82	25
SM 36:1-d9	740.6	184	82	25
SM 36:2	729.6	184	82	25
SM 36:2-d17	746.6	184	82	25
SM 36:2-d18	747.6	184	82	25
SM 36:2-d34	763.6	184	82	25
SM 36:2-d9	738.6	184	82	25
SM 36:3	727.6	184	82	25
SM 36:3-d17	744.6	184	82	25
SM 36:3-d18	745.6	184	82	25
SM 36:3-d34	761.6	184	82	25
SM 36:3-d9	736.6	184	82	25
SM 36:4	725.6	184	82	25
SM 38:0	761.7	184	82	25
SM 38:1	759.6	184	82	25
SM 38:1-d17	776.6	184	82	25
SM 38:1-d9	768.6	184	82	25
SM 38:2	757.6	184	82	25
SM 38:2-d17	774.6	184	82	25
SM 38:2-d18	775.6	184	82	25

Table S3.1 Lipid multiple reaction monitoring (MRMs), collision energies, and fragmentor voltages for LC-MS.

Lipid Species	Precursor Ion	Product Ion	Fragmentor (V)	CE (V)
SM 38:2-d34	791.6	184	82	25
SM 38:2-d9	766.6	184	82	25
SM 38:3	755.6	184	82	25
SM 38:3-d17	772.6	184	82	25
SM 38:3-d18	773.6	184	82	25
SM 38:3-d34	789.6	184	82	25
SM 38:3-d9	764.6	184	82	25
SM 38:4	753.6	184	82	25
SM 40:0	789.7	184	82	25
SM 40:1	787.7	184	82	25
SM 40:1-d17	804.7	184	82	25
SM 40:1-d9	796.7	184	82	25
SM 40:2	785.7	184	82	25
SM 40:2-d17	802.7	184	82	25
SM 40:2-d18	803.7	184	82	25
SM 40:2-d34	819.7	184	82	25
SM 40:2-d9	794.7	184	82	25
SM 40:3	783.6	184	82	25
SM 40:3-d17	800.6	184	82	25
SM 40:3-d18	801.6	184	82	25
SM 40:3-d34	817.6	184	82	25
SM 40:3-d9	792.6	184	82	25
SM 40:4	781.6	184	82	25
SM 42:0	817.7	184	82	25
SM 42:1	815.7	184	82	25
SM 42:1-d17	832.7	184	82	25

Table S3.1 Lipid multiple reaction monitoring (MRMs), collision energies, and fragmentor voltages for LC-MS.

Lipid Species	Precursor Ion	Product Ion	Fragmentor (V)	CE (V)
SM 42:1-d9	824.7	184	82	25
SM 42:2	813.7	184	82	25
SM 42:2-d17	830.7	184	82	25
SM 42:2-d18	831.7	184	82	25
SM 42:2-d34	847.7	184	82	25
SM 42:2-d9	822.7	184	82	25
SM 42:3	811.7	184	82	25
SM 42:3-d17	828.7	184	82	25
SM 42:3-d18	829.7	184	82	25
SM 42:3-d34	845.7	184	82	25
SM 42:3-d9	820.7	184	82	25
SM 42:4	809.7	184	82	25
SM 44:0	845.7	184	82	25
SM 44:1	843.7	184	82	25
SM 44:1-d17	860.7	184	82	25
SM 44:1-d9	852.7	184	82	25
SM 44:2	841.7	184	82	25
SM 44:2-d17	858.7	184	82	25
SM 44:2-d18	859.7	184	82	25
SM 44:2-d34	875.7	184	82	25
SM 44:2-d9	850.7	184	82	25
SM 44:3	839.7	184	82	25
SM 44:3-d17	856.7	184	82	25
SM 44:3-d18	857.7	184	82	25
SM 44:3-d34	873.7	184	82	25
SM 44:3-d9	848.7	184	82	25

Table S3.1 Lipid multiple reaction monitoring (MRMs), collision energies, and fragmentor voltages for LC-MS.

Lipid Species	Precursor Ion	Product Ion	Fragmentor (V)	CE (V)
SM 44:4	837.7	184	82	25
SO d18:1 d7	307.4	289.4	112	9
SO d12:1	216.4	198.4	112	9
SO d14:1	244.4	226.4	112	9
SO d16:1	272.4	254.4	112	9
SO d17:1	286.4	268.4	112	9
SO d18:1	300.4	282.4	112	9
SO d18:2	298.4	280.4	112	9
SO d18:2-d17	315.4	297.4	112	9
SO d18:2-d9	307.4	289.4	112	9
SO d19:1	314.4	296.4	112	9
SO d20:1	328.4	310.4	112	9
SO d20:2	326.4	308.4	112	9
SO d20:2-d17	343.4	325.4	112	9
SO d20:2-d9	335.4	317.4	112	9
SO d22:1	356.4	338.4	112	9
SO d22:2	354.4	336.4	112	9
SO d22:2-d17	371.4	353.4	112	9
SO d22:2-d9	363.4	345.4	112	9
SO d24:1	384.4	366.4	112	9
SO d24:2	382.4	364.4	112	9
SO d24:2-d17	399.4	381.4	112	9
SO d24:2-d9	391.4	373.4	112	9
doxSA-C18:0 d3	289.3	271.5	118	13
doxSA-C18:0	286.4	268.4	118	13
doxDHCer m18:0/14:0	496.4	268.3	104	29

Table S3.1 Lipid multiple reaction monitoring (MRMs), collision energies, and fragmentor voltages for LC-MS.

Lipid Species	Precursor Ion	Product Ion	Fragmentor (V)	CE (V)
doxDHCer m18:0/16:0	524.5	268.3	104	29
doxDHCer m18:0/18:0	552.5	268.3	104	29
doxDHCer m18:0/18:1	550.5	268.3	104	29
doxDHCer m18:0/20:0	580.5	268.3	104	29
doxDHCer m18:0/22:0	608.6	268.3	104	29
doxDHCer m18:0/22:1	606.6	268.3	104	29
doxDHCer m18:0/23:0	622.6	268.3	104	29
doxDHCer m18:0/24:0	636.6	268.3	104	29
doxDHCer m18:0/24:1	634.6	268.3	104	29
doxDHCer m18:0/26:0	664.6	268.3	104	29
doxDHCer m18:0/26:1	662.6	268.3	104	29
LPC 18:1-d7	529.4	184.1	100	40
LPC 14:0	468.3	184.1	100	40
LPC 15:0	482.3	184.1	100	40
LPC 16:0	496.3	184.1	100	40
LPC 16:1	494.3	184.1	100	40
LPC 16:1-d17	511.3	184.1	100	40
LPC 16:1-d9	503.3	184.1	100	40
LPC 17:0	510.3	184.1	100	40
LPC 18:0	524.3	184.1	100	40
LPC 18:1	522.3	184.1	100	40
LPC 18:1-d17	539.3	184.1	100	40
LPC 18:1-d9	531.3	184.1	100	40
LPC 18:2	520.3	184.1	100	40
LPC 18:3	518.3	184.1	100	40
LPC 20:0	552.3	184.1	100	40

Table S3.1 Lipid multiple reaction monitoring (MRMs), collision energies, and fragmentor voltages for LC-MS.

Lipid Species	Precursor Ion	Product Ion	Fragmentor (V)	CE (V)
LPC 20:1	550.3	184.1	100	40
LPC 20:1-d17	567.3	184.1	100	40
LPC 20:1-d9	559.3	184.1	100	40
LPC 20:4	544.3	184.1	100	40
LPC 20:5	542.3	184.1	100	40
LPC 22:0	580.3	184.1	100	40
LPC 22:1	578.3	184.1	100	40
LPC 22:1-d17	595.3	184.1	100	40
LPC 22:1-d9	587.3	184.1	100	40
LPC 22:6	568.3	184.1	100	40
LPE 18:1-d7	487.3	44.05	100	40
LPE 14:0	426.3	44.05	100	40
LPE 15:0	440.3	44.05	100	40
LPE 16:0	454.3	44.05	100	40
LPE 16:1	466.3	44.05	100	40
LPE 16:1-d17	483.3	44.05	100	40
LPE 16:1-d9	475.3	44.05	100	40
LPE 17:0	468.3	44.05	100	40
LPE 18:0	482.3	44.05	100	40
LPE 18:1	480.3	44.05	100	40
LPE 18:1-d17	497.3	44.05	100	40
LPE 18:1-d9	489.3	44.05	100	40
LPE 20:0	510.3	44.05	100	40
LPE 20:1	508.3	44.05	100	40
LPE 20:1-d17	525.3	44.05	100	40
LPE 20:1-d9	517.3	44.05	100	40

Table S3.1 Lipid multiple reaction monitoring (MRMs), collision energies, and fragmentor voltages for LC-MS.

Lipid Species	Precursor Ion	Product Ion	Fragmentor (V)	CE (V)
LPE 20:4	502.3	44.05	100	40
LPE 20:5	500.3	44.05	100	40
LPE 22:0	538.3	44.05	100	40
LPE 22:1	536.3	44.05	100	40
LPE 22:1-d17	553.3	44.05	100	40
LPE 22:1-d9	545.3	44.05	100	40
LPE 22:6	526.3	44.05	100	40
PC 15:0/18:1-d7	753.6	184.1	100	40
PC 32:0	734.6	184.1	100	40
PC 32:1	732.6	184.1	100	40
PC 32:1-d17	749.6	184.1	100	40
PC 32:1-d9	741.6	184.1	100	40
PC 32:2	730.6	184.1	100	40
PC 32:2-18	748.6	184.1	100	40
PC 32:2-34	764.6	184.1	100	40
PC 32:2-d17	747.6	184.1	100	40
PC 32:2-d9	739.6	184.1	100	40
PC 34:0	762.6	184.1	100	40
PC 34:1	760.6	184.1	100	40
PC 34:1-d17	777.6	184.1	100	40
PC 34:1-d9	769.6	184.1	100	40
PC 34:2	758.6	184.1	100	40
PC 34:2-d17	775.6	184.1	100	40
PC 34:2-d18	776.6	184.1	100	40
PC 34:2-d34	792.6	184.1	100	40
PC 34:2-d9	767.6	184.1	100	40

Table S3.1 Lipid multiple reaction monitoring (MRMs), collision energies, and fragmentor voltages for LC-MS.

Lipid Species	Precursor Ion	Product Ion	Fragmentor (V)	CE (V)
PC 34:3	756.6	184.1	100	40
PC 34:3-d17	773.6	184.1	100	40
PC 34:3-d18	774.6	184.1	100	40
PC 34:3-d34	790.6	184.1	100	40
PC 34:3-d9	765.6	184.1	100	40
PC 36:0	790.6	184.1	100	40
PC 36:1	788.6	184.1	100	40
PC 36:1-d17	805.6	184.1	100	40
PC 36:1-d9	797.6	184.1	100	40
PC 36:2	786.6	184.1	100	40
PC 36:2	786.6	184.1	100	40
PC 36:2-d17	803.6	184.1	100	40
PC 36:2-d18	804.6	184.1	100	40
PC 36:2-d34	820.6	184.1	100	40
PC 36:2-d9	795.6	184.1	100	40
PC 36:3	784.6	184.1	100	40
PC 36:3-d17	801.6	184.1	100	40
PC 36:3-d18	802.6	184.1	100	40
PC 36:3-d34	818.6	184.1	100	40
PC 36:3-d9	793.6	184.1	100	40
PC 36:4	782.6	184.1	100	40
PC 36:4-d17	799.6	184.1	100	40
PC 36:4-d18	800.6	184.1	100	40
PC 36:4-d34	816.6	184.1	100	40
PC 36:4-d9	791.6	184.1	100	40
PC 36:5	780.6	184.1	100	40

Table S3.1 Lipid multiple reaction monitoring (MRMs), collision energies, and fragmentor voltages for LC-MS.

Lipid Species	Precursor Ion	Product Ion	Fragmentor (V)	CE (V)
PC 36:5-d17	797.6	184.1	100	40
PC 36:5-d18	798.6	184.1	100	40
PC 36:5-d34	814.6	184.1	100	40
PC 36:5-d9	789.6	184.1	100	40
PC 36:6	778.6	184.1	100	40
PC 36:6-d17	795.6	184.1	100	40
PC 36:6-d18	796.6	184.1	100	40
PC 36:6-d34	812.6	184.1	100	40
PC 36:6-d9	787.6	184.1	100	40
PC 38:0	818.7	184.1	100	40
PC 38:1	816.7	184.1	100	40
PC 38:1-d17	833.7	184.1	100	40
PC 38:1-d9	825.7	184.1	100	40
PC 38:2	814.7	184.1	100	40
PC 38:2-d17	831.6	184.1	100	40
PC 38:2-d18	832.6	184.1	100	40
PC 38:2-d34	848.6	184.1	100	40
PC 38:2-d9	823.6	184.1	100	40
PC 38:3	812.7	184.1	100	40
PC 38:3-d17	829.6	184.1	100	40
PC 38:3-d18	830.6	184.1	100	40
PC 38:3-d34	846.6	184.1	100	40
PC 38:3-d9	821.6	184.1	100	40
PC 38:4	810.7	184.1	100	40
PC 38:4-d17	827.6	184.1	100	40
PC 38:4-d18	828.6	184.1	100	40

Table S3.1 Lipid multiple reaction monitoring (MRMs), collision energies, and fragmentor voltages for LC-MS.

Lipid Species	Precursor Ion	Product Ion	Fragmentor (V)	CE (V)
PC 38:4-d34	844.6	184.1	100	40
PC 38:4-d9	819.6	184.1	100	40
PC 38:5	808.7	184.1	100	40
PC 38:5-d17	825.6	184.1	100	40
PC 38:5-d18	826.6	184.1	100	40
PC 38:5-d34	842.6	184.1	100	40
PC 38:5-d9	817.6	184.1	100	40
PC 38:6	806.7	184.1	100	40
PC 38:6-d17	823.6	184.1	100	40
PC 38:6-d18	824.6	184.1	100	40
PC 38:6-d34	840.6	184.1	100	40
PC 38:6-d9	815.6	184.1	100	40
PC 38:7	804.6	184.1	100	40
PC 38:7-d17	821.6	184.1	100	40
PC 38:7-d18	822.6	184.1	100	40
PC 38:7-d34	838.6	184.1	100	40
PC 38:7-d9	813.6	184.1	100	40
PC 40:0	846.7	184.1	100	40
PC 40:1	844.7	184.1	100	40
PC 40:1-d17	861.7	184.1	100	40
PC 40:1-d9	853.7	184.1	100	40
PC 40:2	842.7	184.1	100	40
PC 40:2-d17	859.7	184.1	100	40
PC 40:2-d18	860.7	184.1	100	40
PC 40:2-d34	876.7	184.1	100	40
PC 40:2-d9	851.7	184.1	100	40

Table S3.1 Lipid multiple reaction monitoring (MRMs), collision energies, and fragmentor voltages for LC-MS.

Lipid Species	Precursor Ion	Product Ion	Fragmentor (V)	CE (V)
PC 40:3	840.7	184.1	100	40
PC 40:3-d17	857.7	184.1	100	40
PC 40:3-d18	858.7	184.1	100	40
PC 40:3-d34	874.7	184.1	100	40
PC 40:3-d9	849.7	184.1	100	40
PC 40:4	838.7	184.1	100	40
PC 40:4-d17	855.7	184.1	100	40
PC 40:4-d18	856.7	184.1	100	40
PC 40:4-d34	872.7	184.1	100	40
PC 40:4-d9	847.7	184.1	100	40
PC 40:5	836.7	184.1	100	40
PC 40:5-d17	853.7	184.1	100	40
PC 40:5-d18	854.7	184.1	100	40
PC 40:5-d34	870.7	184.1	100	40
PC 40:5-d9	845.7	184.1	100	40
PC 40:6	834.7	184.1	100	40
PC 40:6-d17	851.7	184.1	100	40
PC 40:6-d18	852.7	184.1	100	40
PC 40:6-d34	868.7	184.1	100	40
PC 40:6-d9	843.7	184.1	100	40
PC 40:7	832.7	184.1	100	40
PC 40:7-d17	849.7	184.1	100	40
PC 40:7-d18	850.7	184.1	100	40
PC 40:7-d34	866.7	184.1	100	40
PC 40:7-d9	841.7	184.1	100	40
PC 42:0	874.7	184.1	100	40

Table S3.1 Lipid multiple reaction monitoring (MRMs), collision energies, and fragmentor voltages for LC-MS.

Lipid Species	Precursor Ion	Product Ion	Fragmentor (V)	CE (V)
PC 42:1	872.7	184.1	100	40
PC 42:1-d17	889.7	184.1	100	40
PC 42:1-d9	881.7	184.1	100	40
PC 42:2	870.7	184.1	100	40
PC 42:2-d17	887.7	184.1	100	40
PC 42:2-d18	888.7	184.1	100	40
PC 42:2-d34	904.7	184.1	100	40
PC 42:2-d9	879.7	184.1	100	40
PE 15:0/18:1-d7	711.6	570.5	100	40
PE 30:0	664.4	523.5	100	40
PE 31:0	678.4	537.5	100	40
PE 32:0	692.4	551.5	100	40
PE 32:1	690.4	549.5	100	40
PE 32:1-d17	707.4	566.5	100	40
PE 32:1-d9	699.4	558.5	100	40
PE 32:2	688.4	547.5	100	40
PE 32:2-d17	705.4	564.5	100	40
PE 32:2-d18	706.4	565.5	100	40
PE 32:2-d34	722.4	581.5	100	40
PE 32:2-d9	697.4	556.5	100	40
PE 34:0	720.6	579.5	100	40
PE 34:1	718.5	577.5	100	40
PE 34:1-d17	735.5	594.5	100	40
PE 34:1-d9	727.5	586.5	100	40
PE 34:2	716.5	575.5	100	40
PE 34:2-d17	733.5	592.5	100	40

Table S3.1 Lipid multiple reaction monitoring (MRMs), collision energies, and fragmentor voltages for LC-MS.

Lipid Species	Precursor Ion	Product Ion	Fragmentor (V)	CE (V)
PE 34:2-d18	734.5	593.5	100	40
PE 34:2-d34	750.5	609.5	100	40
PE 34:2-d9	725.5	584.5	100	40
PE 36:0	748.6	607.5	100	40
PE 36:1	746.6	605.5	100	40
PE 36:1-d17	763.6	622.5	100	40
PE 36:1-d9	755.6	614.5	100	40
PE 36:2	744.6	603.5	100	40
PE 36:2-d17	761.6	620.5	100	40
PE 36:2-d18	762.6	621.5	100	40
PE 36:2-d34	778.6	637.5	100	40
PE 36:2-d9	753.6	612.5	100	40
PE 36:3	742.5	601.5	100	40
PE 36:3-d17	759.5	618.5	100	40
PE 36:3-d18	760.5	619.5	100	40
PE 36:3-d34	776.5	635.5	100	40
PE 36:3-d9	751.5	610.5	100	40
PE 36:4	740.5	599.5	100	40
PE 36:4-d17	757.5	616.5	100	40
PE 36:4-d18	758.5	617.5	100	40
PE 36:4-d34	774.5	633.5	100	40
PE 36:4-d9	749.5	608.5	100	40
PE 36:5	738.5	597.5	100	40
PE 36:5-d17	755.5	614.5	100	40
PE 36:5-d18	756.5	615.5	100	40
PE 36:5-d34	772.5	631.5	100	40

Table S3.1 Lipid multiple reaction monitoring (MRMs), collision energies, and fragmentor voltages for LC-MS.

Lipid Species	Precursor Ion	Product Ion	Fragmentor (V)	CE (V)
PE 36:5-d9	747.5	606.5	100	40
PE 38:0	776.6	635.5	100	40
PE 38:1	774.6	633.5	100	40
PE 38:1-d17	791.6	650.5	100	40
PE 38:1-d9	783.6	642.5	100	40
PE 38:2	772.6	631.5	100	40
PE 38:2-d17	789.6	648.5	100	40
PE 38:2-d18	790.6	649.5	100	40
PE 38:2-d34	806.6	665.5	100	40
PE 38:2-d9	781.6	640.5	100	40
PE 38:3	770.6	629.5	100	40
PE 38:3-d17	787.6	646.5	100	40
PE 38:3-d18	788.6	647.5	100	40
PE 38:3-d34	804.6	663.5	100	40
PE 38:3-d9	779.6	638.5	100	40
PE 38:4	768.6	627.5	100	40
PE 38:4-d17	785.6	644.5	100	40
PE 38:4-d18	786.6	645.5	100	40
PE 38:4-d34	802.6	661.5	100	40
PE 38:4-d9	777.6	636.5	100	40
PE 38:5	766.6	625.5	100	40
PE 38:5-d17	783.6	642.5	100	40
PE 38:5-d18	784.6	643.5	100	40
PE 38:5-d34	800.6	659.5	100	40
PE 38:5-d9	775.6	634.5	100	40
PE 38:6	764.6	623.5	100	40

Table S3.1 Lipid multiple reaction monitoring (MRMs), collision energies, and fragmentor voltages for LC-MS.

Lipid Species	Precursor Ion	Product Ion	Fragmentor (V)	CE (V)
PE 38:6-d17	781.6	640.5	100	40
PE 38:6-d18	782.6	641.5	100	40
PE 38:6-d34	798.6	657.5	100	40
PE 38:6-d9	773.6	632.5	100	40
PE 40:0	804.7	663.5	100	40
PE 40:1	802.7	661.5	100	40
PE 40:1-d17	819.7	678.5	100	40
PE 40:1-d9	811.7	670.5	100	40
PE 40:2	800.7	659.5	100	40
PE 40:2-d17	817.7	676.5	100	40
PE 40:2-d18	818.7	677.5	100	40
PE 40:2-d34	834.7	693.5	100	40
PE 40:2-d9	809.7	668.5	100	40
PE 40:3	798.6	657.5	100	40
PE 40:3-d17	815.6	674.5	100	40
PE 40:3-d18	816.6	675.5	100	40
PE 40:3-d34	832.6	691.5	100	40
PE 40:3-d9	807.6	666.5	100	40
PE 40:4	796.6	655.5	100	40
PE 40:4-d17	813.6	672.5	100	40
PE 40:4-d18	814.6	673.5	100	40
PE 40:4-d34	830.6	689.5	100	40
PE 40:4-d9	805.6	664.5	100	40
PE 40:5	794.6	653.5	100	40
PE 40:5-d17	811.6	670.5	100	40
PE 40:5-d18	812.6	671.5	100	40

Table S3.1 Lipid multiple reaction monitoring (MRMs), collision energies, and fragmentor voltages for LC-MS.

Lipid Species	Precursor Ion	Product Ion	Fragmentor (V)	CE (V)
PE 40:5-d34	828.6	687.5	100	40
PE 40:5-d9	803.6	662.5	100	40
PE 40:6	792.6	651.5	100	40
PE 40:6-d17	809.6	668.5	100	40
PE 40:6-d18	810.6	669.5	100	40
PE 40:6-d34	826.6	685.5	100	40
PE 40:6-d9	801.6	660.5	100	40
PE 40:7	790.6	649.5	100	40
PE 40:7-d17	807.6	666.5	100	40
PE 40:7-d18	808.6	667.5	100	40
PE 40:7-d34	824.6	683.5	100	40
PE 40:7-d9	799.6	658.5	100	40
DAG 15:0/18:1-d7	605.6	299	100	40
DAG 14:0/16:0	558.5	313	100	40
DAG 14:0/16:1	556.5	311	100	40
DAG 14:0/16:1-d17	573.5	328	100	40
DAG 14:0/16:1-d9	565.5	320	100	40
DAG 14:0/18:0	586.5	341	100	40
DAG 14:0/18:1	584.5	339	100	40
DAG 14:0/18:1-d17	601.5	356	100	40
DAG 14:0/18:1-d9	593.5	348	100	40
DAG 15:0/16:0	572.5	313	100	40
DAG 15:0/16:1	570.5	311	100	40
DAG 15:0/16:1-d17	587.5	328	100	40
DAG 15:0/16:1-d9	579.5	320	100	40
DAG 15:0/18:0	600.5	341	100	40

Table S3.1 Lipid multiple reaction monitoring (MRMs), collision energies, and fragmentor voltages for LC-MS.

Lipid Species	Precursor Ion	Product Ion	Fragmentor (V)	CE (V)
DAG 15:0/18:1	598.5	339	100	40
DAG 15:0/18:1-d17	615.5	356	100	40
DAG 15:0/18:1-d9	607.5	348	100	40
DAG 16:0/16:0	586.5	313	100	40
DAG 16:0/16:1	584.5	313	100	40
DAG 16:0/16:1-d17	601.5	313	100	40
DAG 16:0/16:1-d9	593.5	313	100	40
DAG 16:0/17:0	600.5	313	100	40
DAG 16:0/18:0	614.5	313	100	40
DAG 16:0/18:1	612.5	313	100	40
DAG 16:0/18:1-d17	629.5	313	100	40
DAG 16:0/18:1-d9	621.5	313	100	40
DAG 16:0/18:2	610.5	313	100	40
DAG 16:0/20:0	642.5	313	100	40
DAG 16:0/20:4	634.5	313	100	40
DAG 16:0/20:5	632.5	313	100	40
DAG 16:0/22:0	670.5	313	100	40
DAG 16:0/22:6	658.5	313	100	40
DAG 16:0/24:0	698.5	313	100	40
DAG 16:1/18:0	612.5	311	100	40
DAG 16:1/18:1	610.5	311	100	40
DAG 16:1/18:2	608.5	311	100	40
DAG 16:1/20:0	640.5	311	100	40
DAG 16:1/20:4	632.5	311	100	40
DAG 16:1/20:5	630.5	311	100	40
DAG 16:1/22:0	668.5	311	100	40

Table S3.1 Lipid multiple reaction monitoring (MRMs), collision energies, and fragmentor voltages for LC-MS.

Lipid Species	Precursor Ion	Product Ion	Fragmentor (V)	CE (V)
DAG 16:1/22:6	656.5	311	100	40
DAG 16:1/24:0	696.5	311	100	40
DAG 16:1-d17/18:0	629.5	328	100	40
DAG 16:1-d17/18:1	627.5	328	100	40
DAG 16:1-d17/18:1-d17	644.5	328	100	40
DAG 16:1-d9/18:0	621.5	320	100	40
DAG 16:1-d9/18:1	619.5	320	100	40
DAG 16:1-d9/18:1-d9	629.5	320	100	40
DAG 17:0/17:0	614.5	327	100	40
DAG 17:0/18:0	628.5	327	100	40
DAG 17:0/18:1	626.5	327	100	40
DAG 17:0/18:1-d17	643.5	327	100	40
DAG 17:0/18:1-d9	635.5	327	100	40
DAG 17:0/18:2	624.5	327	100	40
DAG 17:0/20:0	656.5	327	100	40
DAG 17:0/20:5	646.5	327	100	40
DAG 17:0/22:0	684.5	327	100	40
DAG 17:0/22:6	672.5	327	100	40
DAG 18:0/18:0	642.5	341	100	40
DAG 18:0/18:1	640.5	341	100	40
DAG 18:0/18:1-d17	657.5	341	100	40
DAG 18:0/18:1-d9	649.5	341	100	40
DAG 18:0/18:2	638.5	341	100	40
DAG 18:0/20:0	670.5	341	100	40
DAG 18:0/20:4	662.5	341	100	40
DAG 18:0/20:5	660.5	341	100	40

Table S3.1 Lipid multiple reaction monitoring (MRMs), collision energies, and fragmentor voltages for LC-MS.

Lipid Species	Precursor Ion	Product Ion	Fragmentor (V)	CE (V)
DAG 18:0/22:0	698.5	341	100	40
DAG 18:0/22:6	686.5	341	100	40
DAG 18:0/24:0	726.5	341	100	40
DAG 18:1/18:1	638.5	339	100	40
DAG 18:1/18:2	636.5	339	100	40
DAG 18:1/20:0	668.5	339	100	40
DAG 18:1/20:4	660.5	339	100	40
DAG 18:1/20:5	658.5	339	100	40
DAG 18:1/22:0	696.5	339	100	40
DAG 18:1/22:6	684.5	339	100	40
DAG 18:1/24:0	724.5	339	100	40
DAG 18:1-d17/18:1	655.5	356	100	40
DAG 18:1-d17/18:1-d17	672.5	356	100	40
DAG 18:1-d17/18:2	653.5	356	100	40
DAG 18:1-d17/20:0	685.5	356	100	40
DAG 18:1-d17/20:4	677.5	356	100	40
DAG 18:1-d17/20:5	675.5	356	100	40
DAG 18:1-d17/22:0	713.5	356	100	40
DAG 18:1-d17/22:6	701.5	356	100	40
DAG 18:1-d17/24:0	741.5	356	100	40
DAG 18:1-d9/18:1	647.5	348	100	40
DAG 18:1-d9/18:1-d9	656.5	348	100	40
DAG 18:1-d9/18:2	645.5	348	100	40
DAG 18:1-d9/20:0	677.5	348	100	40
DAG 18:1-d9/20:4	669.5	348	100	40
DAG 18:1-d9/20:5	667.5	348	100	40

Table S3.1 Lipid multiple reaction monitoring (MRMs), collision energies, and fragmentor voltages for LC-MS.

Lipid Species	Precursor Ion	Product Ion	Fragmentor (V)	CE (V)
DAG 18:1-d9/22:0	705.5	348	100	40
DAG 18:1-d9/22:6	693.5	348	100	40
DAG 18:1-d9/24:0	733.5	348	100	40
DAG 18:2/18:2	634.5	337	100	40
DAG 18:2/20:0	666.5	337	100	40
DAG 18:2/20:4	658.5	337	100	40
DAG 18:2/20:5	656.5	337	100	40
DAG 18:2/22:0	694.5	337	100	40
DAG 18:2/22:6	682.5	337	100	40
DAG 18:2/24:0	722.5	337	100	40
TAG 15:0/18:1-d7/15:0 (d30:0)	829.8	523.5	100	40
TAG 48:0 (d32:0)	824.8	551.5	100	40
TAG 48:1 (d32:0)	822.8	551.5	100	40
TAG 48:1-d17 (d32:0)	839.8	551.5	100	40
TAG 48:1-d9 (d32:0)	831.8	551.5	100	40
TAG 48:2 (d32:1)	820.8	549.5	100	40
TAG 48:2 (d32:2)	820.8	547.5	100	40
TAG 48:2-d17 (d32:1)	837.8	549.5	100	40
TAG 48:2-d17 (d32:2-d17)	837.8	564.5	100	40
TAG 48:2-d18 (d32:1)	838.8	549.5	100	40
TAG 48:2-d18 (d32:2-d18)	838.8	565.5	100	40
TAG 48:2-d34 (d32:1)	854.8	549.5	100	40
TAG 48:2-d34 (d32:2-d34)	854.8	581.5	100	40
TAG 48:2-d9 (d32:1)	829.8	549.5	100	40
TAG 48:2-d9 (d32:2-d9)	829.8	556.5	100	40
TAG 48:3 (d32:2)	818.8	547.5	100	40

Table S3.1 Lipid multiple reaction monitoring (MRMs), collision energies, and fragmentor voltages for LC-MS.

Lipid Species	Precursor Ion	Product Ion	Fragmentor (V)	CE (V)
TAG 48:3-d17 (d32:2)	835.8	547.5	100	40
TAG 48:3-d18 (d32:2-d9)	836.8	556.5	100	40
TAG 48:3-d34 (d32:2-d17)	852.8	564.5	100	40
TAG 48:3-d9 (d32:2)	827.8	547.5	100	40
TAG 50:0 (d32:0)	852.8	551.5	100	40
TAG 50:1 (d32:0)	850.8	551.5	100	40
TAG 50:1-d17 (d32:0)	867.8	551.5	100	40
TAG 50:1-d9 (d32:0)	859.8	551.5	100	40
TAG 50:2 (d32:0)	848.8	551.5	100	40
TAG 50:2 (d32:1)	848.8	549.5	100	40
TAG 50:2 (d32:2)	848.8	547.5	100	40
TAG 50:2-d17 (d32:1)	865.8	549.5	100	40
TAG 50:2-d17 (d32:2-d17)	865.8	564.5	100	40
TAG 50:2-d18 (d32:1-d9)	882.8	566.5	100	40
TAG 50:2-d18 (d32:2-d18)	866.8	565.5	100	40
TAG 50:2-d34 (d32:1-d17)	882.8	566.5	100	40
TAG 50:2-d34 (d32:2-d34)	882.8	581.5	100	40
TAG 50:2-d9 (d32:1)	857.8	549.5	100	40
TAG 50:2-d9 (d32:2-d9)	857.8	556.5	100	40
TAG 50:3 (d32:0)	846.8	551.5	100	40
TAG 50:3 (d32:1)	846.8	549.5	100	40
TAG 50:3 (d32:2)	846.8	547.5	100	40
TAG 50:3-d17 (d32:1-d17)	863.8	566.5	100	40
TAG 50:3-d17 (d32:2)	863.8	547.5	100	40
TAG 50:3-d18 (d32:2-d9)	864.8	556.5	100	40
TAG 50:3-d27 (d32:2-d18)	873.8	565.5	100	40

Table S3.1 Lipid multiple reaction monitoring (MRMs), collision energies, and fragmentor voltages for LC-MS.

Lipid Species	Precursor Ion	Product Ion	Fragmentor (V)	CE (V)
TAG 50:3-d34 (d32:2-d17)	880.8	564.5	100	40
TAG 50:3-d51 (d32:2-d34)	897.8	581.5	100	40
TAG 50:3-d9 (d32:1-d9)	855.8	558.5	100	40
TAG 50:3-d9 (d32:2)	855.8	547.5	100	40
TAG 52:0 (d32:0)	880.8	551.5	100	40
TAG 52:0 (d34:0)	880.8	579.5	100	40
TAG 52:1 (d36:1)	878.8	605.5	100	40
TAG 52:1-d17 (d36:1-d17)	895.8	622.5	100	40
TAG 52:1-d9 (d36:1-d9)	887.8	614.5	100	40
TAG 52:2 (d34:1)	876.8	577.5	100	40
TAG 52:2 (d34:2)	876.8	575.5	100	40
TAG 52:2-d17 (d34:1)	893.8	577.5	100	40
TAG 52:2-d17 (d34:2-d17)	893.8	592.5	100	40
TAG 52:2-d18 (d34:1-d9)	894.8	586.5	100	40
TAG 52:2-d18 (d34:2-d18)	894.8	593.5	100	40
TAG 52:2-d34 (d34:1-d17)	910.8	594.5	100	40
TAG 52:2-d34 (d34:2-d34)	910.8	609.5	100	40
TAG 52:2-d9 (d34:1)	885.8	577.5	100	40
TAG 52:2-d9 (d34:2-d9)	885.8	584.5	100	40
TAG 52:3 (d34:1)	874.8	577.5	100	40
TAG 52:3 (d34:2)	874.8	575.5	100	40
TAG 52:3-d17 (d34:1-d17)	891.8	594.5	100	40
TAG 52:3-d17 (d34:2)	891.8	575.5	100	40
TAG 52:3-d18 (d34:2-d9)	892.8	584.5	100	40
TAG 52:3-d27 (d34:2-d18)	901.8	593.5	100	40
TAG 52:3-d34 (d34:2-d17)	908.8	592.5	100	40

Table S3.1 Lipid multiple reaction monitoring (MRMs), collision energies, and fragmentor voltages for LC-MS.

Lipid Species	Precursor Ion	Product Ion	Fragmentor (V)	CE (V)
TAG 52:3-d51 (d34:2-d34)	925.8	609.5	100	40
TAG 52:3-d9 (d34:1-d9)	883.8	586.5	100	40
TAG 52:3-d9 (d34:2)	883.8	575.5	100	40
TAG 52:4 (d32:0)	872.8	551.5	100	40
TAG 52:4 (d34:2)	872.8	575.5	100	40
TAG 52:4 (d34:3)	872.8	573.5	100	40
TAG 52:4-d17 (d34:2-d17)	889.8	592.5	100	40
TAG 52:4-d17 (d34:3)	889.8	573.5	100	40
TAG 52:4-d18 (d34:2-d18)	890.8	593.5	100	40
TAG 52:4-d18 (d34:3-d9)	890.8	582.5	100	40
TAG 52:4-d27 (d34:3-d18)	899.8	591.5	100	40
TAG 52:4-d34 (d34:2-d34)	906.8	609.5	100	40
TAG 52:4-d34 (d34:3-d17)	906.8	590.5	100	40
TAG 52:4-d51 (d34:3-d34)	923.8	607.5	100	40
TAG 52:4-d9 (d34:2-d9)	881.8	584.5	100	40
TAG 52:4-d9 (d34:3)	881.8	573.5	100	40
TAG 52:5 (d32:0)	870.8	551.5	100	40
TAG 52:5 (d32:1)	870.8	549.5	100	40
TAG 52:5 (d34:2)	870.8	575.5	100	40
TAG 52:5-d17 (d32:1-d17)	887.8	566.5	100	40
TAG 52:5-d17 (d34:2-d17)	887.8	592.5	100	40
TAG 52:5-d18 (d34:2-d34)	888.8	593.5	100	40
TAG 52:5-d34 (d34:2-d34)	904.8	609.5	100	40
TAG 52:5-d9 (d32:1-d9)	879.8	558.5	100	40
TAG 52:5-d9 (d34:2-d9)	879.8	584.5	100	40
TAG 52:6 (d30:0)	868.8	523.5	100	40

Table S3.1 Lipid multiple reaction monitoring (MRMs), collision energies, and fragmentor voltages for LC-MS.

Lipid Species	Precursor Ion	Product Ion	Fragmentor (V)	CE (V)
TAG 54:0 (d36:0)	908.9	607.6	100	40
TAG 54:0 (d38:0)	908.9	635.6	100	40
TAG 54:1 (d36:1)	906.9	605.6	100	40
TAG 54:1-d17 (d36:1-d17)	923.9	622.6	100	40
TAG 54:1-d9 (d36:1-d9)	915.9	614.6	100	40
TAG 54:2 (d36:1)	904.9	605.6	100	40
TAG 54:2 (d36:2)	904.9	603.6	100	40
TAG 54:2-d17 (d36:1)	921.9	605.6	100	40
TAG 54:2-d17 (d36:2-d17)	921.9	620.6	100	40
TAG 54:2-d18 (d36:2-d18)	922.9	621.6	100	40
TAG 54:2-d34 (d36:1-d17)	938.9	622.6	100	40
TAG 54:2-d34 (d36:2-d34)	938.9	637.6	100	40
TAG 54:2-d9 (d36:1)	913.9	605.6	100	40
TAG 54:2-d9 (d36:1-d9)	922.9	614.6	100	40
TAG 54:2-d9 (d36:2-d9)	913.9	612.6	100	40
TAG 54:3 (d36:2)	902.9	603.6	100	40
TAG 54:3-d17 (d36:2)	919.9	603.6	100	40
TAG 54:3-d18 (d36:2-d9)	920.9	612.6	100	40
TAG 54:3-d27 (d36:2-d18)	929.9	621.6	100	40
TAG 54:3-d34 (d36:2-d17)	936.9	620.6	100	40
TAG 54:3-d51 (d36:2-d34)	953.9	637.6	100	40
TAG 54:3-d9 (d36:2)	911.9	603.6	100	40
TAG 54:4 (d34:1)	900.8	577.5	100	40
TAG 54:4 (d36:2)	900.8	603.5	100	40
TAG 54:4 (d36:3)	900.8	601.5	100	40
TAG 54:4-d17 (d34:1-d17)	917.8	594.5	100	40

Table S3.1 Lipid multiple reaction monitoring (MRMs), collision energies, and fragmentor voltages for LC-MS.

Lipid Species	Precursor Ion	Product Ion	Fragmentor (V)	CE (V)
TAG 54:4-d17 (d36:2-d17)	917.8	620.5	100	40
TAG 54:4-d17 (d36:3)	917.8	601.5	100	40
TAG 54:4-d18 (d36:2-d18)	918.8	621.5	100	40
TAG 54:4-d18 (d36:3-d9)	918.8	610.5	100	40
TAG 54:4-d27 (d36:3-d18)	927.8	619.5	100	40
TAG 54:4-d34 (d36:2-d34)	934.8	637.5	100	40
TAG 54:4-d34 (d36:3-d17)	934.8	618.5	100	40
TAG 54:4-d51 (d36:3-d34)	951.8	635.5	100	40
TAG 54:4-d9 (d34:1-d9)	909.8	586.5	100	40
TAG 54:4-d9 (d36:2-d9)	909.8	612.5	100	40
TAG 54:4-d9 (d36:3)	909.8	601.5	100	40
TAG 54:5 (d36:4)	898.8	599.5	100	40
TAG 54:5-d17 (d36:4)	915.8	599.5	100	40
TAG 54:5-d18 (d36:4-d9)	916.8	608.5	100	40
TAG 54:5-d27 (d36:4-d18)	925.8	617.5	100	40
TAG 54:5-d34 (d36:4-d17)	932.8	616.5	100	40
TAG 54:5-d51 (d36:4-d34)	949.8	633.5	100	40
TAG 54:5-d9 (d36:4)	907.8	599.5	100	40
TAG 54:6 (d32:0)	896.8	551.5	100	40
TAG 54:6 (d34:1)	896.8	577.5	100	40
TAG 54:6 (d34:2)	896.8	575.5	100	40
TAG 54:6 (d36:5)	896.8	597.5	100	40
TAG 54:6-d17 (d34:1-d17)	913.8	594.5	100	40
TAG 54:6-d17 (d34:2-d17)	913.8	592.5	100	40
TAG 54:6-d17 (d36:5)	913.8	597.5	100	40
TAG 54:6-d18 (d34:2-d18)	914.8	593.5	100	40

Table S3.1 Lipid multiple reaction monitoring (MRMs), collision energies, and fragmentor voltages for LC-MS.

Lipid Species	Precursor Ion	Product Ion	Fragmentor (V)	CE (V)
TAG 54:6-d18 (d36:5-d9)	914.8	606.5	100	40
TAG 54:6-d27 (d36:5-d18)	923.8	615.5	100	40
TAG 54:6-d34 (d34:2-d34)	930.8	609.5	100	40
TAG 54:6-d34 (d36:5-d17)	930.8	614.5	100	40
TAG 54:6-d51 (d36:5-d34)	947.8	631.5	100	40
TAG 54:6-d9 (d34:1-d9)	905.8	586.5	100	40
TAG 54:6-d9 (d34:2-d9)	905.8	584.5	100	40
TAG 54:6-d9 (d36:5)	905.8	597.5	100	40
TAG 56:0 (d40:0)	936.9	663.5	100	40
TAG 56:1 (d32:0)	934.9	551.5	100	40
TAG 56:1 (d38:0)	934.9	635.5	100	40
TAG 56:1 (d40:1)	934.9	661.5	100	40
TAG 56:1-d17 (d32:0)	951.9	551.5	100	40
TAG 56:1-d17 (d38:0)	951.9	635.5	100	40
TAG 56:1-d17 (d40:1-d17)	951.9	678.5	100	40
TAG 56:1-d9 (d32:0)	943.9	551.5	100	40
TAG 56:1-d9 (d38:0)	943.9	635.5	100	40
TAG 56:1-d9 (d40:1-d9)	943.9	670.5	100	40
TAG 56:2 (d36:1)	932.9	605.5	100	40
TAG 56:2 (d38:1)	932.9	633.5	100	40
TAG 56:2-d17 (d36:1)	949.9	605.5	100	40
TAG 56:2-d17 (d38:1)	949.9	633.5	100	40
TAG 56:2-d18 (d36:1-d9)	950.9	605.5	100	40
TAG 56:2-d18 (d38:1-d9)	950.9	642.5	100	40
TAG 56:2-d34 (d36:1-d17)	966.9	622.5	100	40
TAG 56:2-d34 (d38:1-d17)	966.9	650.5	100	40

Table S3.1 Lipid multiple reaction monitoring (MRMs), collision energies, and fragmentor voltages for LC-MS.

Lipid Species	Precursor Ion	Product Ion	Fragmentor (V)	CE (V)
TAG 56:2-d9 (d36:1)	941.9	605.5	100	40
TAG 56:2-d9 (d38:1)	941.9	633.5	100	40
TAG 56:3 (d36:2)	930.9	603.5	100	40
TAG 56:3 (d38:2)	930.9	631.5	100	40
TAG 56:3-d17 (d36:2)	947.9	603.5	100	40
TAG 56:3-d17 (d38:2)	947.9	631.5	100	40
TAG 56:3-d18 (d36:2-d9)	948.9	612.5	100	40
TAG 56:3-d18 (d38:2-d9)	948.9	640.5	100	40
TAG 56:3-d27 (d36:2-d18)	957.9	621.5	100	40
TAG 56:3-d27 (d38:2-d18)	957.9	649.5	100	40
TAG 56:3-d34 (d36:2-d17)	964.9	620.5	100	40
TAG 56:3-d34 (d38:2-d17)	964.9	648.5	100	40
TAG 56:3-d51 (d36:2-d34)	981.9	637.5	100	40
TAG 56:3-d51 (d38:2-d34)	981.9	665.5	100	40
TAG 56:3-d9 (d36:2)	939.9	603.5	100	40
TAG 56:3-d9 (d38:2)	939.9	631.5	100	40
TAG 56:4 (d36:2)	928.9	603.5	100	40
TAG 56:4 (d38:3)	928.8	629.5	100	40
TAG 56:4-d17 (d36:2)	945.9	603.5	100	40
TAG 56:4-d17 (d38:3)	945.8	629.5	100	40
TAG 56:4-d18 (d36:2-d9)	946.9	612.5	100	40
TAG 56:4-d18 (d38:3-d9)	946.8	638.5	100	40
TAG 56:4-d27 (d38:3-d18)	955.8	647.5	100	40
TAG 56:4-d34 (d36:2-d17)	962.9	620.5	100	40
TAG 56:4-d34 (d38:3-d17)	962.8	646.5	100	40
TAG 56:4-d51 (d38:3-d34)	979.8	663.5	100	40

Table S3.1 Lipid multiple reaction monitoring (MRMs), collision energies, and fragmentor voltages for LC-MS.

Lipid Species	Precursor Ion	Product Ion	Fragmentor (V)	CE (V)
TAG 56:4-d9 (d36:2)	937.9	603.5	100	40
TAG 56:4-d9 (d38:3)	937.8	629.5	100	40
TAG 56:5 (d32:0)	926.8	551.5	100	40
TAG 56:5 (d36:1)	926.8	605.5	100	40
TAG 56:5 (d36:2)	926.8	603.5	100	40
TAG 56:5 (d38:4)	926.8	627.5	100	40
TAG 56:5-d17 (d36:1-d17)	943.8	622.5	100	40
TAG 56:5-d17 (d36:2)	943.8	603.5	100	40
TAG 56:5-d17 (d38:4)	943.8	627.5	100	40
TAG 56:5-d18 (d36:2)	944.8	612.5	100	40
TAG 56:5-d18 (d38:4-d9)	944.8	636.5	100	40
TAG 56:5-d27 (d38:4-d18)	953.8	645.5	100	40
TAG 56:5-d34 (d36:2-d17)	960.8	620.5	100	40
TAG 56:5-d34 (d38:4-d17)	960.8	644.5	100	40
TAG 56:5-d51 (d38:4-d34)	977.8	661.5	100	40
TAG 56:5-d9 (d36:1-d9)	935.8	614.5	100	40
TAG 56:5-d9 (d36:2)	935.8	603.5	100	40
TAG 56:5-d9 (d38:4)	935.8	627.5	100	40
TAG 56:6 (d34:0)	924.9	579.5	100	40
TAG 56:6 (d36:1)	924.9	605.6	100	40
TAG 56:6 (d36:2)	924.9	607.6	100	40
TAG 56:6 (d36:2)	924.8	603.5	100	40
TAG 56:6 (d38:5)	924.8	625.5	100	40
TAG 56:6-d17 (d36:2)	941.8	603.5	100	40
TAG 56:6-d17 (d38:5)	941.8	625.5	100	40
TAG 56:6-d18 (d36:2-d9)	942.8	612.5	100	40

Table S3.1 Lipid multiple reaction monitoring (MRMs), collision energies, and fragmentor voltages for LC-MS.

Lipid Species	Precursor Ion	Product Ion	Fragmentor (V)	CE (V)
TAG 56:6-d18 (d38:5-d9)	942.8	634.5	100	40
TAG 56:6-d27 (d38:5-d18)	951.8	643.5	100	40
TAG 56:6-d34 (d36:2-d17)	958.8	620.5	100	40
TAG 56:6-d34 (d38:5-d17)	958.8	642.5	100	40
TAG 56:6-d51 (d38:5-d34)	975.8	659.5	100	40
TAG 56:6-d9 (d36:2)	933.8	603.5	100	40

Table S3.2 Dietary fatty acid composition.

Fatty Acid Composition (%)	Cis Unsaturated HFD	Trans Unsaturated HFD
SFA	23.6	26.7
MUFA	63.9	62.5
PUFA	12.4	10.9
Total C18:1	62.2	62.4
C14:0	0.4	0.2
C16:0	16.0	16.5
C16:1 (9Z)	1.3	0
C17:0	0.2	0.1
C18:0	6.5	9.2
C18:1 (9Z)	59.0	23.3
C18:1 (11Z)	3.0	0
other cis C18:1	0.1	10.6
C18:1 (9E)	0.0	3.5
C18:1 (11E)	0.0	6
other trans C18:1	0.1	19
C18:2 (9Z, 12Z)	11.2	6.1
C18:2 (9E, 12E)	0.0	0.2
other trans C18:2	0.0	4.1
C18:3	0.8	0.3
total trans C18:3	0.0	0.2
C20:0	0.3	0.3
C20:1	0.4	0.1
C20:2	0.2	0
C20:4 (5Z, 8Z, 11Z, 14Z)	0.1	0
C22:0	0.1	0.3
C24:0	0.0	0.1

Table S3.3 Orbitrap high-resolution (QE) mass spectrometry lipid analysis.

Lipid Species	Precursor Ion	Product Ion
Lysophosphatidylcholine (LPC)		
18:1(d7) LPC	529.3999	184.0734
LPC(14:0)	468.3084	184.0734
LPC(16:0)	496.3405	184.0734
LPC(16:1)	494.3246	184.0734
LPC(18:0)	524.3721	184.0734
LPC(18:1)	522.3566	184.0734
LPC(18:2)	520.3407	184.0734
LPC(18:3)	518.3249	184.0734
LPC(20:0)	552.4039	184.0734
LPC(20:1)	550.3877	184.0734
LPC(20:2)	548.3721	184.0734
LPC(20:3)	546.3563	184.0734
LPC(20:4)	544.3405	184.0734
LPC(22:0)	580.4346	184.0734
LPC(22:1)	578.4194	184.0734
LPC(22:3)	574.3880	184.0734
LPC(22:4)	572.3725	184.0734
LPC(22:5)	570.3556	184.0734
LPC(22:6)	568.3405	184.0734
LPC(24:0)	608.4656	184.0734
LPC(24:1)	606.4502	184.0734
Lysophosphatidylethanolamine (LPE)		
18:1(d7) LPE	487.3533	346.4
LPE(16:0)	454.2929	313.3
LPE(18:0)	482.3247	341.3

Table S3.3 Orbitrap high-resolution (QE) mass spectrometry lipid analysis.

Lipid Species	Precursor Ion	Product Ion
LPE(18:1)	480.3087	339.3
LPE(18:2)	478.2931	337.3
LPE(20:3)	504.3080	363.3
LPE(20:4)	502.2937	361.3
LPE(22:5)	528.3093	387.3
LPE(22:6)	526.2927	385.3
Phosphatidylcholine (PC)		
15:0-18:1(d7) PC	753.6151	184.0734
PC(32:0)	734.5704	184.0734
PC(32:1)	732.5546	184.0734
PC(32:2)	730.5389	184.0734
PC(32:3)	728.5238	184.0734
PC(34:0)	762.6011	184.0734
PC(34:1)	760.5860	184.0734
PC(34:2)	758.5704	184.0734
PC(34:3)	756.5545	184.0734
PC(34:4)	754.5388	184.0734
PC(34:5)	752.5232	184.0734
PC(36:1)	788.6172	184.0734
PC(36:2)	786.6018	184.0734
PC(36:3)	784.5859	184.0734
PC(36:4)	782.5701	184.0734
PC(36:5)	780.5546	184.0734
PC(36:6)	778.5391	184.0734
PC(36:7)	776.5225	184.0734
PC(36:0)	790.6304	184.0734

Table S3.3 Orbitrap high-resolution (QE) mass spectrometry lipid analysis.

Lipid Species	Precursor Ion	Product Ion
PC(38:1)	816.6466	184.0734
PC(38:2)	814.6334	184.0734
PC(38:3)	812.6169	184.0734
PC(38:4)	810.6016	184.0734
PC(38:5)	808.5853	184.0734
PC(38:6)	806.5699	184.0734
PC(38:7)	804.5544	184.0734
PC(38:8)	802.5393	184.0734
PC(40:2)	842.6628	184.0734
PC(40:3)	840.6475	184.0734
PC(40:4)	838.6324	184.0734
PC(40:5)	836.6166	184.0734
PC(40:6)	834.6016	184.0734
PC(40:7)	832.5853	184.0734
PC(40:8)	830.5697	184.0734
PC(42:4)	866.6641	184.0734
PC(42:5)	864.6492	184.0734
PC(42:6)	862.6326	184.0734
PC(42:7)	860.6176	184.0734
PC(42:8)	858.5995	184.0734
PC(42:9)	856.5840	184.0734
PC(42:10)	854.5703	184.0734
Phosphatidylethanolamine (PE)		
15:0-18:1(d7) PE	711.5670	570.6
PE 34:1	718.5397	577.5
PE 34:2	716.5229	575.5

Table S3.3 Orbitrap high-resolution (QE) mass spectrometry lipid analysis.

Lipid Species	Precursor Ion	Product Ion
PE 36:1	746.5696	605.6
PE 36:2	744.5558	603.6
PE 36:3	742.5398	601.5
PE 36:4	740.5230	599.5
PE 36:5	738.5079	597.5
PE 38:5	766.5388	625.5
PE 38:6	764.5223	623.5
PE 38:7	762.5068	621.5
PE 40:7	790.5390	649.5
PE 40:8	788.5209	647.5
Diacylglycerol (DAG)		
15:0-18:1(d7) DG	605.5858	346.3
DG 32:0	586.5417	313.3
DG 32:1	584.5258	339.3
DG 32:2	582.5099	311
DG 34:0	614.5727	313.3
DG 34:1	612.5576	313.3
DG 34:2	610.5408	313.3
DG 34:3	608.5259	337.3
DG 36:0	642.6047	341.3
DG 36:1	640.5890	341.3
DG 36:2	638.5724	339.3
DG 36:3	636.5574	339.3
DG 36:4	634.5411	337.3
DG 38:1	668.6195	369.3
DG 38:2	666.6041	339.3

Table S3.3 Orbitrap high-resolution (QE) mass spectrometry lipid analysis.

Lipid Species	Precursor Ion	Product Ion
DG 38:3	664.5876	339.3
DG 38:4	662.5729	339.3
DG 38:5	660.5569	339.3
DG 38:6	658.5408	337.3
Triacylglycerol (TAG)		
15:0-18:1(d7)-15:0 TG	829.7999	570.5
TG(48:0)	824.7711	551.5
TG(48:1)	822.7556	549.5
TG(48:2)	820.7396	549.5
TG(48:3)	818.7233	575.5
TG(50:0)	852.8030	579.5
TG(50:1)	850.7874	577.5
TG(50:2)	848.7714	575.5
TG(50:3)	846.7550	575.5
TG(50:4)	844.7386	575.5
TG(50:5)	842.7229	575.5
TG(50:6)	840.7082	573.5
TG(50:7)	838.6925	571.5
TG(52:0)	880.8342	579.5
TG(52:1)	878.8138	579.5
TG(52:2)	876.7993	577.5
TG(52:3)	874.7872	575.5
TG(52:4)	872.7712	575.5
TG(52:5)	870.7539	603.5
TG(52:6)	868.7397	603.5
TG(52:7)	866.7242	599.5

Table S3.3 Orbitrap high-resolution (QE) mass spectrometry lipid analysis.

Lipid Species	Precursor Ion	Product Ion
TG(52:8)	864.7097	597.5
TG(54:1)	906.8501	605.5
TG(54:2)	904.8340	605.5
TG(54:3)	902.8186	603.5
TG(54:4)	900.8030	601.5
TG(54:5)	898.7865	577.5
TG(54:6)	896.7709	575.5
TG(54:7)	894.7560	573.5
TG(54:8)	892.7405	571.5
TG(56:1)	934.8813	635.6
TG(56:2)	932.8657	633.6
TG(56:3)	930.8497	631.6
TG(56:4)	928.8342	629.6
TG(56:5)	926.8177	605.5
TG(56:6)	924.8026	603.5
TG(56:7)	922.7872	577.5
TG(56:8)	920.7714	575.5
TG(58:1)	962.9119	663.6
TG(58:2)	960.8968	661.6
TG(58:3)	958.8812	661.6
TG(58:4)	956.8651	659.6
TG(58:5)	954.8492	633.6
TG(58:6)	952.8335	605.5
TG(58:7)	950.8183	605.5
TG(58:8)	948.8023	603.5
TG(60:1)	990.9429	605.5
TG(60:2)	988.9284	689.6

Table S3.3 Orbitrap high-resolution (QE) mass spectrometry lipid analysis.

Lipid Species	Precursor Ion	Product Ion
TG(60:3)	986.9127	687.6
TG(60:4)	984.8966	687.6
TG(60:5)	982.8820	659.6
TG(60:6)	980.8641	681.6
TG(60:7)	978.8497	631.6
TG(60:8)	976.8337	631.6
Cholesteryl Esters (ChE)		
ChE 18:1-d7	675.6782	376.4
ChE(16:0)	642.6198	369.4
ChE(16:1)	640.6038	369.4
ChE(18:0)	670.6506	369.4
ChE(18:1)	668.6349	369.4
ChE(18:2)	666.6195	369.4
ChE(18:3)	664.6035	369.4
ChE(20:1)	696.6658	369.4
ChE(20:2)	694.6506	369.4
ChE(20:3)	692.6348	369.4
ChE(20:4)	690.6194	369.4
ChE(20:5)	688.6036	369.4
ChE(22:4)	718.6506	369.4
ChE(22:5)	716.6349	369.4
ChE(22:6)	714.6194	369.4
ChE(24:3)	748.6976	369.4
ChE(24:4)	746.6824	369.4
ChE(24:5)	744.6667	369.4
ChE(24:6)	742.6507	369.4

Table S3.4 Mouse qPCR primer sequences

Gene	Forward primer sequence (5'-3')	Reverse primer sequence (5'-3')
Sptlc1	GTTGCAGGAGCGTTCTGATCT	GGCCGGACACGATGTTGTAG
Sptlc2	GTGAGGAACGGGTACTTGAGG	CAACCAGCATGGGTGTTTCTT
Sptlc3	ACACAATCCTAAGACCCAGCA	AGACTGGCTTATCCTCAGCATA
Sptssa	ACCGTGTTCAATTCGATGCTG	CTGGGGCATGAAGACGTAGC
Sptssb	CGTGAAGGAGTATTTTGCCTGG	GCCACAATGGTCAGTATGATGGT
Ormdl1	ACAGTGAGGTAAACCCCAATACT	GCAAAAACACATACATCCCCAGA
Ormdl2	CACAGCGAAGTAAACCCCAAC	AGGGTCCAGACAACAGGAATG
Ormdl3	CCAACCTTATCCACAACCTGG	GACCCCGTAGTCCATCTGC
Degs1	GAATGGGTCTACACGGACCAG	AGTCATGGAGTGGTTAAGGCA
Fads3	TGACCTACCAGGCGACAAGT	CAATCAACAGGGGTTTCAGGAA
Cert	AGTGCCTCTGACGATGTTCAC	ACCAGTTGCCAATTTGCATCA
Cers2	TATGACTACTTCTGGTGGGAACG	GTATCGAATGACGAGAAAGAGCA
Cers4	CTGGTGGCTGTGCGAATTG	CCGGGTTGGGCTTTATCTTTC
Cers5	CGGGGAAAGGTGTCTAAGGAT	GTTCATGCAGTTGGCACCATT
Sgms1	GAAGGAAGTGGTTTACTGGTCAC	GACTCGGTACAGTGGGGGT
Sgms2	CCACCAACACTTACACAAGCC	GCACCCTTTCGTAACCCGTT
Smpd1	ACTCCACGGTTCTTTGGGTTC	CGGCGCTATGGCACTGAAT
Smpd2	TGGGACATCCCCTACCTGAG	TAGGTGAGCGATAGCCTTTGC
Smpd3	ACACGACCCCCTTTCCTAATA	GGCGCTTCTCATAGGTGGTG
Sgpp1	GATGCAGAGACCGAGGTTCG	CGGCAAGTTGCTCACTTTGAC
Sgpp2	CACCCACTGGAATATCGACCC	AAGTCTCACAACGGGAGGAAA
Sphk1	ACTGATACTCACCGAACGGAA	CCATCACCGGACATGACTGC
Sphk2	ACAGCGACTACGCCCAAAG	GTGGGTAGGTGTAGATGCAGA
Sgpl1	CTGAAGGACTTCGAGCCTTATTT	GACACTCCACGCAATGAGC

Table S3.5 Top 100 differentially correlated genes with *SPTLC2* and *SPTLC3* in human liver.

Gene Name	Gene Description	*SPTLC3*	*SPTLC2*	Average	Variance
A1CF	APOBEC1 complementation factor	0.695	-0.484	0.1055	0.695021
TPM4	tropomyosin 4	-0.619	0.559	-0.03	0.693842
GRB14	growth factor receptor bound protein 14	0.639	-0.537	0.051	0.691488
GAS2	growth arrest specific 2	0.602	-0.551	0.0255	0.664705
GPR176	G protein-coupled receptor 176	-0.581	0.567	-0.007	0.658952
MYOF	myoferlin	-0.496	0.651	0.0775	0.657805
TTR	transthyretin	0.635	-0.511	0.062	0.656658
UPB1	beta-ureidopropionase 1	0.589	-0.554	0.0175	0.653225
KLB	klotho beta	0.692	-0.45	0.121	0.652082
GBA3	glucosylceramidase beta 3 (gene/pseudogene)	0.705	-0.436	0.1345	0.650941
EPHX2	epoxide hydrolase 2	0.661	-0.479	0.091	0.6498
RBP4	retinol binding protein 4	0.612	-0.524	0.044	0.645248
MTTP	microsomal triglyceride transfer protein	0.693	-0.443	0.125	0.645248
KIF3C	kinesin family member 3C	-0.571	0.562	-0.0045	0.641845
APOB	apolipoprotein B	0.672	-0.458	0.107	0.63845
PAH	phenylalanine hydroxylase	0.629	-0.5	0.0645	0.637321
AMBP	alpha-1-microglobulin/bikunin precursor	0.579	-0.546	0.0165	0.632813
DDC	dopa decarboxylase	0.667	-0.458	0.1045	0.632813
MB21D2	Mab-21 domain containing 2	-0.559	0.566	0.0035	0.632813
MARC1	mitochondrial amidoxime reducing component 1	0.619	-0.501	0.059	0.6272
FAM57A	family with sequence similarity 57 member A	-0.619	0.5	-0.0595	0.626081
UBASH3B	ubiquitin associated and SH3 domain containing B	-0.472	0.647	0.0875	0.626081
ADH6	alcohol dehydrogenase 6 (class V)	0.645	-0.472	0.0865	0.623845
AFAP1	actin filament associated protein 1	-0.586	0.53	-0.028	0.622728

Table S3.5 Top 100 differentially correlated genes with *SPTLC2* and *SPTLC3* in human liver.

Gene Name	Gene Description	*SPTLC3*	*SPTLC2*	Average	Variance
PFKP	phosphofructokinase, platelet	-0.517	0.599	0.041	0.622728
TF	transferrin	0.613	-0.502	0.0555	0.621613
MTMR2	myotubularin related protein 2	-0.459	0.655	0.098	0.620498
ABCC6P1	ATP binding cassette subfamily C member 6 pseudogene 1	0.628	-0.484	0.072	0.618272
GJB1	gap junction protein beta 1	0.628	-0.484	0.072	0.618272
GFPT2	glutamine-fructose-6-phosphate transaminase 2	-0.596	0.514	-0.041	0.61605
IQGAP2	IQ motif containing GTPase activating protein 2	0.714	-0.396	0.159	0.61605
MAOB	monoamine oxidase B	0.633	-0.477	0.078	0.61605
SERPIND1	serpin family D member 1	0.621	-0.487	0.067	0.613832
F2	coagulation factor II, thrombin	0.588	-0.519	0.0345	0.612725
HK1	hexokinase 1	-0.522	0.585	0.0315	0.612725
SMLR1	small leucine rich protein 1	0.627	-0.479	0.074	0.611618
SLC19A3	solute carrier family 19 member 3	0.608	-0.496	0.056	0.609408
CHSY1	chondroitin sulfate synthase 1	-0.481	0.622	0.0705	0.608305
HLF	HLF, PAR bZIP transcription factor	0.63	-0.472	0.079	0.607202
SLC22A9	solute carrier family 22 member 9	0.563	-0.539	0.012	0.607202
LDLRAD3	low density lipoprotein receptor class A domain containing 3	-0.475	0.626	0.0755	0.606101
LRP12	LDL receptor related protein 12	-0.529	0.572	0.0215	0.606101
GATM	glycine amidinotransferase	0.657	-0.443	0.107	0.605
IQGAP1	IQ motif containing GTPase activating protein 1	-0.424	0.676	0.126	0.605
LOXL2	lysyl oxidase like 2	-0.581	0.519	-0.031	0.605
SPOCK1	SPARC (osteonectin), cwcv and kazal like domains proteoglycan 1	-0.55	0.55	0	0.605
ACSM2B	acyl-CoA synthetase medium chain family member 2B	0.636	-0.463	0.0865	0.603901

Table S3.5 Top 100 differentially correlated genes with *SPTLC2* and *SPTLC3* in human liver.

Gene Name	Gene Description	*SPTLC3*	*SPTLC2*	Average	Variance
CYP4F3	cytochrome P450 family 4 subfamily F member 3	0.593	-0.505	0.044	0.602802
AGMAT	agmatinase	0.61	-0.487	0.0615	0.601705
ABCC6	ATP binding cassette subfamily C member 6	0.601	-0.495	0.053	0.600608
PTK7	protein tyrosine kinase 7 (inactive)	-0.555	0.541	-0.007	0.600608
ZNF385B	zinc finger protein 385B	0.663	-0.433	0.115	0.600608
AGMO	alkylglycerol monooxygenase	0.657	-0.438	0.1095	0.599513
PROX1	prospero homeobox 1	0.654	-0.441	0.1065	0.599513
ANKS4B	ankyrin repeat and sterile alpha motif domain containing 4B	0.674	-0.42	0.127	0.598418
ALB	albumin	0.606	-0.488	0.059	0.598418
ARHGAP23	Rho GTPase activating protein 23	-0.51	0.584	0.037	0.598418
PDLIM4	PDZ and LIM domain 4	-0.596	0.498	-0.049	0.598418
PON1	paraoxonase 1	0.624	-0.47	0.077	0.598418
ASGR2	asialoglycoprotein receptor 2	0.564	-0.527	0.0185	0.595141
TPBG	trophoblast glycoprotein	-0.564	0.526	-0.019	0.59405
EHHADH	enoyl-CoA hydratase and 3-hydroxyacyl CoA dehydrogenase	0.686	-0.4	0.143	0.589698
RNF145	ring finger protein 145	-0.461	0.625	0.082	0.589698
RGN	regucalcin	0.575	-0.511	0.032	0.589698
NR1H4	nuclear receptor subfamily 1 group H member 4	0.563	-0.522	0.0205	0.588613
ABCC1	ATP binding cassette subfamily C member 1	-0.571	0.513	-0.029	0.587528
BHMT2	betaine--homocysteine S-methyltransferase 2	0.585	-0.499	0.043	0.587528
CPB2	carboxypeptidase B2	0.626	-0.458	0.084	0.587528
SLC30A10	solute carrier family 30 member 10	0.632	-0.452	0.09	0.587528
FABP1	fatty acid binding protein 1	0.575	-0.505	0.035	0.5832
METTL9	methyltransferase like 9	-0.503	0.577	0.037	0.5832

Table S3.5 Top 100 differentially correlated genes with *SPTLC2* and *SPTLC3* in human liver.

Gene Name	Gene Description	*SPTLC3*	*SPTLC2*	Average	Variance
AGXT2	alanine--glyoxylate aminotransferase 2	0.643	-0.436	0.1035	0.582121
SLC47A1	solute carrier family 47 member 1	0.626	-0.453	0.0865	0.582121
ACSM2A	acyl-CoA synthetase medium chain family member 2A	0.627	-0.451	0.088	0.581042
ANGPTL3	angiopoietin like 3	0.62	-0.458	0.081	0.581042
CYP39A1	cytochrome P450 family 39 subfamily A member 1	0.652	-0.426	0.113	0.581042
FOXC2	forkhead box C2	-0.602	0.476	-0.063	0.581042
GALNT7	polypeptide N-acetylgalactosaminyltransferase 7	-0.509	0.569	0.03	0.581042
RASA3	RAS p21 protein activator 3	-0.499	0.579	0.04	0.581042
APOH	apolipoprotein H	0.599	-0.478	0.0605	0.579965
EHD2	EH domain containing 2	-0.526	0.551	0.0125	0.579965
RUNX1	runt related transcription factor 1	-0.601	0.476	-0.0625	0.579965
TCEA3	transcription elongation factor A3	0.542	-0.534	0.004	0.578888
XXYLT1	xyloside xylosyltransferase 1	-0.536	0.538	0.001	0.576738
IFNWP19	interferon omega 1 pseudogene 19	-0.579	0.495	-0.042	0.576738
MTHFD2	methylenetetrahydrofolate dehydrogenase (NADP+ dependent) 2, methenyltetrahydrofolate cyclohydrolase	-0.574	0.5	-0.037	0.576738
CYTH3	cytohesin 3	-0.512	0.561	0.0245	0.575665
DGAT2	diacylglycerol O-acyltransferase 2	0.625	-0.448	0.0885	0.575665
F5	coagulation factor V	0.632	-0.441	0.0955	0.575665
DRP2	dystrophin related protein 2	-0.586	0.486	-0.05	0.574592
SERPINH1	serpin family H member 1	-0.628	0.444	-0.092	0.574592
CTTNBP2NL	CTTNBP2 N-terminal like	-0.44	0.631	0.0955	0.573521
CERCAM	cerebral endothelial cell adhesion molecule	-0.583	0.486	-0.0485	0.571381

Table S3.5 Top 100 differentially correlated genes with *SPTLC2* and *SPTLC3* in human liver.

Gene Name	Gene Description	*SPTLC3*	*SPTLC2*	Average	Variance
CREB3L1	cAMP responsive element binding protein 3 like 1	-0.609	0.46	-0.0745	0.571381
KNG1	kininogen 1	0.613	-0.456	0.0785	0.571381
TUBA1A	tubulin alpha 1a	-0.53	0.539	0.0045	0.571381
HGD	homogentisate 1,2-dioxygenase	0.598	-0.47	0.064	0.570312
ITIH2	inter-alpha-trypsin inhibitor heavy chain 2	0.585	-0.483	0.051	0.570312
SLC17A1	solute carrier family 17 member 1	0.616	-0.452	0.082	0.570312
CALU	calumenin	-0.46	0.607	0.0735	0.569245
PIPOX	pipecolic acid and sarcosine oxidase	0.634	-0.433	0.1005	0.569245
APOC3	apolipoprotein C3	0.598	-0.468	0.065	0.568178
CD44	CD44 molecule (Indian blood group)	-0.469	0.597	0.064	0.568178
ALDH1A1	aldehyde dehydrogenase 1 family member A1	0.611	-0.454	0.0785	0.567113
HNF4A	hepatocyte nuclear factor 4 alpha	0.619	-0.446	0.0865	0.567113
ORM2	orosomucoid 2	0.582	-0.483	0.0495	0.567113
UGT2B4	UDP glucuronosyltransferase family 2 member B4	0.615	-0.45	0.0825	0.567113
APOC1	apolipoprotein C1	0.556	-0.508	0.024	0.566048
HPX	hemopexin	0.604	-0.46	0.072	0.566048
KLKB1	kallikrein B1	0.621	-0.442	0.0895	0.564985

Chapter 5 References

[1] D. M. Dreon, H. A. Fernstrom, H. Campos, P. Blanche, P. T. Williams, and R. M. Krauss, "Change in dietary saturated fat intake is correlated with change in mass of large low-density-lipoprotein particles in men," *Am. J. Clin. Nutr.*, vol. 67, no. 5, pp. 828–836, May 1998, doi: 10.1093/ajcn/67.5.828.

[2] A. Mente, L. de Koning, H. S. Shannon, and S. S. Anand, "A systematic review of the evidence supporting a causal link between dietary factors and coronary heart disease," *Arch. Intern. Med.*, vol. 169, no. 7, pp. 659–669, Apr. 2009, doi: 10.1001/archinternmed.2009.38.

[3] S. H. Zhang, R. L. Reddick, J. A. Piedrahita, and N. Maeda, "Spontaneous hypercholesterolemia and arterial lesions in mice lacking apolipoprotein E," *Science*, vol. 258, no. 5081, pp. 468–471, Oct. 1992, doi: 10.1126/science.1411543.

[4] S. Ishibashi, M. S. Brown, J. L. Goldstein, R. D. Gerard, R. E. Hammer, and J. Herz, "Hypercholesterolemia in low density lipoprotein receptor knockout mice and its reversal by adenovirus-mediated gene delivery," *J. Clin. Invest.*, vol. 92, no. 2, pp. 883–893, Aug. 1993, doi: 10.1172/JCI116663.

[5] Y. Nakashima, A. S. Plump, E. W. Raines, J. L. Breslow, and R. Ross, "ApoE-deficient mice develop lesions of all phases of atherosclerosis throughout the arterial tree," *Arterioscler. Thromb. J. Vasc. Biol.*, vol. 14, no. 1, pp. 133–140, Jan. 1994, doi: 10.1161/01.atv.14.1.133.

[6] S. Ishibashi, J. L. Goldstein, M. S. Brown, J. Herz, and D. K. Burns, "Massive xanthomatosis and atherosclerosis in cholesterol-fed low density lipoprotein receptor-negative mice," *J. Clin. Invest.*, vol. 93, no. 5, pp. 1885–1893, May 1994, doi: 10.1172/JCI117179.

[7] R. M. Machado, E. R. Nakandakare, E. C. R. Quintao, P. M. Cazita, M. K. Koike, V. S. Nunes, F. D. Ferreira, M. S. Afonso, R. P. A. Bombo, A. Machado-Lima, F. G. Soriano, S. Catanozi, and A. M. Lottenberg, "Omega-6 polyunsaturated fatty acids prevent atherosclerosis development in LDLr-KO mice, in spite of displaying a pro-inflammatory profile similar to trans fatty acids," *Atherosclerosis*, vol. 224, no. 1, pp. 66–74, Sep. 2012, doi: 10.1016/j.atherosclerosis.2012.06.059.

[8] K. Simons and G. van Meer, "Lipid sorting in epithelial cells," *Biochemistry*, vol. 27, no. 17, pp. 6197–6202, Aug. 1988, doi: 10.1021/bi00417a001.

[9] G. van Meer, "Lipid traffic in animal cells," *Annu. Rev. Cell Biol.*, vol. 5, pp. 247–275, 1989, doi: 10.1146/annurev.cb.05.110189.001335.

[10] K. Simons and E. Ikonen, "Functional rafts in cell membranes," *Nature*, vol. 387, no. 6633, pp. 569–572, Jun. 1997, doi: 10.1038/42408.

[11] T. Harder, P. Scheiffele, P. Verkade, and K. Simons, “Lipid domain structure of the plasma membrane revealed by patching of membrane components,” *J. Cell Biol.*, vol. 141, no. 4, pp. 929–942, May 1998, doi: 10.1083/jcb.141.4.929.

[12] A. Cremesti, F. Paris, H. Grassmé, N. Holler, J. Tschopp, Z. Fuks, E. Gulbins, and R. Kolesnick, “Ceramide enables fas to cap and kill,” *J. Biol. Chem.*, vol. 276, no. 26, pp. 23954–23961, Jun. 2001, doi: 10.1074/jbc.M101866200.

[13] C. R. Bollinger, V. Teichgräber, and E. Gulbins, “Ceramide-enriched membrane domains,” *Biochim. Biophys. Acta BBA - Mol. Cell Res.*, vol. 1746, no. 3, pp. 284–294, Dec. 2005, doi: 10.1016/j.bbamcr.2005.09.001.

[14] E. R. Smith, A. H. Merrill, L. M. Obeid, and Y. A. Hannun, “Effects of sphingosine and other sphingolipids on protein kinase C,” *Methods Enzymol.*, vol. 312, pp. 361–373, 2000, doi: 10.1016/s0076-6879(00)12921-0.

[15] L. M. Obeid, C. M. Linardic, L. A. Karolak, and Y. A. Hannun, “Programmed cell death induced by ceramide,” *Science*, vol. 259, no. 5102, pp. 1769–1771, Mar. 1993, doi: 10.1126/science.8456305.

[16] D. K. Perry and Y. A. Hannun, “The role of ceramide in cell signaling,” *Biochim. Biophys. Acta*, vol. 1436, no. 1–2, pp. 233–243, Dec. 1998, doi: 10.1016/s0005-2760(98)00145-3.

[17] S. Spiegel and A. H. Merrill, “Sphingolipid metabolism and cell growth regulation,” *FASEB J. Off. Publ. Fed. Am. Soc. Exp. Biol.*, vol. 10, no. 12, pp. 1388–1397, Oct. 1996, doi: 10.1096/fasebj.10.12.8903509.

[18] M. L. Allende, H. Zhu, M. Kono, L. E. Hoachlander-Hobby, V. L. Huso, and R. L. Proia, “Genetic defects in the sphingolipid degradation pathway and their effects on microglia in neurodegenerative disease,” *Cell. Signal.*, vol. 78, p. 109879, Feb. 2021, doi: 10.1016/j.cellsig.2020.109879.

[19] B. Ogretmen, “Sphingolipid metabolism in cancer signalling and therapy,” *Nat. Rev. Cancer*, vol. 18, no. 1, pp. 33–50, Jan. 2018, doi: 10.1038/nrc.2017.96.

[20] M.-H. Li, T. Sanchez, G. L. Milne, J. D. Morrow, T. Hla, and F. Ferrer, “S1P/S1P2 signaling induces cyclooxygenase-2 expression in Wilms tumor,” *J. Urol.*, vol. 181, no. 3, pp. 1347–1352, Mar. 2009, doi: 10.1016/j.juro.2008.10.140.

[21] M.-H. Li, T. Sanchez, A. Pappalardo, K. R. Lynch, T. Hla, and F. Ferrer, “Induction of antiproliferative connective tissue growth factor expression in Wilms’ tumor cells by sphingosine-1-phosphate receptor 2,” *Mol. Cancer Res. MCR*, vol. 6, no. 10, pp. 1649–1656, Oct. 2008, doi: 10.1158/1541-7786.MCR-07-2048.

[22] J. Liang, M. Nagahashi, E. Y. Kim, K. B. Harikumar, A. Yamada, W.-C. Huang, N. C. Hait, J. C. Allegood, M. M. Price, D. Avni, K. Takabe, T. Kordula, S. Milstien, and S. Spiegel, “Sphingosine-1-phosphate links persistent STAT3 activation, chronic intestinal

inflammation, and development of colitis-associated cancer," *Cancer Cell*, vol. 23, no. 1, pp. 107–120, Jan. 2013, doi: 10.1016/j.ccr.2012.11.013.

[23] W.-C. Huang, M. Nagahashi, K. P. Terracina, and K. Takabe, "Emerging Role of Sphingosine-1-phosphate in Inflammation, Cancer, and Lymphangiogenesis," *Biomolecules*, vol. 3, no. 3, pp. 408–434, 2013, doi: 10.3390/biom3030408.

[24] I. V. Tiper, J. E. East, P. B. Subrahmanyam, and T. J. Webb, "Sphingosine 1-phosphate signaling impacts lymphocyte migration, inflammation and infection," *Pathog. Dis.*, vol. 74, no. 6, p. ftw063, Aug. 2016, doi: 10.1093/femspd/ftw063.

[25] M. Knapp, A. Lisowska, P. Zabielski, W. Musiał, and M. Baranowski, "Sustained decrease in plasma sphingosine-1-phosphate concentration and its accumulation in blood cells in acute myocardial infarction," *Prostaglandins Other Lipid Mediat.*, vol. 106, pp. 53–61, Oct. 2013, doi: 10.1016/j.prostaglandins.2013.10.001.

[26] F. Potì, F. Gualtieri, S. Sacchi, G. Weißen-Plenz, G. Varga, M. Brodde, C. Weber, M. Simoni, and J.-R. Nofer, "KRP-203, sphingosine 1-phosphate receptor type 1 agonist, ameliorates atherosclerosis in LDL-R-/- mice," *Arterioscler. Thromb. Vasc. Biol.*, vol. 33, no. 7, pp. 1505–1512, Jul. 2013, doi: 10.1161/ATVBAHA.113.301347.

[27] K. J. E. Sattler, S. Elbasan, P. Keul, M. Elter-Schulz, C. Bode, M. H. Gräler, M. Bröcker-Preuss, T. Budde, R. Erbel, G. Heusch, and B. Levkau, "Sphingosine 1-phosphate levels in plasma and HDL are altered in coronary artery disease," *Basic Res. Cardiol.*, vol. 105, no. 6, pp. 821–832, Nov. 2010, doi: 10.1007/s00395-010-0112-5.

[28] Y. Liu, R. Wada, T. Yamashita, Y. Mi, C. X. Deng, J. P. Hobson, H. M. Rosenfeldt, V. E. Nava, S. S. Chae, M. J. Lee, C. H. Liu, T. Hla, S. Spiegel, and R. L. Proia, "Edg-1, the G protein-coupled receptor for sphingosine-1-phosphate, is essential for vascular maturation," *J. Clin. Invest.*, vol. 106, no. 8, pp. 951–961, Oct. 2000, doi: 10.1172/JCI10905.

[29] K. Mizugishi, T. Yamashita, A. Olivera, G. F. Miller, S. Spiegel, and R. L. Proia, "Essential role for sphingosine kinases in neural and vascular development," *Mol. Cell. Biol.*, vol. 25, no. 24, pp. 11113–11121, Dec. 2005, doi: 10.1128/MCB.25.24.11113-11121.2005.

[30] M. Kono, Y. Mi, Y. Liu, T. Sasaki, M. L. Allende, Y.-P. Wu, T. Yamashita, and R. L. Proia, "The sphingosine-1-phosphate receptors S1P1, S1P2, and S1P3 function coordinately during embryonic angiogenesis," *J. Biol. Chem.*, vol. 279, no. 28, pp. 29367–29373, Jul. 2004, doi: 10.1074/jbc.M403937200.

[31] T. Kimura, T. Watanabe, K. Sato, J. Kon, H. Tomura, K. Tamama, A. Kuwabara, T. Kanda, I. Kobayashi, H. Ohta, M. Ui, and F. Okajima, "Sphingosine 1-phosphate stimulates proliferation and migration of human endothelial cells possibly through the lipid receptors, Edg-1 and Edg-3," *Biochem. J.*, vol. 348 Pt 1, no. Pt 1, pp. 71–76, May 2000.

[32] S. An, Y. Zheng, and T. Bleu, “Sphingosine 1-phosphate-induced cell proliferation, survival, and related signaling events mediated by G protein-coupled receptors Edg3 and Edg5,” *J. Biol. Chem.*, vol. 275, no. 1, pp. 288–296, Jan. 2000, doi: 10.1074/jbc.275.1.288.

[33] S. Wang, P. Robinet, J. D. Smith, and K. Gulshan, “ORMDL orosomucoid-like proteins are degraded by free-cholesterol-loading-induced autophagy,” *Proc. Natl. Acad. Sci. U. S. A.*, vol. 112, no. 12, pp. 3728–3733, Mar. 2015, doi: 10.1073/pnas.1422455112.

[34] M. F. Moffatt, M. Kabesch, L. Liang, A. L. Dixon, D. Strachan, S. Heath, M. Depner, A. von Berg, A. Bufe, E. Rietschel, A. Heinzmann, B. Simma, T. Frischer, S. A. G. Willis-Owen, K. C. C. Wong, T. Illig, C. Vogelberg, S. K. Weiland, E. von Mutius, G. R. Abecasis, M. Farrall, I. G. Gut, G. M. Lathrop, and W. O. C. Cookson, “Genetic variants regulating ORMDL3 expression contribute to the risk of childhood asthma,” *Nature*, vol. 448, no. 7152, pp. 470–473, Jul. 2007, doi: 10.1038/nature06014.

[35] D. P. B. McGovern, A. Gardet, L. Törkvist, P. Goyette, J. Essers, K. D. Taylor, B. M. Neale, R. T. H. Ong, C. Lagacé, C. Li, T. Green, C. R. Stevens, C. Beauchamp, P. R. Fleshner, M. Carlson, M. D’Amato, J. Halfvarson, M. L. Hibberd, M. Lördal, L. Padyukov, A. Andriulli, E. Colombo, A. Latiano, O. Palmieri, E.-J. Bernard, C. Deslandres, D. W. Hommes, D. J. de Jong, P. C. Stokkers, R. K. Weersma, NIDDK IBD Genetics Consortium, Y. Sharma, M. S. Silverberg, J. H. Cho, J. Wu, K. Roeder, S. R. Brant, L. P. Schumm, R. H. Duerr, M. C. Dubinsky, N. L. Glazer, T. Haritunians, A. Ippoliti, G. Y. Melmed, D. S. Siscovick, E. A. Vasiliauskas, S. R. Targan, V. Annese, C. Wijmenga, S. Pettersson, J. I. Rotter, R. J. Xavier, M. J. Daly, J. D. Rioux, and M. Seielstad, “Genome-wide association identifies multiple ulcerative colitis susceptibility loci,” *Nat. Genet.*, vol. 42, no. 4, pp. 332–337, Apr. 2010, doi: 10.1038/ng.549.

[36] J. C. Barrett, D. G. Clayton, P. Concannon, B. Akolkar, J. D. Cooper, H. A. Erlich, C. Julier, G. Morahan, J. Nerup, C. Nierras, V. Plagnol, F. Pociot, H. Schuilenburg, D. J. Smyth, H. Stevens, J. A. Todd, N. M. Walker, S. S. Rich, and Type 1 Diabetes Genetics Consortium, “Genome-wide association study and meta-analysis find that over 40 loci affect risk of type 1 diabetes,” *Nat. Genet.*, vol. 41, no. 6, pp. 703–707, Jun. 2009, doi: 10.1038/ng.381.

[37] J. C. Barrett, S. Hansoul, D. L. Nicolae, J. H. Cho, R. H. Duerr, J. D. Rioux, S. R. Brant, M. S. Silverberg, K. D. Taylor, M. M. Barmada, A. Bitton, T. Dassopoulos, L. W. Datta, T. Green, A. M. Griffiths, E. O. Kistner, M. T. Murtha, M. D. Regueiro, J. I. Rotter, L. P. Schumm, A. H. Steinhart, S. R. Targan, R. J. Xavier, NIDDK IBD Genetics Consortium, C. Libioulle, C. Sandor, M. Lathrop, J. Belaiche, O. Dewit, I. Gut, S. Heath, D. Laukens, M. Mni, P. Rutgeerts, A. Van Gossum, D. Zelenika, D. Franchimont, J.-P. Hugot, M. de Vos, S. Vermeire, E. Louis, Belgian-French IBD Consortium, Wellcome Trust Case Control Consortium, L. R. Cardon, C. A. Anderson, H. Drummond, E. Nimmo, T. Ahmad, N. J. Prescott, C. M. Onnie, S. A. Fisher, J. Marchini, J. Ghori, S. Bumpstead, R. Gwilliam, M. Tremelling, P. Deloukas, J. Mansfield, D. Jewell, J. Satsangi, C. G. Mathew, M. Parkes, M. Georges, and M. J. Daly, “Genome-wide association defines more than 30

distinct susceptibility loci for Crohn's disease," *Nat. Genet.*, vol. 40, no. 8, pp. 955–962, Aug. 2008, doi: 10.1038/ng.175.

[38] S. M. Hammad, N. L. Baker, J. M. El Abiad, S. D. Spassieva, J. S. Pierce, B. Rembiesa, J. Bielawski, M. F. Lopes-Virella, R. L. Klein, and DCCT/EDIC Group of Investigators, "Increased Plasma Levels of Select Deoxy-ceramide and Ceramide Species are Associated with Increased Odds of Diabetic Neuropathy in Type 1 Diabetes: A Pilot Study," *Neuromolecular Med.*, vol. 19, no. 1, pp. 46–56, Mar. 2017, doi: 10.1007/s12017-016-8423-9.

[39] A. S. Havulinna, M. Sysi-Aho, M. Hilvo, D. Kauhanen, R. Hurme, K. Ekroos, V. Salomaa, and R. Laaksonen, "Circulating Ceramides Predict Cardiovascular Outcomes in the Population-Based FINRISK 2002 Cohort," *Arterioscler. Thromb. Vasc. Biol.*, vol. 36, no. 12, pp. 2424–2430, Dec. 2016, doi: 10.1161/ATVBAHA.116.307497.

[40] A. Othman, C. H. Saely, A. Muendlein, A. Vonbank, H. Drexel, A. von Eckardstein, and T. Hornemann, "Plasma 1-deoxysphingolipids are predictive biomarkers for type 2 diabetes mellitus," *BMJ Open Diabetes Res. Care*, vol. 3, no. 1, p. e000073, 2015, doi: 10.1136/bmjdrc-2014-000073.

[41] E. B. Smith, "Intimal and medial lipids in human aortas," *Lancet Lond. Engl.*, vol. 1, no. 7128, pp. 799–803, Apr. 1960, doi: 10.1016/s0140-6736(60)90680-2.

[42] J. Iqbal, M. T. Walsh, S. M. Hammad, and M. M. Hussain, "Sphingolipids and Lipoproteins in Health and Metabolic Disorders," *Trends Endocrinol. Metab. TEM*, vol. 28, no. 7, pp. 506–518, Jul. 2017, doi: 10.1016/j.tem.2017.03.005.

[43] S. L. Schissel, J. Tweedie-Hardman, J. H. Rapp, G. Graham, K. J. Williams, and I. Tabas, "Rabbit aorta and human atherosclerotic lesions hydrolyze the sphingomyelin of retained low-density lipoprotein. Proposed role for arterial-wall sphingomyelinase in subendothelial retention and aggregation of atherogenic lipoproteins.," *J. Clin. Invest.*, vol. 98, no. 6, pp. 1455–1464, Sep. 1996, doi: 10.1172/JCI118934.

[44] K. J. Williams and I. Tabas, "The response-to-retention hypothesis of early atherogenesis," *Arterioscler. Thromb. Vasc. Biol.*, vol. 15, no. 5, pp. 551–561, May 1995, doi: 10.1161/01.atv.15.5.551.

[45] C. M. Devlin, A. R. Leventhal, G. Kuriakose, E. H. Schuchman, K. J. Williams, and I. Tabas, "Acid sphingomyelinase promotes lipoprotein retention within early atheromata and accelerates lesion progression," *Arterioscler. Thromb. Vasc. Biol.*, vol. 28, no. 10, pp. 1723–1730, Oct. 2008, doi: 10.1161/ATVBAHA.108.173344.

[46] Y. Fan, F. Shi, J. Liu, J. Dong, H. H. Bui, D. A. Peake, M.-S. Kuo, G. Cao, and X.-C. Jiang, "Selective reduction in the sphingomyelin content of atherogenic lipoproteins inhibits their retention in murine aortas and the subsequent development of atherosclerosis," *Arterioscler. Thromb. Vasc. Biol.*, vol. 30, no. 11, pp. 2114–2120, Nov. 2010, doi: 10.1161/ATVBAHA.110.213363.

[47] H. Obinata and T. Hla, “Sphingosine 1-phosphate and inflammation,” *Int. Immunol.*, vol. 31, no. 9, pp. 617–625, Aug. 2019, doi: 10.1093/intimm/dxz037.

[48] A. Skoura, J. Michaud, D.-S. Im, S. Thangada, Y. Xiong, J. D. Smith, and T. Hla, “Sphingosine-1-phosphate receptor-2 function in myeloid cells regulates vascular inflammation and atherosclerosis,” *Arterioscler. Thromb. Vasc. Biol.*, vol. 31, no. 1, pp. 81–85, Jan. 2011, doi: 10.1161/ATVBAHA.110.213496.

[49] J.-R. Nofer, M. Bot, M. Brodde, P. J. Taylor, P. Salm, V. Brinkmann, T. van Berkel, G. Assmann, and E. A. L. Biessen, “FTY720, a synthetic sphingosine 1 phosphate analogue, inhibits development of atherosclerosis in low-density lipoprotein receptor-deficient mice,” *Circulation*, vol. 115, no. 4, pp. 501–508, Jan. 2007, doi: 10.1161/CIRCULATIONAHA.106.641407.

[50] F. Poti, S. Costa, V. Bergonzini, M. Galletti, E. Pignatti, C. Weber, M. Simoni, and J.-R. Nofer, “Effect of sphingosine 1-phosphate (S1P) receptor agonists FTY720 and CYM5442 on atherosclerosis development in LDL receptor deficient (LDL-R$^{-/-}$) mice,” *Vascul. Pharmacol.*, vol. 57, no. 1, pp. 56–64, Aug. 2012, doi: 10.1016/j.vph.2012.03.003.

[51] T.-S. Park, R. L. Panek, S. B. Mueller, J. C. Hanselman, W. S. Rosebury, A. W. Robertson, E. K. Kindt, R. Homan, S. K. Karathanasis, and M. D. Rekhter, “Inhibition of sphingomyelin synthesis reduces atherogenesis in apolipoprotein E-knockout mice,” *Circulation*, vol. 110, no. 22, pp. 3465–3471, Nov. 2004, doi: 10.1161/01.CIR.0000148370.60535.22.

[52] M. R. Hojjati, Z. Li, H. Zhou, S. Tang, C. Huan, E. Ooi, S. Lu, and X.-C. Jiang, “Effect of Myriocin on Plasma Sphingolipid Metabolism and Atherosclerosis in apoE-deficient Mice,” *J. Biol. Chem.*, vol. 280, no. 11, pp. 10284–10289, Mar. 2005, doi: 10.1074/jbc.M412348200.

[53] E. N. Glaros, W. S. Kim, C. M. Quinn, W. Jessup, K.-A. Rye, and B. Garner, “Myriocin slows the progression of established atherosclerotic lesions in apolipoprotein E gene knockout mice,” *J. Lipid Res.*, vol. 49, no. 2, pp. 324–331, Feb. 2008, doi: 10.1194/jlr.M700261-JLR200.

[54] X. C. Jiang, F. Paultre, T. A. Pearson, R. G. Reed, C. K. Francis, M. Lin, L. Berglund, and A. R. Tall, “Plasma sphingomyelin level as a risk factor for coronary artery disease,” *Arterioscler. Thromb. Vasc. Biol.*, vol. 20, no. 12, pp. 2614–2618, Dec. 2000, doi: 10.1161/01.atv.20.12.2614.

[55] A. Schlitt, S. Blankenberg, D. Yan, H. von Gizycki, M. Buerke, K. Werdan, C. Bickel, K. J. Lackner, J. Meyer, H. J. Rupprecht, and X.-C. Jiang, “Further evaluation of plasma sphingomyelin levels as a risk factor for coronary artery disease,” *Nutr. Metab.*, vol. 3, p. 5, Jan. 2006, doi: 10.1186/1743-7075-3-5.

[56] D. H. Deutschman, J. S. Carstens, R. L. Klepper, W. S. Smith, M. T. Page, T. R. Young, L. A. Gleason, N. Nakajima, and R. A. Sabbadini, “Predicting obstructive coronary artery

disease with serum sphingosine-1-phosphate," *Am. Heart J.*, vol. 146, no. 1, pp. 62–68, Jul. 2003, doi: 10.1016/S0002-8703(03)00118-2.

[57] G. Chiri-Osmond, "Mayo Clinic Launches First-in-U.S. Blood Test that Assesses Risk of Heart Attack Using Plasma Ceramides." [Online]. Available: https://newsnetwork.mayoclinic.org/discussion/mayo-clinic-launches-first-in-u-s-blood-test-that-assesses-risk-of-heart-attack-using-plasma-ceramides/

[58] M. C. Sullards, J. C. Allegood, S. Kelly, E. Wang, C. A. Haynes, H. Park, Y. Chen, and A. H. Merrill, "Structure-Specific, Quantitative Methods for Analysis of Sphingolipids by Liquid Chromatography–Tandem Mass Spectrometry: 'Inside-Out' Sphingolipidomics," in *Methods in Enzymology*, vol. 432, Elsevier, 2007, pp. 83–115. doi: 10.1016/S0076-6879(07)32004-1.

[59] Y. A. Hannun and L. M. Obeid, "Principles of bioactive lipid signalling: lessons from sphingolipids," *Nat. Rev. Mol. Cell Biol.*, vol. 9, no. 2, pp. 139–150, Feb. 2008, doi: 10.1038/nrm2329.

[60] N. C. Zitomer, T. Mitchell, K. A. Voss, G. S. Bondy, S. T. Pruett, E. C. Garnier-Amblard, L. S. Liebeskind, H. Park, E. Wang, M. C. Sullards, A. H. Merrill, and R. T. Riley, "Ceramide synthase inhibition by fumonisin B1 causes accumulation of 1-deoxysphinganine: a novel category of bioactive 1-deoxysphingoid bases and 1-deoxydihydroceramides biosynthesized by mammalian cell lines and animals," *J. Biol. Chem.*, vol. 284, no. 8, pp. 4786–4795, Feb. 2009, doi: 10.1074/jbc.M808798200.

[61] F. S. Eichler, T. Hornemann, A. McCampbell, D. Kuljis, A. Penno, D. Vardeh, E. Tamrazian, K. Garofalo, H.-J. Lee, L. Kini, M. Selig, M. Frosch, K. Gable, A. von Eckardstein, C. J. Woolf, G. Guan, J. M. Harmon, T. M. Dunn, and R. H. Brown, "Overexpression of the wild-type SPT1 subunit lowers desoxysphingolipid levels and rescues the phenotype of HSAN1," *J. Neurosci. Off. J. Soc. Neurosci.*, vol. 29, no. 46, pp. 14646–14651, Nov. 2009, doi: 10.1523/JNEUROSCI.2536-09.2009.

[62] A. Penno, M. M. Reilly, H. Houlden, M. Laurá, K. Rentsch, V. Niederkofler, E. T. Stoeckli, G. Nicholson, F. Eichler, R. H. Brown, A. von Eckardstein, and T. Hornemann, "Hereditary sensory neuropathy type 1 is caused by the accumulation of two neurotoxic sphingolipids," *J. Biol. Chem.*, vol. 285, no. 15, pp. 11178–11187, Apr. 2010, doi: 10.1074/jbc.M109.092973.

[63] M. Bertea, M. F. Rütti, A. Othman, J. Marti-Jaun, M. Hersberger, A. von Eckardstein, and T. Hornemann, "Deoxysphingoid bases as plasma markers in diabetes mellitus," *Lipids Health Dis.*, vol. 9, p. 84, Aug. 2010, doi: 10.1186/1476-511X-9-84.

[64] T. Muthusamy, T. Cordes, M. K. Handzlik, L. You, E. W. Lim, J. Gengatharan, A. F. M. Pinto, M. G. Badur, M. J. Kolar, M. Wallace, A. Saghatelian, and C. M. Metallo, "Serine restriction alters sphingolipid diversity to constrain tumour growth," *Nature*, vol. 586, no. 7831, pp. 790–795, Oct. 2020, doi: 10.1038/s41586-020-2609-x.

[65] T. Cordes, R. S. Kuna, G. H. McGregor, S. V. Khare, J. Gengatharan, T. Muthusamy, and C. M. Metallo, “1-Deoxysphingolipid synthesis compromises anchorage-independent growth and plasma membrane endocytosis in cancer cells,” *J. Lipid Res.*, vol. 63, no. 10, p. 100281, Oct. 2022, doi: 10.1016/j.jlr.2022.100281.

[66] M. L. Gantner, K. Eade, M. Wallace, M. K. Handzlik, R. Fallon, J. Trombley, R. Bonelli, S. Giles, S. Harkins-Perry, T. F. C. Heeren, L. Sauer, Y. Ideguchi, M. Baldini, L. Scheppke, M. I. Dorrell, M. Kitano, B. J. Hart, C. Cai, T. Nagasaki, M. G. Badur, M. Okada, S. M. Woods, C. Egan, M. Gillies, R. Guymer, F. Eichler, M. Bahlo, M. Fruttiger, R. Allikmets, P. S. Bernstein, C. M. Metallo, and M. Friedlander, “Serine and Lipid Metabolism in Macular Disease and Peripheral Neuropathy,” *N. Engl. J. Med.*, vol. 381, no. 15, pp. 1422–1433, Oct. 2019, doi: 10.1056/NEJMoa1815111.

[67] A. H. Merrill and R. D. Williams, “Utilization of different fatty acyl-CoA thioesters by serine palmitoyltransferase from rat brain.,” *J. Lipid Res.*, vol. 25, no. 2, pp. 185–188, Feb. 1984, doi: 10.1016/S0022-2275(20)37838-X.

[68] A. H. Merrill, D. W. Nixon, and R. D. Williams, “Activities of serine palmitoyltransferase (3-ketosphinganine synthase) in microsomes from different rat tissues.,” *J. Lipid Res.*, vol. 26, no. 5, pp. 617–622, May 1985, doi: 10.1016/S0022-2275(20)34349-2.

[69] G. Han, S. D. Gupta, K. Gable, S. Niranjanakumari, P. Moitra, F. Eichler, R. H. Brown, J. M. Harmon, and T. M. Dunn, “Identification of small subunits of mammalian serine palmitoyltransferase that confer distinct acyl-CoA substrate specificities,” *Proc. Natl. Acad. Sci.*, vol. 106, no. 20, pp. 8186–8191, May 2009, doi: 10.1073/pnas.0811269106.

[70] T. Hornemann, A. Penno, M. F. Rütti, D. Ernst, F. Kivrak-Pfiffner, L. Rohrer, and A. von Eckardstein, “The SPTLC3 subunit of serine palmitoyltransferase generates short chain sphingoid bases,” *J. Biol. Chem.*, vol. 284, no. 39, pp. 26322–26330, Sep. 2009, doi: 10.1074/jbc.M109.023192.

[71] A. N. Kimberlin, S. Majumder, G. Han, M. Chen, R. E. Cahoon, J. M. Stone, T. M. Dunn, and E. B. Cahoon, “Arabidopsis 56-amino acid serine palmitoyltransferase-interacting proteins stimulate sphingolipid synthesis, are essential, and affect mycotoxin sensitivity,” *Plant Cell*, vol. 25, no. 11, pp. 4627–4639, Nov. 2013, doi: 10.1105/tpc.113.116145.

[72] L. Zhao, S. Spassieva, K. Gable, S. D. Gupta, L.-Y. Shi, J. Wang, J. Bielawski, W. L. Hicks, M. P. Krebs, J. Naggert, Y. A. Hannun, T. M. Dunn, and P. M. Nishina, “Elevation of 20-carbon long chain bases due to a mutation in serine palmitoyltransferase small subunit b results in neurodegeneration,” *Proc. Natl. Acad. Sci. U. S. A.*, vol. 112, no. 42, pp. 12962–12967, Oct. 2015, doi: 10.1073/pnas.1516733112.

[73] M. A. Lone, A. J. Hülsmeier, E. M. Saied, G. Karsai, C. Arenz, A. von Eckardstein, and T. Hornemann, “Subunit composition of the mammalian serine-palmitoyltransferase defines the spectrum of straight and methyl-branched long-chain bases,” *Proc. Natl. Acad. Sci. U. S. A.*, vol. 117, no. 27, pp. 15591–15598, Jul. 2020, doi: 10.1073/pnas.2002391117.

[74] B. Weiss and W. Stoffel, “Human and murine serine-palmitoyl-CoA transferase--cloning, expression and characterization of the key enzyme in sphingolipid synthesis,” *Eur. J. Biochem.*, vol. 249, no. 1, pp. 239–247, Oct. 1997, doi: 10.1111/j.1432-1033.1997.00239.x.

[75] T. Hornemann, S. Richard, M. F. Rütti, Y. Wei, and A. von Eckardstein, “Cloning and initial characterization of a new subunit for mammalian serine-palmitoyltransferase,” *J. Biol. Chem.*, vol. 281, no. 49, pp. 37275–37281, Dec. 2006, doi: 10.1074/jbc.M608066200.

[76] Q.-H. Zhang, R.-X. Yin, H. Gao, F. Huang, J.-Z. Wu, S.-L. Pan, W.-X. Lin, and D.-Z. Yang, “Association of the SPTLC3 rs364585 polymorphism and serum lipid profiles in two Chinese ethnic groups,” *Lipids Health Dis.*, vol. 16, no. 1, p. 1, Jan. 2017, doi: 10.1186/s12944-016-0392-3.

[77] A. A. Hicks, P. P. Pramstaller, A. Johansson, V. Vitart, I. Rudan, P. Ugocsai, Y. Aulchenko, C. S. Franklin, G. Liebisch, J. Erdmann, I. Jonasson, I. V. Zorkoltseva, C. Pattaro, C. Hayward, A. Isaacs, C. Hengstenberg, S. Campbell, C. Gnewuch, A. C. W. Janssens, A. V. Kirichenko, I. R. König, F. Marroni, O. Polasek, A. Demirkan, I. Kolcic, C. Schwienbacher, W. Igl, Z. Biloglav, J. C. M. Witteman, I. Pichler, G. Zaboli, T. I. Axenovich, A. Peters, S. Schreiber, H.-E. Wichmann, H. Schunkert, N. Hastie, B. A. Oostra, S. H. Wild, T. Meitinger, U. Gyllensten, C. M. van Duijn, J. F. Wilson, A. Wright, G. Schmitz, and H. Campbell, “Genetic determinants of circulating sphingolipid concentrations in European populations,” *PLoS Genet.*, vol. 5, no. 10, p. e1000672, Oct. 2009, doi: 10.1371/journal.pgen.1000672.

[78] T. Illig, C. Gieger, G. Zhai, W. Römisch-Margl, R. Wang-Sattler, C. Prehn, E. Altmaier, G. Kastenmüller, B. S. Kato, H.-W. Mewes, T. Meitinger, M. H. de Angelis, F. Kronenberg, N. Soranzo, H.-E. Wichmann, T. D. Spector, J. Adamski, and K. Suhre, “A genome-wide perspective of genetic variation in human metabolism,” *Nat. Genet.*, vol. 42, no. 2, pp. 137–141, Feb. 2010, doi: 10.1038/ng.507.

[79] Y. Wei, D. Wang, F. Topczewski, and M. J. Pagliassotti, “Saturated fatty acids induce endoplasmic reticulum stress and apoptosis independently of ceramide in liver cells,” *Am. J. Physiol. Endocrinol. Metab.*, vol. 291, no. 2, pp. E275-281, Aug. 2006, doi: 10.1152/ajpendo.00644.2005.

[80] K. Hac-Wydro and P. Wydro, “The influence of fatty acids on model cholesterol/phospholipid membranes,” *Chem. Phys. Lipids*, vol. 150, no. 1, pp. 66–81, Nov. 2007, doi: 10.1016/j.chemphyslip.2007.06.213.

[81] S. Parthasarathy, J. C. Khoo, E. Miller, J. Barnett, J. L. Witztum, and D. Steinberg, “Low density lipoprotein rich in oleic acid is protected against oxidative modification: implications for dietary prevention of atherosclerosis,” *Proc. Natl. Acad. Sci. U. S. A.*, vol. 87, no. 10, pp. 3894–3898, May 1990, doi: 10.1073/pnas.87.10.3894.

[82] L. G. Gillingham, S. Harris-Janz, and P. J. H. Jones, “Dietary monounsaturated fatty acids are protective against metabolic syndrome and cardiovascular disease risk factors,” *Lipids*, vol. 46, no. 3, pp. 209–228, Mar. 2011, doi: 10.1007/s11745-010-3524-y.

[83] J. M. Brown, S. Chung, J. K. Sawyer, C. Degirolamo, H. M. Alger, T. Nguyen, X. Zhu, M.-N. Duong, A. L. Wibley, R. Shah, M. A. Davis, K. Kelley, M. D. Wilson, C. Kent, J. S. Parks, and L. L. Rudel, “Inhibition of stearoyl-coenzyme A desaturase 1 dissociates insulin resistance and obesity from atherosclerosis,” *Circulation*, vol. 118, no. 14, pp. 1467–1475, Sep. 2008, doi: 10.1161/CIRCULATIONAHA.108.793182.

[84] R. P. Mensink and M. B. Katan, “Effect of Dietary trans Fatty Acids on High-Density and Low-Density Lipoprotein Cholesterol Levels in Healthy Subjects,” *N. Engl. J. Med.*, vol. 323, no. 7, pp. 439–445, Aug. 1990, doi: 10.1056/NEJM199008163230703.

[85] F. Shao and D. A. Ford, “Elaidic acid increases hepatic lipogenesis by mediating sterol regulatory element binding protein-1c activity in HuH-7 cells,” *Lipids*, vol. 49, no. 5, pp. 403–413, May 2014, doi: 10.1007/s11745-014-3883-x.

[86] F. Sarnyai, É. Kereszturi, K. Szirmai, J. Mátyási, J. I. Al-Hag, T. Csizmadia, P. Lőw, P. Szelényi, V. Tamási, K. Tibori, V. Zámbó, B. Tóth, and M. Csala, “Different Metabolism and Toxicity of TRANS Fatty Acids, Elaidate and Vaccenate Compared to Cis-Oleate in HepG2 Cells,” *Int. J. Mol. Sci.*, vol. 23, no. 13, p. 7298, Jun. 2022, doi: 10.3390/ijms23137298.

[87] X. Jiang, F. Paultre, T. A. Pearson, R. G. Reed, C. K. Francis, M. Lin, L. Berglund, and A. R. Tall, “Plasma Sphingomyelin Level as a Risk Factor for Coronary Artery Disease,” *Arterioscler. Thromb. Vasc. Biol.*, vol. 20, no. 12, pp. 2614–2618, Dec. 2000, doi: 10.1161/01.ATV.20.12.2614.

[88] L. Vendel Nielsen, T. P. Krogager, C. Young, C. Ferreri, C. Chatgilialoglu, O. Nørregaard Jensen, and J. J. Enghild, “Effects of elaidic acid on lipid metabolism in HepG2 cells, investigated by an integrated approach of lipidomics, transcriptomics and proteomics,” *PloS One*, vol. 8, no. 9, p. e74283, 2013, doi: 10.1371/journal.pone.0074283.

[89] M. Suzuki, Y. Ohno, and A. Kihara, “Whole picture of human stratum corneum ceramides, including the chain-length diversity of long-chain bases,” *J. Lipid Res.*, vol. 63, no. 7, p. 100235, Jul. 2022, doi: 10.1016/j.jlr.2022.100235.

[90] C. B. Newgard, J. An, J. R. Bain, M. J. Muehlbauer, R. D. Stevens, L. F. Lien, A. M. Haqq, S. H. Shah, M. Arlotto, C. A. Slentz, J. Rochon, D. Gallup, O. Ilkayeva, B. R. Wenner, W. S. Yancy, H. Eisenson, G. Musante, R. S. Surwit, D. S. Millington, M. D. Butler, and L. P. Svetkey, “A branched-chain amino acid-related metabolic signature that differentiates obese and lean humans and contributes to insulin resistance,” *Cell Metab.*, vol. 9, no. 4, pp. 311–326, Apr. 2009, doi: 10.1016/j.cmet.2009.02.002.

[91] “SPTLC3 - Tissue.” [Online]. Available: https://www.proteinatlas.org/ENSG00000172296-SPTLC3/tissue

[92] A. M. Poss, J. A. Maschek, J. E. Cox, B. J. Hauner, P. N. Hopkins, S. C. Hunt, W. L. Holland, S. A. Summers, and M. C. Playdon, "Machine learning reveals serum sphingolipids as cholesterol-independent biomarkers of coronary artery disease," *J. Clin. Invest.*, vol. 130, no. 3, pp. 1363–1376, Mar. 2020, doi: 10.1172/JCI131838.

[93] D. L. Gorden, D. S. Myers, P. T. Ivanova, E. Fahy, M. R. Maurya, S. Gupta, J. Min, N. J. Spann, J. G. McDonald, S. L. Kelly, J. Duan, M. C. Sullards, T. J. Leiker, R. M. Barkley, O. Quehenberger, A. M. Armando, S. B. Milne, T. P. Mathews, M. D. Armstrong, C. Li, W. V. Melvin, R. H. Clements, M. K. Washington, A. M. Mendonsa, J. L. Witztum, Z. Guan, C. K. Glass, R. C. Murphy, E. A. Dennis, A. H. Merrill, D. W. Russell, S. Subramaniam, and H. A. Brown, "Biomarkers of NAFLD progression: a lipidomics approach to an epidemic," *J. Lipid Res.*, vol. 56, no. 3, pp. 722–736, Mar. 2015, doi: 10.1194/jlr.P056002.

[94] T. Kasumov, L. Li, M. Li, K. Gulshan, J. P. Kirwan, X. Liu, S. Previs, B. Willard, J. D. Smith, and A. McCullough, "Ceramide as a mediator of non-alcoholic Fatty liver disease and associated atherosclerosis," *PloS One*, vol. 10, no. 5, p. e0126910, 2015, doi: 10.1371/journal.pone.0126910.

[95] W. L. Holland, J. T. Brozinick, L.-P. Wang, E. D. Hawkins, K. M. Sargent, Y. Liu, K. Narra, K. L. Hoehn, T. A. Knotts, A. Siesky, D. H. Nelson, S. K. Karathanasis, G. K. Fontenot, M. J. Birnbaum, and S. A. Summers, "Inhibition of ceramide synthesis ameliorates glucocorticoid-, saturated-fat-, and obesity-induced insulin resistance," *Cell Metab.*, vol. 5, no. 3, pp. 167–179, Mar. 2007, doi: 10.1016/j.cmet.2007.01.002.

[96] C. R. Bruce, S. Risis, J. R. Babb, C. Yang, R. S. Lee-Young, D. C. Henstridge, and M. A. Febbraio, "The sphingosine-1-phosphate analog FTY720 reduces muscle ceramide content and improves glucose tolerance in high fat-fed male mice," *Endocrinology*, vol. 154, no. 1, pp. 65–76, Jan. 2013, doi: 10.1210/en.2012-1847.

[97] S. M. Turpin, H. T. Nicholls, D. M. Willmes, A. Mourier, S. Brodesser, C. M. Wunderlich, J. Mauer, E. Xu, P. Hammerschmidt, H. S. Brönneke, A. Trifunovic, G. LoSasso, F. T. Wunderlich, J.-W. Kornfeld, M. Blüher, M. Krönke, and J. C. Brüning, "Obesity-induced CerS6-dependent C16:0 ceramide production promotes weight gain and glucose intolerance," *Cell Metab.*, vol. 20, no. 4, pp. 678–686, Oct. 2014, doi: 10.1016/j.cmet.2014.08.002.

[98] J. M. Adams, T. Pratipanawatr, R. Berria, E. Wang, R. A. DeFronzo, M. C. Sullards, and L. J. Mandarino, "Ceramide content is increased in skeletal muscle from obese insulin-resistant humans," *Diabetes*, vol. 53, no. 1, pp. 25–31, Jan. 2004, doi: 10.2337/diabetes.53.1.25.

[99] J. M. Haus, S. R. Kashyap, T. Kasumov, R. Zhang, K. R. Kelly, R. A. Defronzo, and J. P. Kirwan, "Plasma ceramides are elevated in obese subjects with type 2 diabetes and correlate with the severity of insulin resistance," *Diabetes*, vol. 58, no. 2, pp. 337–343, Feb. 2009, doi: 10.2337/db08-1228.

[100] T. E. Fox, M. C. Bewley, K. A. Unrath, M. M. Pedersen, R. E. Anderson, D. Y. Jung, L. S. Jefferson, J. K. Kim, S. K. Bronson, J. M. Flanagan, and M. Kester, "Circulating sphingolipid biomarkers in models of type 1 diabetes," *J. Lipid Res.*, vol. 52, no. 3, pp. 509–517, Mar. 2011, doi: 10.1194/jlr.M010595.

[101] J. Boon, A. J. Hoy, R. Stark, R. D. Brown, R. C. Meex, D. C. Henstridge, S. Schenk, P. J. Meikle, J. F. Horowitz, B. A. Kingwell, C. R. Bruce, and M. J. Watt, "Ceramides contained in LDL are elevated in type 2 diabetes and promote inflammation and skeletal muscle insulin resistance," *Diabetes*, vol. 62, no. 2, pp. 401–410, Feb. 2013, doi: 10.2337/db12-0686.

[102] L. Song, R. Han, H. Yin, J. Li, Y. Zhang, J. Wang, Z. Yang, J. Bai, and M. Guo, "Sphingolipid metabolism plays a key role in diabetic peripheral neuropathy," *Metabolomics Off. J. Metabolomic Soc.*, vol. 18, no. 6, p. 32, May 2022, doi: 10.1007/s11306-022-01879-7.

[103] M. K. Handzlik, J. M. Gengatharan, K. E. Frizzi, G. H. McGregor, C. Martino, G. Rahman, A. Gonzalez, A. M. Moreno, C. R. Green, L. S. Guernsey, T. Lin, P. Tseng, Y. Ideguchi, R. J. Fallon, A. Chaix, S. Panda, P. Mali, M. Wallace, R. Knight, M. L. Gantner, N. A. Calcutt, and C. M. Metallo, "Insulin-regulated serine and lipid metabolism drive peripheral neuropathy," *Nature*, vol. 614, no. 7946, pp. 118–124, Feb. 2023, doi: 10.1038/s41586-022-05637-6.

[104] M. M. Mielke and C. G. Lyketsos, "Alterations of the sphingolipid pathway in Alzheimer's disease: new biomarkers and treatment targets?," *Neuromolecular Med.*, vol. 12, no. 4, pp. 331–340, Dec. 2010, doi: 10.1007/s12017-010-8121-y.

[105] C. M. C. Bassett, R. S. McCullough, A. L. Edel, T. G. Maddaford, E. Dibrov, D. P. Blackwood, J. A. Austria, and G. N. Pierce, "trans-Fatty acids in the diet stimulate atherosclerosis," *Metabolism*, vol. 58, no. 12, pp. 1802–1808, Dec. 2009, doi: 10.1016/j.metabol.2009.06.010.

[106] T. Monguchi, T. Hara, M. Hasokawa, H. Nakajima, K. Mori, R. Toh, Y. Irino, T. Ishida, K.-I. Hirata, and M. Shinohara, "Excessive intake of trans fatty acid accelerates atherosclerosis through promoting inflammation and oxidative stress in a mouse model of hyperlipidemia," *J. Cardiol.*, vol. 70, no. 2, pp. 121–127, Aug. 2017, doi: 10.1016/j.jjcc.2016.12.012.

[107] Á. Vinué, A. Herrero-Cervera, and H. González-Navarro, "Understanding the Impact of Dietary Cholesterol on Chronic Metabolic Diseases through Studies in Rodent Models," *Nutrients*, vol. 10, no. 7, p. 939, Jul. 2018, doi: 10.3390/nu10070939.

[108] L. H. Tetri, M. Basaranoglu, E. M. Brunt, L. M. Yerian, and B. A. Neuschwander-Tetri, "Severe NAFLD with hepatic necroinflammatory changes in mice fed trans fats and a high-fructose corn syrup equivalent," *Am. J. Physiol. Gastrointest. Liver Physiol.*, vol. 295, no. 5, pp. G987-995, Nov. 2008, doi: 10.1152/ajpgi.90272.2008.

[109] B. A. Neuschwander-Tetri, D. A. Ford, S. Acharya, G. Gilkey, M. Basaranoglu, L. H. Tetri, and E. M. Brunt, "Dietary trans-fatty acid induced NASH is normalized following loss of trans-fatty acids from hepatic lipid pools," *Lipids*, vol. 47, no. 10, pp. 941–950, Oct. 2012, doi: 10.1007/s11745-012-3709-7.

[110] A.-B. Oteng, A. Loregger, M. van Weeghel, N. Zelcer, and S. Kersten, "Industrial Trans Fatty Acids Stimulate SREBP2-Mediated Cholesterogenesis and Promote Non-Alcoholic Fatty Liver Disease," *Mol. Nutr. Food Res.*, vol. 63, no. 19, p. e1900385, Oct. 2019, doi: 10.1002/mnfr.201900385.

[111] T.-S. Park, R. L. Panek, M. D. Rekhter, S. B. Mueller, W. S. Rosebury, A. Robertson, J. C. Hanselman, E. Kindt, R. Homan, and S. K. Karathanasis, "Modulation of lipoprotein metabolism by inhibition of sphingomyelin synthesis in ApoE knockout mice," *Atherosclerosis*, vol. 189, no. 2, pp. 264–272, Dec. 2006, doi: 10.1016/j.atherosclerosis.2005.12.029.

[112] S. D. Gupta, K. Gable, A. Alexaki, P. Chandris, R. L. Proia, T. M. Dunn, and J. M. Harmon, "Expression of the ORMDLS, modulators of serine palmitoyltransferase, is regulated by sphingolipids in mammalian cells," *J. Biol. Chem.*, vol. 290, no. 1, pp. 90–98, Jan. 2015, doi: 10.1074/jbc.M114.588236.

[113] J.-H. Song, G.-T. Kim, K.-H. Park, W.-J. Park, and T.-S. Park, "Bioactive Sphingolipids as Major Regulators of Coronary Artery Disease," *Biomol. Ther.*, vol. 29, no. 4, pp. 373–383, Jul. 2021, doi: 10.4062/biomolther.2020.218.

[114] I. Tabas, K. J. Williams, and J. Borén, "Subendothelial Lipoprotein Retention as the Initiating Process in Atherosclerosis: Update and Therapeutic Implications," *Circulation*, vol. 116, no. 16, pp. 1832–1844, Oct. 2007, doi: 10.1161/CIRCULATIONAHA.106.676890.

[115] A. D. Sniderman, G. Thanassoulis, T. Glavinovic, A. M. Navar, M. Pencina, A. Catapano, and B. A. Ference, "Apolipoprotein B Particles and Cardiovascular Disease: A Narrative Review," *JAMA Cardiol.*, vol. 4, no. 12, pp. 1287–1295, Dec. 2019, doi: 10.1001/jamacardio.2019.3780.

[116] K. Jojima and A. Kihara, "Metabolism of sphingadiene and characterization of the sphingadiene-producing enzyme FADS3," *Biochim. Biophys. Acta BBA - Mol. Cell Biol. Lipids*, vol. 1868, no. 8, p. 159335, Aug. 2023, doi: 10.1016/j.bbalip.2023.159335.

[117] G. Karsai, M. Lone, Z. Kutalik, J. T. Brenna, H. Li, D. Pan, A. Von Eckardstein, and T. Hornemann, "FADS3 is a Δ14Z sphingoid base desaturase that contributes to gender differences in the human plasma sphingolipidome," *J. Biol. Chem.*, vol. 295, no. 7, pp. 1889–1897, Feb. 2020, doi: 10.1074/jbc.AC119.011883.

[118] H. E. Miller and A. J. R. Bishop, "Correlation AnalyzeR: functional predictions from gene co-expression correlations," *BMC Bioinformatics*, vol. 22, no. 1, p. 206, Dec. 2021, doi: 10.1186/s12859-021-04130-7.

[119] S. A. Summers, “Could Ceramides Become the New Cholesterol?,” *Cell Metab.*, vol. 27, no. 2, pp. 276–280, Feb. 2018, doi: 10.1016/j.cmet.2017.12.003.

[120] D. J. Lloyd, J. McCormick, J. Helmering, K. W. Kim, M. Wang, P. Fordstrom, S. A. Kaufman, R. A. Lindberg, and M. M. Véniant, “Generation and characterization of two novel mouse models exhibiting the phenotypes of the metabolic syndrome: Apob48 $^{-/-}$ Lep $^{ob/ob}$ mice devoid of ApoE or Ldlr,” *Am. J. Physiol.-Endocrinol. Metab.*, vol. 294, no. 3, pp. E496–E505, Mar. 2008, doi: 10.1152/ajpendo.00509.2007.

[121] V. P. Gullo, J. McAlpine, K. S. Lam, D. Baker, and F. Petersen, “Drug discovery from natural products,” *J. Ind. Microbiol. Biotechnol.*, vol. 33, no. 7, pp. 523–531, Jul. 2006, doi: 10.1007/s10295-006-0107-2.

[122] Z. Li, T.-S. Park, Y. Li, X. Pan, J. Iqbal, D. Lu, W. Tang, L. Yu, I. J. Goldberg, M. M. Hussain, and X.-C. Jiang, “Serine palmitoyltransferase (SPT) deficient mice absorb less cholesterol,” *Biochim. Biophys. Acta*, vol. 1791, no. 4, pp. 297–306, Apr. 2009, doi: 10.1016/j.bbalip.2009.01.010.

[123] C. A. Fernandez, C. Des Rosiers, S. F. Previs, F. David, and H. Brunengraber, “Correction of 13C mass isotopomer distributions for natural stable isotope abundance,” *J. Mass Spectrom. JMS*, vol. 31, no. 3, pp. 255–262, Mar. 1996, doi: 10.1002/(SICI)1096-9888(199603)31:3<255::AID-JMS290>3.0.CO;2-3.

[124] U. J. F. Tietge, A. Bakillah, C. Maugeais, K. Tsukamoto, M. Hussain, and D. J. Rader, “Hepatic overexpression of microsomal triglyceride transfer protein (MTP) results in increased in vivo secretion of VLDL triglycerides and apolipoprotein B,” *J. Lipid Res.*, vol. 40, no. 11, pp. 2134–2139, Nov. 1999, doi: 10.1016/S0022-2275(20)32437-8.

[125] J. A. Chavez, T. A. Knotts, L.-P. Wang, G. Li, R. T. Dobrowsky, G. L. Florant, and S. A. Summers, “A Role for Ceramide, but Not Diacylglycerol, in the Antagonism of Insulin Signal Transduction by Saturated Fatty Acids,” *J. Biol. Chem.*, vol. 278, no. 12, pp. 10297–10303, Mar. 2003, doi: 10.1074/jbc.M212307200.

[126] F. R. Jornayvaz and G. I. Shulman, “Diacylglycerol Activation of Protein Kinase Cε and Hepatic Insulin Resistance,” *Cell Metab.*, vol. 15, no. 5, pp. 574–584, May 2012, doi: 10.1016/j.cmet.2012.03.005.

[127] M. C. Petersen and G. I. Shulman, “Roles of Diacylglycerols and Ceramides in Hepatic Insulin Resistance,” *Trends Pharmacol. Sci.*, vol. 38, no. 7, pp. 649–665, Jul. 2017, doi: 10.1016/j.tips.2017.04.004.

[128] S. A. Summers, “Ceramides: Nutrient Signals that Drive Hepatosteatosis,” *J. Lipid Atheroscler.*, vol. 9, no. 1, pp. 50–65, Jan. 2020, doi: 10.12997/jla.2020.9.1.50.

[129] K. Minehira, S. G. Young, C. J. Villanueva, L. Yetukuri, M. Oresic, M. K. Hellerstein, R. V. Farese, J. D. Horton, F. Preitner, B. Thorens, and L. Tappy, “Blocking VLDL secretion causes hepatic steatosis but does not affect peripheral lipid stores or insulin sensitivity in

mice," *J. Lipid Res.*, vol. 49, no. 9, pp. 2038–2044, Sep. 2008, doi: 10.1194/jlr.M800248-JLR200.

[130] E. Lopez-Huertas, "Health effects of oleic acid and long chain omega-3 fatty acids (EPA and DHA) enriched milks. A review of intervention studies," *Pharmacol. Res.*, vol. 61, no. 3, pp. 200–207, Mar. 2010, doi: 10.1016/j.phrs.2009.10.007.

[131] E. K. Vassiliou, A. Gonzalez, C. Garcia, J. H. Tadros, G. Chakraborty, and J. H. Toney, "Oleic acid and peanut oil high in oleic acid reverse the inhibitory effect of insulin production of the inflammatory cytokine TNF-α both in vitro and in vivo systems," *Lipids Health Dis.*, vol. 8, no. 1, p. 25, 2009, doi: 10.1186/1476-511X-8-25.

[132] M. [a] del M. C. and S. A.-T. C. Carrillo -, "PAPEL DEL ÁCIDO OLEICO EN EL SISTEMA INMUNE; MECANISMOS DE ACCIÓN; REVISIÓN CIENTÍFICA," *Nutr. Hosp.*, no. 4, pp. 978–990, Jul. 2012, doi: 10.3305/nh.2012.27.4.5783.

[133] H. Sales-Campos, P. Reis De Souza, B. Crema Peghini, J. Santana Da Silva, and C. Ribeiro Cardoso, "An Overview of the Modulatory Effects of Oleic Acid in Health and Disease," *Mini-Rev. Med. Chem.*, vol. 13, no. 2, pp. 201–210, Jan. 2013, doi: 10.2174/1389557511313020003.

[134] S. Li, T. Zhou, C. Li, Z. Dai, D. Che, Y. Yao, L. Li, J. Ma, X. Yang, and G. Gao, "High Metastaticgastric and Breast Cancer Cells Consume Oleic Acid in an AMPK Dependent Manner," *PLoS ONE*, vol. 9, no. 5, p. e97330, May 2014, doi: 10.1371/journal.pone.0097330.

[135] L. Jiang, W. Wang, Q. He, Y. Wu, Z. Lu, J. Sun, Z. Liu, Y. Shao, and A. Wang, "Oleic acid induces apoptosis and autophagy in the treatment of Tongue Squamous cell carcinomas," *Sci. Rep.*, vol. 7, no. 1, p. 11277, Sep. 2017, doi: 10.1038/s41598-017-11842-5.

[136] F. Giulitti, S. Petrungaro, S. Mandatori, L. Tomaipitinca, V. De Franchis, A. D'Amore, A. Filippini, E. Gaudio, E. Ziparo, and C. Giampietri, "Anti-tumor Effect of Oleic Acid in Hepatocellular Carcinoma Cell Lines via Autophagy Reduction," *Front. Cell Dev. Biol.*, vol. 9, p. 629182, Feb. 2021, doi: 10.3389/fcell.2021.629182.

[137] E. Lauretti, L. Iuliano, and D. Praticò, "Extra-virgin olive oil ameliorates cognition and neuropathology of the 3xTg mice: role of autophagy," *Ann. Clin. Transl. Neurol.*, vol. 4, no. 8, pp. 564–574, Aug. 2017, doi: 10.1002/acn3.431.

[138] J. Song, Y.-S. Kim, D. H. Lee, S. H. Lee, H. J. Park, D. Lee, and H. Kim, "Neuroprotective effects of oleic acid in rodent models of cerebral ischaemia," *Sci. Rep.*, vol. 9, no. 1, p. 10732, Jul. 2019, doi: 10.1038/s41598-019-47057-z.

[139] P. Kandel, F. Semerci, R. Mishra, W. Choi, A. Bajic, D. Baluya, L. Ma, K. Chen, A. C. Cao, T. Phongmekhin, N. Matinyan, A. Jiménez-Panizo, S. Chamakuri, I. O. Raji, L. Chang, P. Fuentes-Prior, K. R. MacKenzie, C. L. Benn, E. Estébanez-Perpiñá, K. Venken, D. D. Moore, D. W. Young, and M. Maletic-Savatic, "Oleic acid is an endogenous ligand

of TLX/NR2E1 that triggers hippocampal neurogenesis," *Proc. Natl. Acad. Sci.*, vol. 119, no. 13, p. e2023784119, Mar. 2022, doi: 10.1073/pnas.2023784119.

[140] H. Matsui, T. Yokoyama, K. Sekiguchi, D. Iijima, H. Sunaga, M. Maniwa, M. Ueno, T. Iso, M. Arai, and M. Kurabayashi, "Stearoyl-CoA desaturase-1 (SCD1) augments saturated fatty acid-induced lipid accumulation and inhibits apoptosis in cardiac myocytes," *PloS One*, vol. 7, no. 3, p. e33283, 2012, doi: 10.1371/journal.pone.0033283.

[141] A. Dalla Valle, P. Vertongen, D. Spruyt, J. Lechanteur, V. Suain, N. Gaspard, J.-P. Brion, V. Gangji, and J. Rasschaert, "Induction of Stearoyl-CoA 9-Desaturase 1 Protects Human Mesenchymal Stromal Cells Against Palmitic Acid-Induced Lipotoxicity and Inflammation," *Front. Endocrinol.*, vol. 10, p. 726, Oct. 2019, doi: 10.3389/fendo.2019.00726.

[142] A. Blachnio-Zabielska, M. Baranowski, P. Zabielski, and J. Gorski, "Effect of high fat diet enriched with unsaturated and diet rich in saturated fatty acids on sphingolipid metabolism in rat skeletal muscle," *J. Cell. Physiol.*, vol. 225, no. 3, pp. 786–791, Nov. 2010, doi: 10.1002/jcp.22283.

[143] J. Y. H. Seah, W. S. Chew, F. Torta, C. M. Khoo, M. R. Wenk, D. R. Herr, E. S. Tai, and R. M. van Dam, "Dietary Fat and Protein Intake in Relation to Plasma Sphingolipids as Determined by a Large-Scale Lipidomic Analysis," *Metabolites*, vol. 11, no. 2, p. 93, Feb. 2021, doi: 10.3390/metabo11020093.

[144] "Five billion people unprotected from trans fat leading to heart disease." [Online]. Available: https://www.who.int/news/item/23-01-2023-five-billion-people-unprotected-from-trans-fat-leading-to-heart-disease

[145] E. J. Brandt, R. Myerson, M. C. Perraillon, and T. S. Polonsky, "Hospital Admissions for Myocardial Infarction and Stroke Before and After the Trans-Fatty Acid Restrictions in New York," *JAMA Cardiol.*, vol. 2, no. 6, p. 627, Jun. 2017, doi: 10.1001/jamacardio.2017.0491.

[146] Y. Miyake, Y. Kozutsumi, S. Nakamura, T. Fujita, and T. Kawasaki, "Serine palmitoyltransferase is the primary target of a sphingosine-like immunosuppressant, ISP-1/myriocin," *Biochem. Biophys. Res. Commun.*, vol. 211, no. 2, pp. 396–403, Jun. 1995, doi: 10.1006/bbrc.1995.1827.

[147] T. I. Lima, P.-P. Laurila, M. Wohlwend, J. D. Morel, L. J. E. Goeminne, H. Li, M. Romani, X. Li, C.-M. Oh, D. Park, S. Rodríguez-López, J. Ivanisevic, H. Gallart-Ayala, B. Crisol, F. Delort, S. Batonnet-Pichon, L. R. Silveira, L. Sankabattula Pavani Veera Venkata, A. K. Padala, S. Jain, and J. Auwerx, "Inhibiting de novo ceramide synthesis restores mitochondrial and protein homeostasis in muscle aging," *Sci. Transl. Med.*, vol. 15, no. 696, p. eade6509, May 2023, doi: 10.1126/scitranslmed.ade6509.

[148] P.-P. Laurila, M. Wohlwend, T. Imamura de Lima, P. Luan, S. Herzig, N. Zanou, B. Crisol, M. Bou-Sleiman, E. Porcu, H. Gallart-Ayala, M. K. Handzlik, Q. Wang, S. Jain, D. D'Amico, M. Salonen, C. M. Metallo, Z. Kutalik, T. O. Eichmann, N. Place, J. Ivanisevic,

J. Lahti, J. G. Eriksson, and J. Auwerx, “Sphingolipids accumulate in aged muscle, and their reduction counteracts sarcopenia,” *Nat. Aging*, vol. 2, no. 12, pp. 1159–1175, Dec. 2022, doi: 10.1038/s43587-022-00309-6.